PNL-6807
UC-70

3F

Neutron Measurements of the Fuel Remaining in the TMI II OTSG's

B. D. Geelhood
K. H. Abel

January 1989

Prepared for the U.S. Department of Energy
under Contract DE-AC06-76RLO 1830

Pacific Northwest Laboratory
Operated for the U.S. Department of Energy
by Battelle Memorial Institute

Battelle

PNL-6807

DISCLAIMER

PACIFIC NORTHWEST LABORATORY
operated by
BATTELLE MEMORIAL INSTITUTE
for the
UNITED STATES DEPARTMENT OF ENERGY
under Contract DE-AC06-76RLO 1830

Printed in the United States of America
Available from
National Technical Information Service
United States Department of Commerce
5285 Port Royal Road
Springfield, Virginia 22161

NTIS Price Codes
Microfiche A01

Printed Copy

Pages	Price Codes
001-025	A02
026-050	A03
051-075	A04
076-100	A05
101-125	A06
126-150	A07
151-175	A08
176-200	A09
201-225	A10
226-250	A11
251-275	A12
276-300	A13

PNL-6807
UC-70

NEUTRON MEASUREMENTS OF THE FUEL REMAINING IN THE TMI II OTSG'S

B. D. Geelhood
K. H. Abel

February 1989

Prepared for
the U.S. Department of Energy
under Contract DE-AC06-76RLO 1830

Pacific Northwest Laboratory
Richland, Washington 99352

EXECUTIVE SUMMARY

MEASUREMENTS MADE

Polypropylene tubes containing a string of 18 copper rods were inserted into the lower head region and each J-leg of the two once-through steam generators (OTSG) of the unit two reactor at Three Mile Island. The object was to measure the neutron flux present in those regions and estimate the amount of residual fuel remaining in each OTSG. The neutron flux from any residual fuel induces a radioisotope, ^{64}Cu, in the copper coupons. The ^{64}Cu activity is detected by coincidence counting the two 511-keV gamma rays produced by the annihilation of the positron emitted in the decay of ^{64}Cu. The copper coupons were placed between two 6-inch diameter, 6-inch long NaI(Tl) crystals and the electronics produced a coincidence count whenever the two gamma rays were uniquely detected. The net coincidence count is proportional to the amount of ^{64}Cu activity in the coupon.

CALCULATIONS MADE

The coincidence count data were reduced to estimates of the neutron flux in the various regions of the OTSGs. The flux estimates from several measurements were combined statistically to produce estimates of the flux in each OTSG region. These estimates are listed in Table 1. The table contains weighted average values in the column headed "Wtd Ave FLUX" for each area (J-leg or bowl) of the OTSG. In some OTSG areas, the neutron flux was below the limit of detection and no significant non-zero flux estimate was possible. The column labeled "FLUX LTV" contains a less-than-value where the mean of the neutron flux has a 95% chance of being below that value and only a 5% chance of being above it. The "LTV" is 1.645-sigma above either the mean flux or the minimum detectable flux. The neutron flux in the 1B/J-leg and both A and B bowls was below the minimum detectable level.

The neutron flux value is a fundamental and direct intermediate result of the ^{64}Cu measurements. It is also relatively independent of the debris environment model at the bottom of the OTSGs. The relatively low measured flux value indicates a low danger of criticality.

A reasonable model of the debris configuration and other physics-based considerations was used to estimate the amount of residual fuel remaining in each OTSG. Several models were considered, which gave reasonably consistent estimates of the amount of fuel. Fuel estimates from two such models are also listed in Table 1. One model listed estimated the residual fuel required to produce the ^{64}Cu based on the ratio of neutron capture in the copper coupons compared to the other major neutron capturing materials in the OTSG. The other model estimated the fuel based on experimental data from a mockup. Both schemes produce reasonable estimates of the total fuel present without requiring fuel distribution details that are not available.

TABLE 1. Summary of OTSG Neutron Flux Measurements with Fuel Estimates Based on 1) the Neutron Capture Model Using the Flux Removal Cross Sections and 2) Experimental Mockup Data Using ^{3}He Sensor Data (increased to cover systematic error estimates)

LOCATION	Wtd Ave FLUX n/sec/cm²	FLUX LTV n/sec/cm²	DEBRIS AREA cm²	Capture model Removal σ FUEL EST kg	FUEL LTV kg	Experimental (corrected) FUEL EST kg	FUEL LTV kg
1A/J-leg	0.016(3)	0.020	1.1E4	3.61	4.51	3.43	4.3
2A/J-leg	0.009(3)	0.014	1.1E4	2.03	3.16	1.93	3.0
A/BOWL	----	0.006	2.5E4	----	3.08	----	2.9
A sum				5.64	10.75	5.36	10.2
1B/J-leg	----	0.005	1.1E4	----	1.13	----	1.1
2B/J-leg	0.024(3)	0.030	1.1E4	5.42	6.77	5.14	6.4
B/BOWL	----	0.004	2.5E4	----	2.05	----	1.9
B sum				5.42	9.95	5.14	9.4

Details of these models and some of the other agreeing modeling work can be found in the body of the report. These neutron flux estimates agree with estimates based on debris volume (video evidence) and the gamma-ray measurements. In spite of modeling uncertainties, these estimates could not underestimate reality by more than a factor of two. In fact, the LTVs in the table may be considered reasonable upper limits without an additional multiplicative factor.

CONCLUSIONS

The PNL equipment was well suited to the neutron flux measurement task and worked well the entire time. The neutron flux measurements indicate the amount of residual fuel in the OTSGs is less than 10 kg each.

CONTENTS

FIGURES

TABLES

1.0 COINCIDENCE MEASUREMENT SYSTEM

1.1 INTRODUCTION

This chapter describes the experimental equipment used to determine ^{64}Cu activity in the neutron-activated copper coupons. The techniques used for initial setup of the counting system and for quality control of data are also explained. Modifications to the equipment or procedures which might yield slightly improved results in future measurements are also discussed.

1.2 COPPER COUPONS

Natural copper was placed in each area of the OTSGs in the form of 18 individual coupons. These copper coupons were 1/4-inch diameter rods, 4 inches long, with the ends machined to a convex surface to allow the string to bend slightly. Each coupon weighed 28.60 grams and was labeled with an alphabetic character identifying the string followed by a sequence number (1 to 18). Each coupon was individually weighed on a Mettler PC4400 scale and none deviated from the average by more than 0.05 g. This 0.2% maximum error in the weight is insignificant to the measurement task.

Eighteen copper coupons, supplied by Pacific Northwest Laboratory[a], were placed in a 1/2-inch diameter polypropylene tube for emplacement in the bottom of the OTSG by insertion from the manway at the top of the OTSG down through a steam tube. The front or leading end of the polypropylene tube was sealed and a bullet-shaped plug inserted. The coupons were loaded sequentially in the polypropylene tube with coupon #1 at the bullet end (front) of the string and coupon #18 at the rear of the string. The 18 copper coupons were preceded and followed in the string by small GM counters to measure the local gamma-ray dose as the string was inserted. Additional copper rods were used as ballast behind the rear GM counter to insure that the string would not float up from the bottom surface of the OTSG bowl or J-leg. The tubes remained watertight for all the OTSG measurements and the coupons were not contaminated by OTSG water.

1.3 SENSORS AND ELECTRONICS

The copper coupons were placed in a plexiglass holder that was a half-inch thick between two 6-inch diameter, 6-inch long NaI(Tl) crystals. The holder had seven holes drilled on half-inch centers to hold the coupons upright and centered vertically on the crystal face. The holder was made of

(a) Operated for the U.S. Department of Energy by Battelle Memorial Institute under Contract DE-AC06-76RLO 1830.

low Z material to minimize attenuation of 511-keV gamma rays by the holder. The half-inch thickness and hole spacing were chosen to allow coupon placement and retrieval between the crystals.

Each NaI(Tl) crystal was viewed with a 5-inch diameter photomultiplier tube (PMT). No preamplifier was used since the cable to the main amplifier was relatively short. Since PMT gain is electronically cleaner than preamplifier gain, the PMTs were biased relatively high at 1200 volts. The two PMTs of a sensor system shared a common high voltage power supply since the adjustment required to match the gains could be made at the amplifiers.

The NaI(Tl) crystals and attached PMTs were mounted in plexiglass cradles to maintain a fixed horizontal position. The horizontal position was chosen to reduce the probability of cosmic rays interacting in both crystals. The crystals were also enclosed in a 4-inch thick lead cave to reduce the coincidence background from cosmic rays and surrounding natural radioactivity. A few of the lead bricks at the top of the cave over the coupon holder were temporarily removed to insert the copper coupons. The position of the cave in the basement of a concrete turbine building also contributed additional cosmic ray shielding. During initial setup of the counting system on site at TMI, the NaI(Tl) crystals were carefully washed with alcohol to remove possible radioactive contamination that might contribute to the coincidence background. The PMT bases were also carefully washed with alcohol to minimize or eliminate electronic noise from dirty connections.

Figure 1.1 is a schematic diagram of the sensor electronics used to make the coincidence measurements. One portion of the electronics was used to make the ^{64}Cu measurements. The other portion was used in the setup and quality assurance measurements to insure proper performance of the sensors during the measurements.

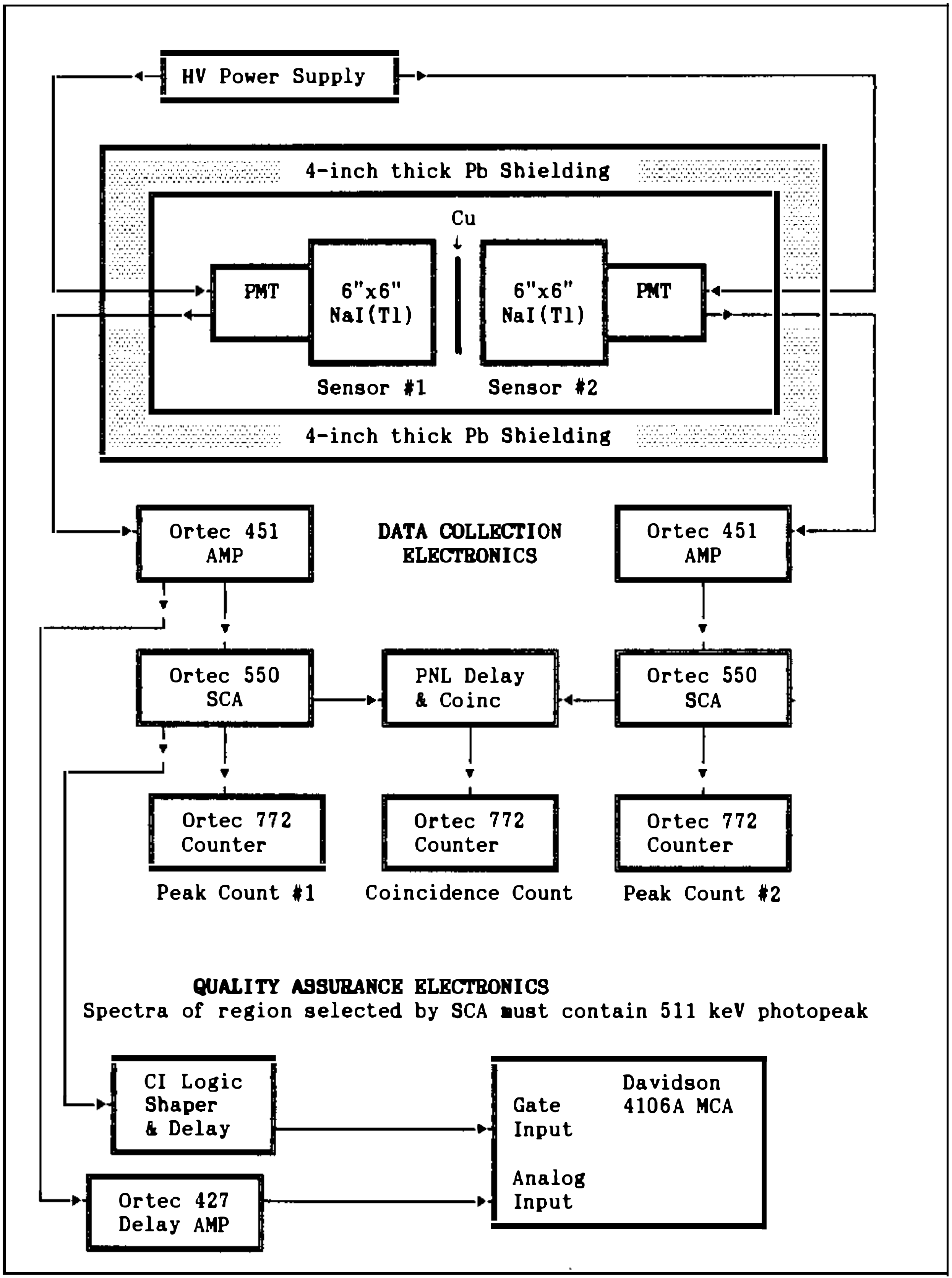

FIGURE 1.1. Schematic of Sensor and Electronics

The signal cable from each PMT base was brought out through a crack in the lead cave wall to the input of an Ortec 451 spectroscopy amplifier. The gain settings were typically 500 coarse and 11.00 fine. The shaping time constant was 1 microsecond. The base line restore (BLR) was set to automatic. The delay option was out. The signal input was negative for the "A" pair and positive for the "B" pair since the bases of the PMTs were wired differently. The signals were checked on an oscilloscope during setup to insure correct polarity and that the pulse shape was as expected. They were checked occasionally during the 3-week measurement period to insure continued proper performance. The gain of each amplifier was set to place the 511-keV photopeak from ^{22}Na in channel 159 of the multichannel analyzer (MCA).

The unipolar output of the amplifier was connected to the input of the Ortec 550 single-channel analyzer (SCA). The SCAs were operated in window mode with the lower level threshold nominally set to 1.25 and the window nominally set to 5.25. The SCA output was a logic pulse whenever the analog input pulse amplitude was within the window settings (the region of the 511-keV photopeak). The threshold and window settings were made and periodically rechecked using the electronics (Logic shaper & delay, delayed amplifier, and multichannel analyzer) shown in the lower part of Figure 1.1 as Quality Assurance Electronics. The settings for the SCA were used to select a region of data collection on the MCA by requiring coincidence between the SCA output and the delayed amplifier pulse for MCA storage. The SCA window selected completely enclosed the 511-keV photopeak. The SCA window was slightly larger than the photopeak to insure that measurement the system would not be sensitive to slight gain shifts. If the SCA window were narrower, the background coincidence rate would be slightly (possibly 10%) less, but a slight gain shift would have greatly changed sensor efficiency. Given the one-time nature of the measurement and the personnel dose, additional assurance of proper operation was felt more preferable than slightly lower background rates and minimum detectable levels.

The front output from each SCA (sensor #1 and #2) was connected to the positive input of an Ortec 772 counter with a 50-ohm terminator. The terminator removed possible ringing that might have led to double counting. The threshold for the positive input was adjusted to about half the typical height of the logic pulse. This was done on an extender cable monitoring both the logic pulse and the threshold level at the input to the comparator circuit. If the threshold is near the average logic pulse amplitude, counts could be lost due to a slight reduction in the logic pulse amplitude. Conversely, if the threshold is too low, the counter is susceptible to counting either ringing or electronic noise. The count of each individual SCA output is used to ensure that chance coincidence does not significantly contribute to the coincidence count. It also serves as a quality control check that the crystals and electronics are functioning properly. The photopeak counts for the two sensors should be approximately equal. The individual photopeak counts were dominated by cosmic-ray and other natural radioactivity rather than the ^{64}Cu positron, so a constant value of the individual counts ensured that the background rates had not significantly changed during a measurement.

The rear output from each SCA (sensor #1 and #2) was connected to a PNL built delay and coincidence circuit. The logic pulse from both sensors (#1 and #2) was delayed by an adjustable amount. The delay settings were adjusted for time overlap while monitoring the delayed SCA pulses from a relatively hot ^{22}Na source on an oscilloscope. The delayed pulses were made 1 microsecond wide by the delaying circuit (one-shot pair). Thus the coincidence time gate was 1 µs. The coincidence logic pulse was the output of an AND gate with the delayed and shaped SCA pulses as input.

The coincidence window of 1 µs was short enough to make the chance rate small compared to the coincidence count. The chance rate is the rate two physically unrelated events occur within a short time window and therefore appear to be related. The chance rate is given by

$$\text{ChanceRate} = 2 * [\text{Rate \#1}] * [\text{Rate \#2}] * \text{CoincidenceTime}$$

The factor "2" is included since either pulse could be first. Typical background individual rates at TMI were about 50 cpm so the chance coincidence rate from background was about 8.3E-5 cpm, which is very small compared to the 0.55 cpm background coincidence rate. With the hot GPU ^{22}Na source, the typical individual rates were 80K cpm for a chance rate of 213 cpm, which is small compared to the measured 31K cpm coincidence rate. The 1 µs time was also large compared to the time jitter of the photopeak pulses out of the SCA. It was clear while adjusting the delays that coincidence events were not being missed due to slight changes in time of pulse arrival.

The logic pulse out of the coincidence box was connected with a 50-ohm terminator to the positive input of an Ortec 772 counter. The threshold was carefully adjusted as described above for the counter on the individual SCAs. All the counters were controlled by a single Ortec timer.

The quality control electronics were connected to only one amplifier and SCA at a time. The delay amplifier provided a fixed time delay for the analog pulse from the amplifier. This allowed time for the SCA pulse to reach the coincidence input of the MCA slightly before the analog pulse as required for proper coincidence mode MCA operation. The logic shaper and delay stretched the logic pulse to satisfy the MCA requirements and allowed an adjustable delay for correct arrival time of the coincidence pulse relative to the fixed delay of the analog pulse.

1.4 QUALITY ASSURANCE EFFORTS

Periodically during the three weeks of measurements at TMI, the GPU ^{22}Na source [5.49E5 dpm on 9/11/88] was counted in each of the two sensor pairs. The mean coincidence count rate was plotted and compared to the previously established value. It was constant within acceptable deviations for the entire measurement period. If the coincidence rate had shifted, it could imply that the gain may have shifted, requiring either amplifier gain or SCA threshold adjustment.

Also the coincidence rate with the weaker PNL ^{22}Na source [3.47E3 dpm on 8/18/88] was measured periodically. The count rates from the weaker PNL source were closer to that expected from the ^{64}Cu coupons. Sometimes nuclear counting systems experience different difficulties at various counting rates. If the system developed a gain shift at high count rate, constant values at high count rates may not insure proper operation at the lower rates of the OTSG measurements. The coincidence counts were constant within acceptable deviations for the entire measurement period.

Background count rates were measured daily to insure the background remained reasonably constant as well. The daily background measurements were statistically combined to provide a system background estimate, thus minimizing the error in the net count for each ^{64}Cu measurement. The combination of the two sources and background exercised the system at counting rates ranging from very low to high.

As time permitted, coincidence spectra of the ^{22}Na source were acquired for each of the four crystals. The 511-keV photopeak channel was monitored and the amplifier gains were slightly adjusted if necessary to hold the photopeak in the originally selected channel (159). The width of the SCA window was also monitored and held constant.

Initially the two older amplifiers experienced some gain shifting. These were replaced after initial setup and before any copper coupon measurements were made. The two newer amplifiers had been in use with the ^3He sensors at PNL. After they were placed into the counting system the gain shift problem was better. Additionally, a cooling fan was placed in the electronics cabinet and the cabinet top removed to avoid gain drift due to heat buildup in the electronics.

The individual 511-keV photopeak count out of the #2 amplifier of the B system was consistently twice as high as the counts out of the other three amplifiers when the caves were empty. This was traced to afterpulses following large cosmic-ray events landing in the 511-keV region. Since 1) this high individual rate did not affect the coincidence count rate and 2) the rate of these afterpulses was unlikely to change during the measurement period, the high individual rate was accepted. Also on this amplifier the coarse gain setting required to place the photopeak in channel 159 was twice that of the other three. The individual count rates held steady during the measurement period, and no problem with the ^{64}Cu measurements were encountered due to this annoyance.

One morning the temperature in the cable spreading room was higher than usual and gain shifts were noticed. In an effort to correct the electronic gain shift problem a cable between one PMT and amplifier became strained and broke contact. This was immediately replaced. The temperature returned to normal before the coupons were removed from the OTSG. No impact on the ^{64}Cu measurements occurred.

No delays in the measurements occurred due to PNL equipment problems. All ^{64}Cu measurements were of equally high quality. No malfunction occurred to compromise the data.

1.5 RECOMMENDED EQUIPMENT IMPROVEMENTS

The coincidence background rate was higher than we would have liked. The background rate establishes the minimum detectable level, so background reduction is important to ^{64}Cu activation measurements. The sensors used had to work in the field rather than just in the PNL laboratory. Also, short lead time somewhat limited our options.

The background rate for the sensors used at TMI was about 0.55 cpm and the background rate for the low-level counting system at PNL was about 0.12 cpm. Thus a decrease in the TMI background by more than a factor of 5 would not have been likely.

The background rate could be reduced for any future measurements by utilizing an active shield against cosmic-ray events. This could entail using a 1-inch thick sheet of plastic scintillator under the NaI(Tl) crystals. The plastic scintillator could be used to provide an additional anticoincidence pulse requirement for the coincidence pulse from the positron decay. The plastic scintillator has fast response and could detect cosmic particles. A pulse from the plastic indicating a cosmic-ray event would be delayed [for slower NaI(Tl) response] and stretched to about 10 μs to block any simultaneous or near-simultaneous occurrences of SCA (511-keV photopeak) pulse coincidences. Cosmic-rays contribute to the coincidence background by 1) directly producing positrons, 2) producing high-energy gamma rays that pair produce with subsequent positron annihilation, 3) corner clipping both crystals and depositing just the right amount of energy in each to satisfy the SCAs, and 4) producing ringing pulses that satisfy the SCAs following huge events. The problem with ringing pulses could also be eliminated by modifying the SCAs to go dead for 10 μs following a large pulse (large being defined as a pulse greater than the upper discriminator).

Another option in reducing the background rate would be to use more lead to make a thicker cave.

Instead of reducing the background, another option for reducing the MDL would have been to use more copper. This would have required placing several strings down the J-leg in the deployment and counting more coupons at one time. This option was not practical.

The source holder could have had the holes for the copper coupons slightly closer together to improve the relative efficiency for counting the extreme positions. Also nine holes in the holder would have allowed counting all the coupons at the same time. A 9-coupon count would have a MDL which is two-thirds that of a 6-coupon count.

1.6 CONCLUSION

The equipment was well suited to the measurement and worked well the entire time.

2.0 METHOD OF NEUTRON FLUX DETERMINATION

2.1 INTRODUCTION

This section describes the calculations employed to determine the neutron flux at the coupon locations in the OTSGs. The neutron flux is derived from the ^{64}Cu activity measured in the copper coupons after retrieval from various locations in the OTSGs. The ^{64}Cu activity measurement was accomplished by coincidence detection [2 6"x 6" NaI(Tl) crystals] of the two 511-keV gamma rays produced during the annihilation of the positron emitted during 19.3% of the radioactive decays of ^{64}Cu.

2.2 NUMBER OF ^{63}Cu ATOMS IN COUPON

The number of atoms of ^{63}Cu in the 28.60 gram copper coupon at the start of the neutron activation is

$$NO(63) = \frac{(6.022045E23 \text{ atoms/mole})*(28.60 \text{ grams/coupon})*(0.692\ ^{63}Cu/Cu)}{(63.546 \text{ grams/mole})}$$

$$NO(63) = 1.875E23 \text{ atoms of } ^{63}Cu \text{ per coupon}$$

where we have used Avogadro's number, the coupon weight, the ^{63}Cu isotopic abundance, and the atomic weight of copper.

2.3 ACTIVATION OF ^{64}Cu

During the activation, the number of atoms of ^{63}Cu, N63A, present in the coupon is reduced. The reaction rate is

$$\frac{d}{dt} N63A(t) = - N63A(t) * \sigma * \Phi$$

where "σ"=4.4E-24 cm^2 is the neutron capture cross section[a] of ^{63}Cu and "Φ" is the neutron flux measured in neutrons/(second*cm^2). In fact, the number of ^{63}Cu atoms does not change significantly during the activation because the $\sigma * \Phi$ product is small.

---

[a] C.M Lederer and V. Shirley. 1978. Table of Isotopes, 7th Edition. John Wiley & Sons, Inc, New York.

Note the approximation of assigning an effective neutron capture cross section rather than considering the product, $\sigma * \Phi$, as a convolution of the capture cross section as a function of neutron energy and the energy distribution of the neutron flux. The convolution process is more exact but beyond the scope of this problem. Note that Φ only appears in the formalism as the $\sigma * \Phi$ product, which would allow scaling of the resulting flux with the value of the detailed convolution. The convolution process would include neutron capture into non-thermal resonances. Proper use of the convolution process would require a reasonable model of the neutron energy spectrum in the OTSG environment. Lacking information on quantities of non-thermal neutron poisons in the OTSG, such a model would be more misleading than useful. Omitting capture into copper by non-thermal resonances increases the neutron flux estimate to produce the measured activity. This is a conservative approximation for the task of setting an upper limit on the amount of residual fuel.

The neutron radiative capture cross section measured at 2200 m/sec is σ=4.50(2) barns and the radiative capture resonance integral I_γ=4.97(8) barns[a] for ^{63}Cu. However, in the aqueous OTSG environment, the thermal flux dominates. The neutron flux overestimation (ignoring resonance capture) will be considerably less than a factor of 2.1 [(4.5+4.97)/4.5]. When resonance capture is ignored in the fuel estimating model, most of this error cancels out.

At the same time, the number of atoms of ^{64}Cu, N64A(t), (which was initially zero at the start of the neutron activation) also changes with a reaction rate given by

$$\frac{d}{dt} N64A(t) = + N63A(t) * \sigma * \Phi - \lambda * N64A(t)$$

where "λ" is the radioactive decay constant, which is expressed in decays per unit time. The decay constant, λ, is related to the half life, t(1/2), of an isotope by $\lambda = \ln(2) / t(1/2)$. For ^{64}Cu, with a 12.699-hour half life, the decay constant is either 5.4583E-2 decays/hour or 1.5162E-5 decays/second depending on choice of units. The first term on the right of the above rate equation corresponds to a gain from the neutron activation of the ^{63}Cu and the second term to a loss due to radioactive decay of ^{64}Cu. Initially the first term dominates. Then as the number of ^{64}Cu atoms increases, the two terms become equal. At equilibrium (after a long activation time), the number of ^{64}Cu atoms is a constant since the production rate and decay rate are equal.

(a) S. F. Mughabhab, M. Divadeenam, and N. E. Holden. 1981. <u>Neutron Cross Sections Volume 1 Neutron Resonance Parameters and Thermal Cross Sections Part A Z=1-60</u>, Academic Press, New York.

These differential equations can be solved for the number of atoms at the end of the activation period, t=Ta, subject to the initial conditions of N64A(t=0)=0 and N63A(t=0)=N0(63) at the start of the activation. The solutions are

$$N63A(t=Ta) = N0(63) * e^{-(\sigma * \Phi * Ta)}$$

$$N64A(t=Ta) = \frac{\sigma * \Phi * N0(63)}{\lambda - \sigma * \Phi} * \left[e^{-(\sigma*\Phi*Ta)} - e^{-(\lambda*Ta)} \right]$$

The value of N64A can be accurately approximated (because of the very small size of $\sigma*\Phi$) by

$$N64A(t=Ta) = \frac{\sigma * \Phi * N0(63)}{\lambda} * \left[1 - e^{-(\lambda * Ta)} \right]$$

Now one can easily solve for the neutron flux, "Φ", since the function is linear in Φ

$$\Phi = \frac{\lambda * N64A(t=Ta)}{\sigma * N0(63)} \Bigg/ \left[1 - e^{-(\lambda * Ta)} \right]$$

where "Ta" is the time duration of the activation. Note "Φ" will have the same time units as λ. After measurement of the ^{64}Cu activity, λ*N64A(t=Ta), at the end of the activation period, all the parameters are known.

2.4 DECAY OF THE COPPER ACTIVITY

The ^{64}Cu activity will decay during the experimental period and must be correctly taken into account.

2.4.1 Decay Before the Start of a Counting Period

The number of ^{64}Cu atoms in the copper coupon decreases after the coupon has been removed from the neutron flux. The number of ^{64}Cu atoms at the start of a counting period, N64S, is given by

$$N64S = N64A * e^{-(\lambda * Td)}$$

where "N64A" is the number of atoms at the end of the activation period and "Td" is the time delay between the end of the activation period and the start of the count.

For the OTSG measurements, a delay of between one and two hours was experienced after string removal and the start of the first ^{64}Cu measurement. The time between end of activation and start of counting was used to 1) remove the strings from the contaminated OTSG area, 2) decontaminate the string, 3) remove the coupons from the string, radiologically monitor the coupons to insure that they were contamination free, and 4) transfer them into the counting system.

2.4.2 Decay During the Counting Period

Isotopes with very long half lives can be assumed not to decay sufficiently during a relatively short counting time and thus no change will occur in the counting rate during the counting period. However, the 12.699-hour half life of ^{64}Cu will not be short relative to some of our longer counting times, so a correction must be made for decay during the counting time. The number of counts observed can be given by

$$Cts = \int_{t=0}^{t=Tc} Eff * \lambda * N64S * e^{-(\lambda * t)} * dt$$

where "Tc" is the counting time, "Eff" is the sensor efficiency in counts per decay, and "N64S" is the number of atoms at the start of the counting period from the previous section. The integration uses a change of variable $x = (\lambda * t)$ to yield

$$Cts = Eff*N64S * \int_{t=0}^{x=\lambda*Tc} e^{-x} * dx = Eff*N64S * \left[- e^{-x} \right]_{t=0}^{\lambda*Tc}$$

which becomes

$$Cts = Eff * N64S * \left[1 - e^{-(\lambda * Tc)} \right]$$

Thus from the value of the sensor counts, "Cts", one can obtain the number of ^{64}Cu atoms at the start of the counting period, "N64S". As a check, consider the small Tc expansion

$$Cts = Eff * N64S * \left[(\lambda * Tc) - (\lambda * Tc)^2/2 + ... \right]$$

which equals the usual { Eff*λ*N64S*Tc } if only the first term in the series expansion is considered.

2.5 SENSOR EFFICIENCY

The previous section used the sensor efficiency, "Eff", to convert between the count rate and the decay rate. The efficiency desired is the ratio of net coincidence counts to ^{64}Cu decays. The coincidence was between detections in the 511-keV photopeak regions of the two NaI(Tl) crystals used at TMI.

2.5.1 Absolute Efficiency Values

Several methods of obtaining the absolute efficiency will be considered.

2.5.1.1 Calculations Based on Sensor Parameters

First consider some relatively simple numerically calculated efficiency values based on NaI(Tl) data in the Harshaw catalog and geometry considerations. These calculations will set the scale for what can be expected as a reasonable ^{64}Cu efficiency value. For a pair of 6-inch diameter, 6-inch long NaI(Tl) crystals separated by 0.5 inches the fractional solid angle, Ω, for a gamma ray to enter one of the crystals from a point centered between the crystals is

$$\Omega = \frac{1 - \cos(\theta)}{2} = 0.458$$

where θ = ArcTan(D/a), the crystal diameter, D, is 6 inches, and the distance between the crystals, "a" is 0.5 inches. Then the probability of one gamma ray entering either of the two crystals is 0.917. However, one must also consider the probability that the gamma ray will interact within the NaI(Tl) crystal. The total cross section for a 511-keV annihilation gamma ray in NaI(Tl) is 0.34 cm^{-1} for an interaction length of 2.94 cm (1.16 inches). The fraction of gamma rays emitted by the point source which interact in a crystal is given by the integral over angles within the fractional solid angle for entering the crystal. Each increment of angle is weighted by the probability of the gamma ray interacting in the crystal along a path in that direction. This interaction probability is $1-e^{-d/L}$ where "d" is the distance the gamma ray travels through the crystal at each angle and "L" is the interaction length.

This integral was numerically calculated for two cases 1) crystal separation of 0.5 inches (closest possible with our 0.5-inch thick copper rod holder between the crystals) [source 0.25 inches from crystal] and 2) crystal separation of 0.75 inches (allowing for packing around crystal) [source 0.375 inches from the crystal]. The following text (using case 1) explains the calculations leading to the entries in Table 2.1. The probability for a single 511-keV gamma ray entering and interacting in one 6"x 6" crystal is 40.8%.

The photofraction (fraction of interacting gamma rays producing a count in the photopeak) is about 80% for a 511-keV gamma ray in a 6"x 6" crystal. The probability of a pair of 511-keV gamma rays depositing full energy in the two-crystal system is 47.7%, which is twice the single-crystal fractional solid angle integral weighted by $[1-e^{-d/L}]^2$ times the square of the photofraction. The single-crystal solid angle is multiplied by two because there are two crystals for the first gamma ray to pass through. The second gamma ray always goes in the opposite direction from the first so an extra solid angle factor is not needed. However, both gamma rays must interact and deposit full energy to satisfy a full energy coincidence criterion.

Figure 2.1 shows the ^{64}Cu decay scheme. Only 19.3% of the ^{64}Cu decays emit a positron. Thus the calculated ^{64}Cu efficiency for coincidence detection of both annihilation gamma rays in the 511-keV photopeak is (47.7%)*0.193 or 9.21%. This efficiency estimate is for a point ^{64}Cu source not a rod. Since the ^{64}Cu activity is distributed over the ¼-inch diameter, 4-inch long rod, this estimate will be an upper limit. For points off the crystal axis one of the gamma rays will have a shorter path in the crystal resulting in a lower interaction probability.

2.5.1.2 Comparison to a Standardized ^{22}Na Source

The absolute ^{64}Cu detection efficiency can be estimated by comparison to a standardized ^{22}Na source. The use of the ^{22}Na source is not practical because 1) it is a point source and the ^{64}Cu is a rod shaped source, and 2) the 1274-keV gamma ray of ^{22}Na interferes. Although accurate standardization using the ^{22}Na source was not practical, the following exercise is instructive in demonstrating the difficulties. Figure 2.1 shows the decay scheme of both ^{64}Cu and ^{22}Na.

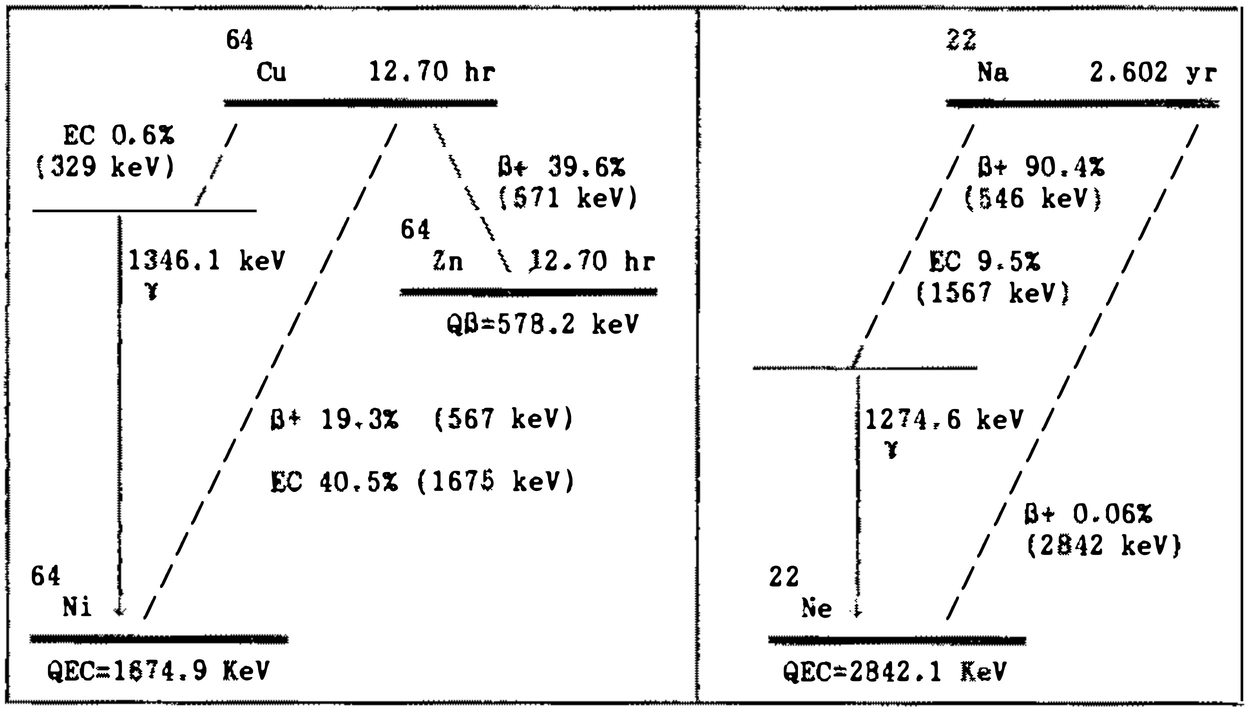

FIGURE 2.1. Decay Schemes of ^{64}Cu and ^{22}Na

Like ^{64}Cu, ^{22}Na also decays by positron (β^+) emission which produces a pair of 511-keV annihilation gamma rays. The ^{22}Na source can be used to adjust the electronics (photopeak windows and timing) for maximum detection efficiency for the pair of 511-keV gamma rays. It can also be used to insure system stability during a multiday measurement period.

For ^{22}Na (2.602-year half life), 90.46% of the total radioactive decays result in positron emission and 9.5% result in an electron capture. However, nearly all of the ^{22}Na decays pass through the 1.274-MeV excited state of ^{22}Ne with subsequent 1.274-MeV gamma-ray emission. This 1.274-MeV gamma-ray emission somewhat spoils the ^{22}Na calibration process for positron annihilation gamma rays. If the 1.274-MeV gamma ray interacts with one of the two NaI(Tl) crystals, its energy will add to the 511-keV gamma-ray energy and remove the interaction from the 511-keV photopeak region. Thus the ^{22}Na coincidence count rate of detections in both 511-keV photopeak regions can be significantly less than the coincidence detection rate of positron annihilation gamma rays.

Calculations of ^{22}Na probabilities and efficiencies in the manner of the previous section are instructive. Results for both cases may be found in Table 2.1. The total cross section for a 511-keV gamma ray in NaI(Tl) is 0.34 cm^{-1} for an interaction length of 2.94 cm (1.16 inches). The total cross section for a 1.27-MeV gamma ray in NaI(Tl) is 0.18 cm^{-1} for an interaction length of 5.55 cm (2.19 inches). The probability for a single 511-keV gamma ray entering and interacting in one 6"x 6" crystal is 40.8%. For a single 1274-keV gamma ray the probability is 33.7%.

When the probability of detecting the subsequent 1274-keV gamma ray in either crystal (67.5%) is considered, the probability of a coincidence between two 511-keV photopeak counts without considering the 1274-keV gamma (47.7%) must be reduced by the probability that the 1274-keV gamma ray not interfere (1-.675). The probability of coincidence in the 511-keV region becomes 0.477*0.325 or 15.5% of the ^{22}Na positron emissions to the 1274-keV excited state. The efficiency for the 511-keV region coincidence increases when the crystal separation is slightly increased because the 1274-keV gamma is less likely to interfere.

The efficiency for ^{22}Na is the product of detection probabilities and the fraction of decays following each possible decay path. Thus the ^{22}Na efficiency is (15.5%)*0.904 + (47.7%)*0.0006 or 14.04%.

The last item in the Table 2.1 is the efficiency for making a detection in both crystals with sufficient energy to be above the lower limit of the 511-keV region in both crystals. This will occur when both 511-keV gamma rays deposit full energy (47.7%) or when one 511-keV gamma ray deposits full energy in one crystal but the other 511-keV gamma ray does not but the 1274-keV makes up the difference. The combined probability of 1) both 511-keV gamma rays interacting in the crystals (0.746), 2) one depositing full energy (0.8), 3) the other not depositing full energy (0.2), and 4) the 1274-keV gamma interacting in the "not" crystal (0.337) is 0.0402. This must be multiplied by 2 since either crystal could have had the full 511-keV energy to yield 8.04%. The combined probability of 1) one 511-keV gamma ray interacting in one crystal (0.408), 2) it depositing full energy (0.8), 3) the other 511-keV gamma ray entering the other crystal but not interacting (1- 0.408/0.4585 = 0.110), and 4) the 1274-keV gamma interacting in the not crystal (0.337) is 0.012. Similarly this must be multiplied by 2 to yield 2.42%. Thus the ^{22}Na efficiency for an above threshold coincidence is 0.904*(47.7%+ 8.04% + 2.42%)=52.6%.

TABLE 2.1. Calculated ^{64}Cu and ^{22}Na Efficiencies

6"x 6" NaI(Tl) crystal separation	0.50 inch	0.75 inch
	Probability of	
a gamma entering one 6"x 6" crystal	45.85%.	43.80%
1274 keV gamma ray interacting in one 6"x 6" crystal	33.7%.	31.1%
511 keV gamma ray interacting in one 6"x 6" crystal	40.8%	38.0%
511 keV pair interacting in two NaI(Tl) crystals	74.6%	68.4%
511 keV pair depositing full energy in two NaI(Tl)	47.7%	43.8%
511 keV photopeak coincidence (with 1274 problem)	15.5%	16.5%
	Efficiency (100%*cts/decay)	
511 keV photopeak coincidence ^{64}Cu (path=19.3%)	9.21%	8.45%
511 keV photopeak coincidence ^{22}Na (path=90.4%)	14.0%	14.9%
511 keV and above coincidence ^{22}Na (path=90.4%)	52.6%	48.0%

These calculated results can be compared to ^{22}Na measurements in order to judge how realistic they are. The GPU ^{22}Na source was labeled as 1.17 μCi on 11/11/82 which had decayed to 9029 d/s by 9/28/88.

The coincidence rate between windows containing the 511-keV photopeaks was 1060 cps yielding a ^{22}Na efficiency of 0.117 cts/decay. This is slightly lower than the 14% expected from the above calculation. If the calculation were scaled to match the ^{22}Na efficiency, the scaled ^{64}Cu efficiency would be 7.7% for case 1 or 6.6% for case 2.

When a spectrum of the ^{22}Na detections in a single crystal was made with no coincidence requirement, the count rate above the 511-keV photopeak region was 2887 cps, yielding a 32% efficiency. This compares reasonably well to the 33.7% calculated probability of the 1274-keV gamma interacting in a single crystal. The experimental value may be a little high since some of the interacting 1274-keV gamma rays will deposit less than 511 keV in the crystal.

The coincidence rate between detections in or above the 511-keV photopeak region was obtained by changing the SCA mode from window to integral. The observed integral mode coincidence rate was 3650 cps corresponding to a 40.4% efficiency. This is considerably lower than the last entry in Table 2.1 perhaps indicating that the calculated efficiency for ^{64}Cu is too high. Matching the integral mode efficiency would scale the calculated ^{64}Cu efficiency estimate to 7.1% (9.21%*40.4/52.6) for case 1 or 7.1% for case 2.

2.5.1.3 Comparison to Efficiency of Packard-5 system at PNL

An alternate method, which experimentally determines the efficiency for the distributed copper rods, involves 1) counting copper rods (which were activated at GPU by a neutron source in a cave) with the two NaI(Tl) coincidence systems used at TMI, 2) flying the rods back to PNL, and 3) counting the rods on the calibrated Packard-5 system. The Packard-5 efficiency for ^{64}Cu distributed in a 6-inch long, 1/4-inch diameter copper rod is 19.39 d/c or 5.157%. The efficiency for a 4-inch long rod will be slightly greater than for the 6-inch log rod. Our best estimate of the efficiency for a 4-inch long rod is 19.04 d/c or 5.252% based on efficiency measurements of 20.44 d/c on a 4-inch diameter disk and 21.20 d/c on a 6-inch diameter disk. The rod length correction scales as the square root of the d/c values at the two disk diameters since only a one-dimensional scaling is necessary for the rod. The Packard-5 system consists of two 9-inch diameter crystals separated by 1 inch.

The activated copper rods and identical unactivated copper rods were both flown back and counted at PNL after counting at TMI. Cosmic-ray induced ^{64}Cu activity from the plane ride was equally present in both activated and unactivated rods so it could be subtracted out.

Seven copper rods were placed for activation in a concrete block cave with a neutron source. The rods were removed on 9-28-88 at 14:22 EDT after being in the cave for about 120 hours. Since this produced 99.85% of maximum or saturation ^{64}Cu activity in the rods, the exact entrance time was not important.

TABLE 2.2. Packard-5 Count Data for Rods Activated in Cave

Label	Item counted	Count Start Time Pacific Daylight	Duration (min)	Count (cts)	Count Rate (cpm)
P1	8 rods cosmic only	9-29-88 @ 15:08	60	94	1.566
P2	1 rod L2 activated	9-29-88 @ 16:16	60	746	12.43
P3	1 rod L6 activated	9-29-88 @ 17:33	60	740	12.333
P4	1 rod L6 activated	9-29-88 @ 17:33	1120	8143	7.2705
P5	22 rods cosmic	9-30-88 @ 13:47	3260	1510	0.46319
P6	22 rods cosmic	10-3-88 @ 14:11	1318	162	0.12291
P7	empty	10-10-88 @ 14:22	100	15	0.15

The background count rate with no activity in the system was taken as 0.1229 cpm from the last count after considerable decay time. This was justified based on the 0.15 cpm background from the empty cave. (The presence of the copper mass absorbs radiation scattered from one crystal into the other and reduces the system coincidence background.)

Based on the 5.252% ^{64}Cu counting efficiency for 1/4"-inch diameter, 4-inch long copper rod, the activating neutron flux can be calculated and is listed in Table 2.3 below.

TABLE 2.3. Neutron Flux Estimates Based on Packard-5 Measurements

Label	Item counted	Flux estimate n/(s*cm²)	% Error	decays/min per rod at t=0
P1	8 rods cosmic only	0.33(4)	12.2%	16
P2	1 rod L2 activated	23.60(87)	3.7%	1166
P3	1 rod L6 activated	25.10(93)	3.7%	1241
P4	1 rod L6 activated	24.28(27)	1.1%	1200
P5	22 rods cosmic	0.297(18)	6.1%	14
P6	22 rods cosmic	used as background estimate		
	Flux seen by rod	24.0(3)	1.2%	1184

The data is not sufficient to make a claim that the ^{64}Cu activity in rod L6 was significantly greater than that in rod L2. The average activity in the three rod measurements indicated a flux of 24.32 n/(s*cm²). However the cosmic rays induced an activity during the airplane ride to PNL which would account for a 0.30 n/(s*cm²) flux. Using the P4 measurement as the most accurate, the estimated neutron flux in the cave at TMI was 24.0(3) n/(s*cm²).

The ^{64}Cu decay rate when the rods were removed from the source was 1184 d/m. Table 2.4 lists the efficiencies at TMI required to match the 1184 d/m decay rate to the observed counting rates.

TABLE 2.4. Data from Sensors Used at GPU

Label	Rod	Cts/min at t=0	Efficiency
LA1	L2	60.73	5.129%
LB2	L6	55.82	4.714%
LA2	L6	56.85	4.802%
LB2	L2	53.80	4.544%
LA4	L6	55.93	4.724%
LB4	L2	55.24	4.666%
LA10	L2	58.13	4.910%
LB11	L6	54.50	4.603%
	AVERAGE	56.38	4.762%
	Std Err	2.21	0.187%

The resulting absolute efficiency estimate for the two systems used at GPU was 4.8(2)%. The fractional error in this calibration is only 3.9% which is acceptable considering the 2.8% counting statistics obtained for the single, activated rod counts at GPU. This efficiency value is less than the previous estimates for a point source as it should be.

2.5.1.4 Computer Code Modeling with EGS4

Harry Miley modeled the TMI measurement system geometry with the EGS4 (electron gamma shower) code from SLAC. He found the TMI system efficiency (counts/decay) for a 1/4-inch diameter, 4-inch long copper rod to be 7.72% with the 6"x 6" NaI(Tl) crystal pair and 1/2" separation. He found the Packard-5 efficiency for a 1/4-inch diameter, 6-inch long copper rod to be 8.78% with the 9"x 8" NaI(Tl) crystal pair with 1" separation. The 8.78% was 70% higher than the 5.16% experimental calibration value. The ratio between the TMI system and the Packard-5 (0.879) allows scaling between these systems which indicates 4.53% is the TMI efficiency.

This code did not take into account that the positron could escape the copper rod and be annihilated at another location. If the positron was annihilated in one of the crystals, it would carry kinetic energy into the crystal, possibly increasing the deposited energy enough to produce a pulse above the photopeak region. This would lower the efficiency from that calculated by the code. If the positron was annihilated at any position farther from the crystal axis, it would also have a lower efficiency.

2.5.1.5 Selection of Absolute Efficiency Value

A ^{64}Cu efficiency for the copper rods is less than a theoretical point source or a sealed disk source since 1) the rods are distributed sources and 2) the 511-keV gamma rays can interact in the thickness of the copper rod. When a ^{64}Cu decay or positron annihilation occurs off axis, one gamma ray of the 511-keV pair will travel considerably less distance in the crystal than the distance used in the on axis calculation reducing the coincidence probability. When a gamma ray interacts before entering the crystal, it will not have sufficient energy to cause a coincidence count.

The efficiency value used to reduce the coincidence counts to ^{64}Cu activity is 4.8(2)%. This value was obtained from the Packard-5 cross calibration which is considered the most accurate method since no modeling approximations are necessary.

Note that the estimate of the remaining fuel is proportional to the flux measurement and the flux estimate is inversely proportional to the efficiency used. Given the coincidence count, using the lowest efficiency value of those reasonably supportable yields the highest estimate for the amount of residual fuel. This is conservative in that we seek to place an upper limit on the amount of residual fuel in the OTSGs.

2.5.2 Relative Efficiency Based on Position

The efficiency for counting the copper coupons varies depending on which of the seven positions in the plastic sample holder the copper coupon occupies. When single coupons are counted only the center position was used. However, when multiple coupons were counted, the non-central positions were also used. The relative efficiencies for detection at each position are listed in Table 2.5 below. These values were obtained by placing either the GPU ^{22}Na source or a neutron activated copper rod in each position and comparing the count at that position to the count in the central position. For the copper rod values ^{64}Cu decay was taken into account. The efficiencies observed were not exactly symmetric about the central position since the source holder was not exactly centered on the crystals. The actual OTSG flux measurements were accomplished using combinations of 1, 3, 6, and 7 rods counts. The average relative efficiency factors for these three multiple-rod configurations are also listed in the table.

TABLE 2.5. Relative Efficiencies at the Rod Positions

Position	Relative Efficiency System #1		Relative Efficiency System #2	
	GPU ^{22}Na Point	Cu rod Extended	GPU ^{22}Na Point	Cu rod Extended
	outer wall near post		cave center wall	
1	0.8638 *	0.654 *	0.9076	0.716
2	0.9489	0.857	0.9788	0.919
3	0.9895	0.994	1.0009	0.977
4	1.0000	1.000	1.0000	1.000
5	0.9909	0.947	0.9878	0.970
6	0.9610	0.918	0.9388	0.865
7	0.8928	0.708	0.8457 *	0.688 *
	cave center wall		cave outer wall	
7-position average	0.9496	0.868	0.9514	0.876
6-position average	0.9639	0.904	0.9690	0.906
3-position average	0.9935	0.981	0.9962	0.983

* omitted in 6-position average since lowest efficiency position not used

The point source efficiency for the extreme positions is about 10% to 15% lower than in the central position. The rod source efficiency for the extreme positions is about 30% to 35% lower than in the central position. The difference in efficiency between the ^{22}Na point source and the extended ^{64}Cu rod source is strictly due to less favorable geometry (i.e., the rod ends of the outer rods are in a very unfavorable counting position relative to points on the crystal axis. The relative efficiencies for the point sources only point out that the reduced counting efficiency of the extended rod source can be significant.

The counting efficiencies for multiple rod counts will be reduced by the corresponding average relative efficiency value for the copper rods from the above table. Also since the count provides no information as to relative coupon activity in a multiple coupon measurement, the error in the flux measurement will be arbitrarily increased by 5% to cover this efficiency variation.

3.0 STATISTICAL CONSIDERATIONS

3.1 INTRODUCTION

The statistical nature of this measurement is important and has been separated out from the other aspects for clarity.

3.2 ERROR PROPAGATION

The neutron flux is linearly related to the ^{64}Cu activity in the copper coupons. Therefore, the percentage error in the net ^{64}Cu count and in the neutron flux are the same.

The estimate of the ^{64}Cu count is the coincidence count minus the average background coincidence count. The error estimate for the coincidence counts must be taken as the Poisson standard error [square root of the coincidence count]. This is required since repeated measurements are not feasible due to 1) the substantial ^{64}Cu decay during the counting time, and 2) the long counting times required. The error estimate for the net ^{64}Cu count is taken to be equal to the square root of the sum of 1) the raw coincidence count and 2) the variance of the background estimate. The variance of the background estimate is the standard error in the mean of all the background measurements taken on site. It is not the square root of the background count expected during the one measurement. The Poisson statistical fluctuations during the one measurement have been included in the error estimate of the raw coincidence count and need not be included a second time. For example, when normally distributed data with a mean are transformed to have a mean of zero, the sample variance is not increased by subtracting the mean from each point. In this case, in the variance of the background estimate is small compared to the coincidence count since the average background value is known to much greater precision from the several long background counts obtained over the experimental period. Although the error in the background estimate could have been neglected, it has been included in our data reduction program.

More than one independent measurement of the neutron flux at points in the OTSG were obtained because more than one count of the various copper coupon groups was made. These measurements are not of equal statistical value since they were made at different times, and the ^{64}Cu activity had decayed to different levels for each measurement. The ^{64}Cu decay makes it incorrect to statistically combine the net count values for the independent measurements. Instead the neutron flux estimates must be statistically combined, since the radioactive decay has been taken into account in the calculation of these values. Also some of the later measurements were made for longer counting durations, in an effort to make the later flux measurements comparably significant to the earlier measurements. To combine the several measurements a weighted average was used. Each measurement x_i was weighted by $1/s_i^2$ where s_i is the standard error associated with the i-th measurement, x_i. The weighted mean, $\langle X \rangle$, and its associated standard error in that mean, S_x, are given by

$$\langle X \rangle = \frac{\sum_{i=1}^{N} \frac{x_i}{s_i^2}}{\sum_{i=1}^{N} \frac{1}{s_i^2}} \qquad \text{and} \qquad \frac{1}{S_x^2} = \sum_{i=1}^{N} \frac{1}{s_i^2}$$

This formula can be derived from the Normal distribution by the method of maximum likelihood. It is also a minimum variance unbiased estimate.

Also as an added check the multiple flux measurements can be combined by the normal averaging process to insure that the weighted average has not produced an unrealistic result. The normal average of "N" independent measurements produces a mean, "m", a standard deviation of the distribution of measurements, "s", and a standard error of the estimated mean, "s_m".

$$m = \frac{1}{n} \sum_{i=1}^{N} x_i \qquad s_m = \frac{s}{\sqrt{n}}$$

$$s^2 = \frac{1}{n-1} * \left[\left[\sum_{i=1}^{N} [x_i]^2 \right] - \frac{1}{n} * \left[\sum_{i=1}^{N} x_i \right]^2 \right]$$

Note that we are using this standard average as a double check on the weighted average.

3.3 SIGNIFICANCE OF THE INDIVIDUAL NET ^{64}Cu COUNTS

The significance of a small number of net ^{64}Cu counts is determined by the ability to reject the null hypothesis that the associated coincidence count is due only to the statistical variations in background. The significance is quantized by a false alarm probability, FAP, which is the fractional area under the background distribution function corresponding to an observed count or higher.

If the background distribution function is (or can be approximated by) a normal probability function, the coincidence count increase can be measured in terms of the number of sigmas (standard deviations). This measure has meaning to statisticians and is quite common. However, the normal distribution is not necessarily a good approximation when the number of coincidence counts is relatively small, since the Poisson distribution only approaches the Normal distribution for large counts. Thus the FAP should be calculated directly from the Poisson distribution function with the Poisson mean equal to the expected background count.

Once a FAP is selected, it can be used to calculate a single-count threshold for rejecting the null hypothesis. If sufficient non-background radioactivity is present to make the average signal plus the mean background estimate for a given measurement time equal to the corresponding single-count threshold, there is a 50% chance that the count obtained in a single interval will exceed that threshold. It is therefore generally implied that a 50% detection probability (DP) is desired for a minimum detectable level (MDL) of additional activity. One can require a different detection probability, but the single-count threshold depends only on the selected FAP value and the measurement time, not the detection probability.

The Poisson FAP is calculated by

$$FAP(N;m) = \left[\sum_{I=N}^{\infty} \frac{m^{I}}{I!} * e^{-m} \right]$$

$$FAP(N;m) = 1 - \left[\sum_{I=0}^{N-1} \frac{m^{I}}{I!} * e^{-m} \right]$$

where "FAP(N;m)" is probability of pure background producing a count of "N" or more in an interval given a mean background value of "m" counts for that interval. The infinite sum can be replaced by a finite sum since the Poisson distribution is normalized. The finite sum is often used for numerical calculation of the FAP, but double precision arithmetic is called for to avoid roundoff errors for small FAP values. Note that since the FAP is calculated correctly from the Poisson distribution, the count threshold for a given FAP significance need not be artificially increased for low counts as it might be if the count threshold were calculated using the normal distribution approximation.

The value one selects for the false alarm probability acceptable for a given application is somewhat arbitrary. The selection of the FAP is generally based on the number of measurements made and the expense of acting on a false alarm. Some people like dealing with a 95% confidence level corresponding to a FAP=0.05 or a 1.66-sigma threshold from a normal distribution. A 99% confidence level corresponds to FAP=0.01 or a 2.33-sigma threshold in a normal variable. The most common choice for the FAP is FAP=0.001 or a 3.1-sigma threshold. If a large number of measurements are made and false alarms are expensive to chase down, a higher threshold is used, such as FAP=0.0001 or a 3.73-sigma threshold. A 4.65-sigma threshold of a normally distributed variable corresponds to a FAP=1.7E-6. The FAP values will be listed for each of our measurements to allow individual preference for a FAP threshold to be used in evaluating the significance of an individual measurement.

Generally a count less than 3-sigma [normal distribution FAP > 0.0013] above background is not considered a real increase over background, but only a variation in the background. At a FAP=0.001 threshold, one measurement out of every thousand will exceed that threshold due to background statistical variations. A false alarm probability of less than 0.001 is considered adequate to indicate the presence of ^{64}Cu activity in our copper rods. Although the FAP threshold is in principle independent of possible ^{64}Cu activity, the sensors are set up to uniquely respond to ^{64}Cu and no other radioisotope will be made in the bulk of the copper rods by neutron, gamma-ray, or beta flux experienced in the OTSGs. By not selecting an extremely low FAP value as the threshold we are factoring in the controlled nature of the experiment.

3.4 SIGNIFICANCE OF MULTIPLE COUNTS

When making measurements looking for ^{64}Cu activity, several (typically four) independent measurements were made on the same set of six copper rods and often none of the measurements was greater than the single-count threshold established by the FAP<0.001 requirement. However, the individual measurements of the set were often all above the background value. Intuition indicates that a set of measurements all slightly above the background mean can be just as unlikely as one measurement above the single-count FAP threshold because a set of background measurements should be statistically scattered above and below the mean. Thus when one has several repeated, independent counts exceeding the mean background estimate by less than the single-count FAP threshold, one should consider a real cause for the increase and seek a means of calculating a false alarm probability for the set of measurements rather than only for single measurements.

3.4.1 A Search for a Method to Combine FAPS

A measure of the significance of the independent set of measurements (all above background) is desirable. One might wish to estimate the probability of obtaining a set with the observed or higher values as the product of the individual false alarm probabilities. However, just using the product of individual FAPs is generally incorrect since it does not take into account possible permutations of the measurement order.

3.4.1.1 Dice Rolling Example

Consider the analogous situation of finding the probability of rolling a 5-or-higher on several successive dice rolls. On one toss the probability of rolling a 5 or 6 is only 0.33, but the probability of a 5 or 6 on each of seven consecutive tosses drops to 0.00046, which would satisfy the $FAP<10^{-3}$ requirement. Using the probability product in this case would be correct, as long as all the tosses were greater than or equal to the 5-or-more threshold used. Note that one can not pick out the seven highest tosses from a greater number of tosses and use the product. However, if one wished to claim greater unlikelihood for his seven tosses by calculating the probability of three 5-or-greater and four 6-or-greater tosses corresponding to what was actually rolled on the seven tosses, one would need to be very careful.

When different values are obtained for independent tosses, care must be used to correct for possible equivalent permutations in the measurement order when calculating a combined probability. For example, consider the problem of rolling two dice as detailed in Table 3.1 below. One can toss two dice and get a 4 on one and a 5 on the other. One may then calculate a combined probability, P(4&5), of a 4-or-more on one die, $P(4 \leq n)=3/6$, and 5-or-more on the other, $P(5 \leq n)=2/6$. The product, $P(4 \leq n)*P(5 \leq n)$, is 6/36. However, when one examines the 36 equally probable possible two-dice outcomes found in Table 3.1 below, one finds that the 8 highlighted outcomes satisfy $(4 \leq n)$ on one and $(5 \leq n)$ on the other, not the 6 indicated by the product. The desired combined probability, P(4&5)=8/36, is less than 4-or-more on both, $[P(4 \leq n)]^2=9/36$, but greater than 5-or-more on both, $[P(5 \leq n)]^2=4/36$. Two correct methods of calculating the desired, combined probability P(4&5) exist

$$P(4\&5) = [P(4 \leq n)]^2-[P(4 \leq n<5)]^2 = [3/6]^2-[1/6]^2 = 8/36$$

$$P(4\&5) = [P(5 \leq n)]^2+2*[P(4 \leq n<5)]*[P(5 \leq n)]$$

$$= [2/6]^2+2*[1/6]*[2/6] = 8/36$$

where the 2 in the second term of the second method takes into account that either die could have had the smaller value, 4. As one can easily imagine, handling several tosses with unequal probability for each result can rapidly become a bookkeeping nightmare.

TABLE 3.1. Possible Outcomes for Rolling Two Dice

Die #1 ↓	Die #2 → 1	2	3	4	5	6
1	1+1=2	1+2=3	1+3=4	1+4=5	1+5=6	1+6=7
2	2+1=3	2+2=4	2+3=5	2+4=6	2+5=7	2+6=8
3	3+1=4	3+2=5	3+3=6	3+4=7	3+5=8	3+6=9
4	4+1=5	4+2=6	4+3=7	4+4=8	4+5=9	4+6=10
5	5+1=6	5+2=7	5+3=8	5+4=9	5+5=10	5+6=11
6	6+1=7	6+2=8	6+3=9	6+4=10	6+5=11	6+6=12

3.4.1.2 Poisson Counts Example

Another method one might wish to use for calculating the combined significance of independent counts would be to sum separately the actual counts and the expected background counts and pretend that it was really one longer count. Consider a realistic Poisson count example detailed in Table 3.2 below, with a background mean of 25. If two counts of 34 (25+9) occur, each with FAP=0.04978, the probability of two successive counts with 34-or-more is 2.478E-3 by squaring the FAP. If these two counts are grouped into a single 68 (50+18) count, one can calculate the FAP=8.879E-3 for the longer count. The combined count FAP is greater than the probability of two successive counts with 34-or-more since there are additional possible combinations of two counts which will produce the 18 extra counts. The FAP obtained by combining measurements into a single long count will generally be higher than necessary. The method of combining counts into one long count is a conservative method of calculating a FAP for a group of measurements.

The method used in the previous dice example will be referred to as the combined FAP method. This method, which takes into account permutations of measurement order, can be applied to the example of two Poisson counts. One of the combinations providing 18 extra counts divided between two individual counts is a count of 33 (25+8) with FAP=7.146E-2 and a count 35 (25+10) with FAP=3.384E-2. Combining these two by the same scheme used in the dice example, $[P(35 \le n)]^2 + 2*[P(33 \le n < 35)]*[P(35 \le n)]$ yields a combined FAP of 3.691E-3, which is greater than the product of the two FAPs (2.418E-3). Table 3.2 below lists several of the other possible combinations of dividing 18 extra counts between two measurements along with the combined FAP just calculated. The columns headed "Poisson FAP" are Poisson false alarm probabilities for a single count based on a mean of 25 counts.

TABLE 3.2. Possible Means of Getting 18 Extra Counts in Two Measurements Each with a Background Mean of 25 Counts

Count #1	Poisson FAP #1	Count #2	Poisson FAP #2	Combined FAP	Product of FAPs
34 (25+9)	0.04978	34 (25+9)	0.04978	0.002478	0.002478
35 (25+10)	0.03384	33 (25+8)	0.07146	0.003691	0.002418
36 (25+11)	0.02245	32 (25+7)	0.1001	0.003991	0.002247
37 (25+12)	0.01455	31 (25+6)	0.1367	0.003766	0.001989
38 (25+13)	0.009211	30 (25+5)	0.1821	0.003270	0.001677
39 (25+14)	0.005696	29 (25+4)	0.2366	0.002663	0.001348
40 (25+15)	0.003444	28 (25+3)	0.2998	0.002053	0.001033
41 (25+16)	0.002036	27 (25+2)	0.3706	0.001505	0.0007545
42 (25+17)	0.001177	26 (25+1)	0.4471	0.001051	0.0005262
43 (25+18)	0.000666	25 (25+0)	0.5266	0.000701	0.0003507
68 (50+18)	0.008879			sum = 0.025169	0.0148214

The combined FAP method gives realistic values for the combined FAP. When the two counts are equal the formula gives just the square of the individual FAPs as it should since no extra permutations of measurement order are possible. The combined FAPs are always less likely than the individual FAPs except in the last case, where one of the two measurements matched background. In that last case, the combined FAP is only slightly higher than the lowest individual FAP and the combined FAP would not have been higher if the second FAP were above one half. The combined FAP values are always higher than the product of individual FAPs, which do not consider permutations. They asymptotically approach twice the product as one of the individual FAPs become smaller. In all cases, it is less than half the combined-count FAP making the effort in calculation worthwhile. The sum of the combined FAPs is reasonably higher than the combined-count FAP since the individual combined FAPs overlap areas of probability space.

The scheme combining the counts into one long count results in a FAP which is always higher than the scheme directly combining FAPs. This is understandable in that two independent measurements provide more information than the single longer measurement. Using this extra information should result in a lower FAP value. Note there is a point of diminishing return in dividing counts up into several shorter counts due to loss of precision in very short counts. Also the combined-count FAP is higher than several of the individual Poisson FAPs which is not desired. There is no reason a second above mean measurement should increase the likelihood of the first count belonging to the background distribution.

The fact remains that a set of several successive marginally higher than background counts is just as unlikely as one significantly higher than background count. Note that combining the FAPs of several marginal increased counts can be used to convince someone that a real cause exists for those increases even though each increase is below the single-count threshold calculated for a given FAP. The problem as pointed out before is handling the bookkeeping nightmare associated with combining several counts.

3.4.2 Recipe for Directly Combining FAPS

The solution to the bookkeeping nightmare is using multinomial coefficients. The multinomial coefficient, $(N;n_1,n_2,n_3,\ldots,n_m)$ is the number of ways of putting $N=n_1+n_2+n_3+\ldots+n_m$ different objects into m different boxes with n_k objects in the k-th box for k=1 to m. The multinomial coefficients are defined as

$$(N;n_1,n_2,n_3,\ldots n_m) = \frac{N!}{n_1! * n_2! * n_3! * \ldots n_m!}$$

$$= N! \Big/ \prod_{i=1}^{m} (n_i!)$$

subject to $$N = n_1 + n_2 + n_3 + \ldots + n_m = \sum_{i=1}^{m} n_i$$

The values of the multinomial coefficients for small N values appear in the following table for convenience.

TABLE 3.3. Multinomial Coefficients

N	m	$(N;n_1,\ldots n_m)$	$(N;n_1,\ldots n_m)$	$(N;n_1,\ldots n_m)$
1	1	(1;1)=1		
2	1	(2;2)=1		
	2	(2;1,1)=2		
3	1	(3;3)=1		
	2	(3;1,2)=3		
	3	(3;1,1,1)=6		
4	1	(4;4)=1		
	2	(4;1,3)=4	(4;2,2)=6	
	3	(4;1,1,2)=12		
	4	(4;1,1,1,1)=24		
5	1	(5;5)=1		
	2	(5;1,4)=5	(5;2,3)=10	
	3	(5;1,1,3)=20	(5;1,2,2)=30	
	4	(5;1,1,1,2)=60		
	5	(5;1,1,1,1,1)=120		
6	1	(6;6)=1		
	2	(6;1,5)=6	(6;2,4)=15	(6;3,3)=20
	3	(6;1,1,4)=30	(6;1,2,3)=60	(6;2,2,2)=90
	4	(6;1,1,1,3)=120	(6;1,1,2,2)=180	
	5	(6;1,1,1,1,2)=360		
	6	(6;1,1,1,1,1,1)=720		

If N independent measurements produce a set of N FAPs, arrange them in descending order and label them FAP_i for i=1 to N. These can be used together with $FAP_{N+1}=0$ and $FAP_0=1$ to produce N+1 bands of probability, which we define as

$$P_i = FAP_i - FAP_{i+1} \qquad \text{for } i = 0 \text{ to } N$$

Note that $P_N=FAP_N$ and $P_0=1-FAP_1$. These N+1 probability bands $(P_0\ldots P_N)$ form a set which sum to 1 completely covering the probability space associated with each individual measurement. The N-th power of the summation is

$$\left[\sum_{i=0}^{N} P_i \right]^N = \sum_k c_k * [P_0]^{j0} * [P_1]^{j1} * \ldots * [P_{i=N}]^{jN} = 1$$

where the summation runs over all possible values of the j's subject to the constraint, j0+j1+j2+...+jN=N. The coefficients, c_k, are the multinomial coefficients corresponding to the non-zero j-values. This sum is over all the regions of the probability space combining the N independent measurements. Now to find the combined FAP for the set of N measurements simply remove from the sum those terms which do not satisfy the desired criteria. The criteria are

j0=0	no measurement in the probability band below the lowest FAP
j1≤1	a maximum of 1 measurement in band 1
j1+j2≤2	if none in band #1, then 2 measurements allowed in band #2
:	
:	
j1+j2+...+jN≤N	note jN≥1 is required

For reference, some of the combination formulas for the smaller values of N are listed below. To avoid running superscripts and subscripts together, notation will change. The subscripts on the P's will be combined into the symbol (P_1 becomes P1, P_2 becomes P2, etc.).

For N=2 the normalized probability product is

$$1 = P0^2 + P1^2 + P2^2 + 2*P0*P1 + 2*P0*P1 + 2*P1*P2$$

and the formula for the combined FAP is

$$FAP = P2^2 + 2*P1*P2$$

All the terms with P0 have been dropped since j0=0 is a criteria. Also the term with $P1^2$ has been omitted since j1≤1 is required. Note as general rules 1) no term with P0 is considered and 2) no term without a PN is kept.

For N=3 the normalized probability product is

$$
\begin{aligned}
1 = {} & P0^3 + P1^3 + P2^3 + P3^3 && \text{(3:3) terms} \\
& + 3*P0*P1^2 + 3*P0*P2^2 + 3*P0*P3^2 && \text{(3:1,2)s with P0} \\
& + 3*P0^2*P1 + 3*P0^2*P2 + 3*P0^2*P3 && \\
& + 3*P1*P2^2 + 3*P1*P3^2 && \text{(3:1,2)s with P1} \\
& + 3*P1^2*P2 + 3*P1^2*P3 && \\
& + 3*P2*P3^2 && \text{(3:1,2)s with P2} \\
& + 3*P2^2*P3 && \\
& + 6*P0*P1*P2 + 6*P0*P1*P3 + 6*P0*P2*P3 && \text{(3:1,1,1) terms} \\
& + 6*P1*P2*P3 &&
\end{aligned}
$$

and the formula for the N=3 combined FAP is

$$FAP = P3^3 + 3*P1*P3^2 + 3*P2*P3^2 + 3*P2^2*P3 + 6*P1*P2*P3$$

Note that all the terms with a P0 factor were dropped {$P0^3$, $3*P0*P1^2$, $3*P0*P2^2$, $3*P0*P3^2$, $3*P0^2*P1$, $3*P0^2*P2$, $3*P0^2*P3$, $6*P0*P1*P2$, $6*P0*P1*P3$, & $6*P0*P2*P3$}. Likewise, those without a P3 factor were dropped {$P1^3$, $P2^3$, $3*P1*P2^2$, & $3*P1^2*P2$} since $JN \geq 1$ is required. Also from the (3:1,2) terms, those with a $P1^2$ factor were dropped {$3*P1^2*P3$} since $j1 \leq 1$ is required.

For N=4 the combination formula is

$$
\begin{aligned}
FAP = {} & P4^4 && \text{(4:4) term with P4} \\
& + 4*P1*P4^3 + 4*P2*P4^3 + 4*P3*P4^3 && \text{(4:1,3) terms with P4} \\
& \qquad + 4*P3^3*P4 && \\
& + 6*P2^2*P4^2 + 6*P3^2*P4^2 && \text{(4:2,2) terms with P4} \\
& + 12*P1*P2*P4^2 + 12*P1*P3*P4^2 && \text{(4:1,1,2) terms with P1 \& P4} \\
& \qquad + 12*P1*P3^2*P4 && \\
& + 12*P2*P3*P4^2 && \text{(4:1,1,2) terms with P2 \& P4} \\
& + 12*P2*P3^2*P4 && \\
& + 12*P2^2*P3*P4 && \\
& + 24*P1*P2*P3*P4 && \text{(4:1,1,1,1) term}
\end{aligned}
$$

where the format has been selected for clarity in insuring selection of all the criteria satisfying terms. The (4:1,3) terms $4*P1^3*P4$ & $4*P2^3*P4$ are not allowed [$j1 \leq 1$ & $j1+j2 \leq 2$ criteria] and have been dropped. Likewise the (4:2,2) term $6*P1^2*P4^2$ term has been dropped [$j1 \leq 1$ criteria]. For the more complicated (4:1,1,2) set, first all the terms containing P1 & P4 were selected then the remaining terms with P2 & P4 but not P1 were selected. Several (4:1,1,2) terms were dropped for failure to meet criteria. As the problem becomes more complex, it is necessary to use a system to insure that all the terms satisfying the criteria are included.

For N=5 the combination formula is

$$
\begin{aligned}
FAP = {} & P5^5 && \text{(5:5) term with P5}\\
& +5*P1*P5^4 \;\; +5*P2*P5^4 \;\; +5*P3*P5^4 \;\; +5*P4*P5^4 && \text{(5:1,4)s with P5}\\
& \qquad\qquad\qquad\qquad\qquad\qquad +5*P4^4*P5 && \\
& +10*P2^2*P5^3 \;\; +10*P3^2*P5^3 \;\; +10*P4^2*P5^3 && \text{(5:2,3)s with P5}\\
& \qquad\qquad\quad +10*P3^3*P5^2 \;\; +10*P4^3*P5^2 && \\
& +20*P1*P2*P5^3 \;\; +20*P1*P3*P5^3 \;\; +20*P1*P4*P5^3 && \text{(5:1,1,3)s with P1}\\
& \qquad\qquad\qquad\qquad\qquad\qquad +20*P1*P4^3*P5 && \\
& +20*P2*P3*P5^3 \;\; +20*P2*P4*P5^3 && \text{(5:1,1,3)s with P2}\\
& \qquad\qquad\qquad\quad +20*P2*P4^3*P5 && \\
& +20*P3*P4*P5^3 && \text{(5:1,1,3)s with P3}\\
& +20*P3*P4^3*P5 && \\
& +30*P1*P3^2*P5^2 \;\; +30*P1*P4^2*P5^2 && \text{(5:1,2,2)s with P1}\\
& +30*P2*P3^2*P5^2 \;\; +30*P2*P4^2*P5^2 && \text{(5:1,2,2)s with P2}\\
& +30*P2^2*P3*P5^2 \;\; +30*P2^2*P4*P5^2 && \\
& \qquad\qquad\qquad\quad +30*P2^2*P4^2*P5 && \\
& +30*P3*P4^2*P5^2 && \text{(5:1,2,2)s with P3}\\
& +30*P3^2*P4*P5^2 && \\
& +30*P3^2*P4^2*P5 && \\
& +60*P1*P2*P3*P5^2 \;\; +60*P1*P2*P4*P5^2 \;\; +60*P1*P3*P4*P5^2 && \text{(5:1,1,1,2)s with P1}\\
& \qquad\qquad\qquad\qquad +60*P1*P2*P4^2*P5 \;\; +60*P1*P3*P4^2*P5 && \\
& \qquad\qquad\qquad\qquad\qquad\qquad\qquad\qquad +60*P1*P3^2*P4*P5 && \\
& +60*P2*P3*P4*P5^2 && \text{(5:1,1,1,2)s with P2}\\
& +60*P2*P3*P4^2*P5 && \\
& +60*P2*P3^2*P4*P5 && \\
& +60*P2^2*P3*P4*P5 && \\
& +120*P1*P2*P3*P4*P5 && \text{(5:1,1,1,1,1) term}
\end{aligned}
$$

where terms not satisfying the criteria have been dropped.

This recipe for combining FAPs from a set of measurements has tacitly assumed that the probability distributions were continuous. The scheme directly assumed that a possible measurement value corresponding to all the FAP values in the set existed for each probability distribution of the set. However, the Poisson distribution is discrete rather than continuous. The direct assumption is exactly true for the Poisson case when the background count estimate is the same for each measurement in the set. This would be true if the same sensor were sequentially used for the same counting period for each measurement in the set. Unfortunately, this is not our case. We will have to be willing to ignore the relatively small error in the combined FAP introduced by discrete count values.

3.4.3 Recipe Using the Weighted Mean

An alternative method to estimate the FAP for the combined data set would use the weighted mean, $\langle X \rangle$, of the flux measurements and associated error in that weighted mean, S_x. If the collection of independent flux measurements can be considered normally distributed, one can calculate the probability of measuring the value $\langle X \rangle$ or higher from a distribution with zero mean and S_x as the standard deviation. This probability is obtained by as the probability of $x = \langle X \rangle / S_x$ or higher in a N(0,1) table. A numerical approximation to this valid $0 \le x < \infty$ with an error less than 7.5E-8 is given[a]

$$Z(x) = \frac{1}{[2*\pi]^{\frac{1}{2}}} * e^{-x^2/2}$$

$$t = 1/(1+0.23164*x)$$

$$\begin{aligned} FAP = Q(x) = Z(x) *[\ & 0.31938153 * t - 0.356563782 * t^2 \\ & + 1.781477937 * t^3 - 1.821255978 * t^4 \\ & + 1.330274429 * t^5\ ] \end{aligned}$$

This numerical approximation allows ready calculation of the FAP associated with the weighted mean flux.

However, this method will overestimate the FAP since the error in the weighted mean, S_x, is larger than the similar error calculated under the null hypothesis of zero flux. The overestimate of the FAP will be greatest when the measurement is significantly above zero flux. One way to correct for the over estimation is to use the weighted mean error that one would have if all the counts corresponded to background counts. The error estimate for the net count was the square root of the sum of the raw count and the variance in the background estimate. This was transformed into the error estimate for the neutron flux associated with that count. Under the null hypothesis, the raw count would be the expected background count. The neutron flux error estimate for individual measurements (under the null hypothesis) is the transformation of the square root of the sum of the expected background count and the variance in the background estimate. One can then calculate an estimate of the error in the weighted mean flux corresponding to zero neutron flux.

---

[a] M. Abramowitz and I. Stegun. 1965. Handbook of Mathematical Functions. Dover, New York. eqns 26.2.1 and 26.2.17.

The FAP calculated from the weighted average scheme will be larger than that calculated from the combined FAP scheme since there will generally be combinations of measurements capable of producing the same weighted average that will not satisfy the combined FAP criteria.

Note that one could do the same with the mean of an unweighted or standard average.

3.5 MINIMUM DETECTABLE LEVEL

To avoid confusion, care must be used to define what is meant by minimum detectable level, MDL. The minimum detectable flux will produce a minimum detectable ^{64}Cu activity in the copper samples being counted. Adding the average value of the count due to the minimum detectable ^{64}Cu activity will just meet the significance criteria of FAP≤0.001 or whatever value is selected. If a measurement results in this minimum detectable flux, it will have associated with it an error estimate expressed in terms of the standard error. Now if one wishes to state that this detection implies that the flux was below a set limit with a given degree of confidence one must add some multiple of the standard error to the mean. This limit can be referred to as a less-than-value (LTV) or in the special case that the mean just satisfies the FAP requirement, this limit is referred to as the lower limit of detection (LLD)

As used here, the MDL would have a 50% detection probability since the mean of the distribution will satisfy the FAP criteria.

If one desires to be 95% sure that the flux is less than the LTV and the normal probability distribution is applicable, then the LTV is 1.645 times the standard error (se) above the MDL value. With these definitions one gets a continuous LTV as the measurement drops below meeting the FAP criteria. Mean values for measurements below the MDL are not statistically significant and should be expressed as being less than the LTV=MDL+a*se where "a" is declared.

A lower limit of detection (LLD) corresponding to 4.66-sigma increase above a background mean is an acceptable method for calculating the lower limit of detection according to regulatory guide 4.16 section 3.2 (Dec 85). The claim is that a lower limit sample has a 95% detection probability. An activity with a mean 4.66-sigma above background has a 95% detection probability only when the threshold for detection is 3-sigma above the background mean. The 3-sigma threshold is near the FAP=0.001 threshold (3.092-sigma from a normal distribution).

The derivation of the regulatory guide requirement of an LLD = 4.66-sigma does not completely fit our data. The derivation assumes that the background estimate is known only to the same precision as the activity measurement. This would be the case if the only background count were for the same duration as the activity measuring count. We spent considerable time taking multiple background counts so the background estimate is known to much greater precision. Also as stated in the regulatory guide, the 4.66-sigma requirement assumes that only a single measurement of the activity is made. Multiple measurements are not considered. Note four independent measurements of a sample with a background plus activity mean at the 3-sigma threshold will have a 94% ($1-0.5^4$) chance of detection (being above the 3-sigma threshold on at least one measurement), although a single measurement would have only a 50% chance of detection. Also the duration of the counting is not considered a parameter in the LLD derivation. Activity levels less than the 4.66-sigma LLD could be detected if one were willing to count longer. In the generalized sense, the regulatory guide is requiring that the true activity in a sample be less than a guaranteed value with 95% confidence.

For the case where a measurement can be easily made (considerable activity), one generally quotes a mean value (m) and standard error (se) for the activity level measured, as required in section 5.2 of the regulatory guide. Assuming a normal distribution, the activity has a 95% probability of being below m+1.645*se. The activity has a 99.9% probability of being below m+3.092*se. With this in mind, the weighted mean, <X>, and associated error, S_x, can also be used to estimate a guaranteed less than value, LTV.

$$LTV = \langle X \rangle + 1.645 * S_x \qquad \text{[95.0\% sure it is less than LTV]}$$

$$LTV = \langle X \rangle + 3.092 * S_x \qquad \text{[99.9\% sure it is less than LTV]}$$

As a continuous extension, an estimate of the lowest statistically significant LTV is found when <X>=MDL. Note that the MDL must be greater than zero since it is impossible to produce a negative ^{64}Cu activity in the rods.

Since statistical and other errors have all been propagated into the individual error estimates, s_i, going into the weighted average, the error associated with the weighted mean, S_x, is the correct error estimate to use while finding the minimum detectable level of the weighted average neutron flux. In a manner similar to that used to calculate the significance of the weighted mean, the error, S_x, is simply multiplied by the corresponding sigma level for the desired MDL of the flux. This yields MDL = 3.092 * S_x, (consistent with FAP=0.001 and DP=0.5). The corresponding LTV is 4.737 * S_x, which is 1.645 * S_x higher than the MDL.

For each independent measurement (count), we calculate the minimum detectable level [MDL] of flux given the decay time and count period. This flux level will change as the induced ^{64}Cu decays away and will depend on 1) the number of coupons counted at one time and 2) the length of the counting period. The MDL will decrease inversely with the number of coupons counted at one time. The MDL would decrease inversely as the square root of the counting time if the ^{64}Cu decay during the counting time is not significant. The length of the counting period has two practical limits. It is pointless to count for more than one half life since the lower signal-to-noise data in the second half life compromises the better data in the first half life. Also several groups of coupons must be counted during the first half life, so the time during the first half life must be divided between several counts to obtain the activity levels in the various coupon groups.

The typical coincidence count rate for an empty sensor cave is 0.55 c/m. For a typical count duration of 3000 seconds (50 minutes) using 6 coupons, the MDL neutron flux is 0.036 n/(s*cm^2) if the count started 2 hours after the activation ended. The corresponding MDL for a count of 6 coupons lasting one half life (12.7 hr) is 0.011 n/(s*cm^2), which does not scale with the square root of time from the 50-minute count [0.009 n/(sec*cm^2)] due to ^{64}Cu decay during the counting period. If the minimum LTV or LLD is desired, multiply by 4.737/3.092=1.532 for typical flux levels of 0.055 and 0.017 n/(s*cm^2) respectively. The weighted average flux of all the measurements for both sensor systems allow MDL levels to approach 0.007 n/(s*cm^2) for a given string. This is reasonable since two simultaneous 12.7-hour measurements would have an MDL of 0.011/$\sqrt{2}$ or 0.008 n/(sec*cm^2) and typically the coupons were counted for 12 hours following removal from the OTSG. This 0.007 n/(sec*cm^2) value corresponds to the value of the total background neutron flux levels over land at sea level. One must quickly point out that the flux measured by ^{64}Cu activation is more of a thermal flux and the background cosmic-ray flux is not a thermal flux, but a harder flux containing a large percentage of fast neutrons. The thermal portion of the background cosmic-ray flux can be as little as 7% of the total flux in the absence of moderating materials in the immediate environment. With the boron loaded water in the OTSG, the thermal portion of the background neutron flux could be small.

Table 3.4 lists minimum detectable fluxes for each of the two sensors used during the two measurements (A and B OTSGs).

TABLE 3.4. Minimum Detectable Neutron Fluxes

Item	A-OTSG SENSOR-A	A-OTSG SENSOR-B	B-OTSG SENSOR-A	B-OTSG SENSOR-B	UNITS
Background rate	0.548	0.545	0.594	0.535	c/m
MINIMUM DETECTABLE FLUX [FAP=0.001, DP=0.5]					
50-minute count @ t=2 hour	0.0360	0.0362	0.0373	0.0352	n/(s*cm^2)
12.7-hour count @ t=2 hour	0.0113	0.0113	0.0118	0.0110	n/(s*cm^2)

If the background coincidence counting rate had corresponded to the 0.12 c/m obtained with more sophisticated cosmic cancellation and increased shielding (i.e., the Packard-5 system at PNL), it may have been possible to detect the thermal portion of the background neutron flux.

3.6 COMMENTS

The neutron flux value is a more realistic and fundamental result from the copper coupon counting than kilograms of fuel. The conversion of copper activity to flux is relatively straightforward and not subject to modeling uncertainties. However, the conversion to kilograms of fuel in the OTSG is very much subject to modeling uncertainty. The neutron flux value is a useful intermediate step in the quest for the amount of fuel.

The calculations required to convert the raw coincidence count data into a neutron flux estimate with associated error and significance estimates were done with a BASIC program, FLUX4.BAS. The BASIC program, COMB.BAS, was used to construct combined measurement values from the individual flux measurements. The listings of these programs are provided as an appendix.

4.0 BACKGROUND MEASUREMENTS

4.1 INTRODUCTION

Two coincidence counting systems were used at GPU/TMI-2 to count ^{64}Cu activity following neutron irradiation in the OTSGs. The following is a tabulation of the background coincidence rates which were measured during the experiment. The background measurements have been divided into two sets 1) A-OTSG background measurements and 2) B-OTSG background measurements. Some of the measurements from the time period between the A-OTSG and B-OTSG measurements occur in both background data sets. The rationale for the separation is to minimize the affect of any slight drift in background counting rate over time. Thus background measurements would not influence measurements a long time previously or following.

Some of the A-OTSG background rates were taken with an empty cave and some with 7 copper coupons, which were not activated in the OTSG. There is no statistical difference between the count rates for these two types of background measurements. The average rate for the 7 background copper coupons in the caves was 0.506 cpm for the A sensor pair and 0.522 cpm for the B sensor pair. This was slightly less than the average for the data set but within the error bars. One might reasonably expect a slightly higher background count with the copper coupons present due to ^{64}Cu induced by cosmic-ray neutrons.

The count rates for events in the energy windows around the 511-keV photopeak were also measured. For the A sensor the individual photopeak rates were typically nearly the same at about A1=46 cpm & A2=46 cpm yielding a chance coincidence background rate of 0.0043 cpm. For the B sensor the individual photopeak rates were typically B1=44 cpm & B2=112 cpm yielding a chance coincidence background rate of 0.010 cpm. These chance coincidence rates are well below the actual coincidence background rates of 0.55 cpm. Thus the background coincidence rate is dominated by real events which produce these coincidences. The physical sources of these coincidence counts include 1) cosmic-ray interactions clipping a corner of each crystal, 2) cosmic-ray induced positrons, 3) ringing pulses following huge cosmic-ray events, and 4) positron-emitting contamination in the sensor system.

The average background rate was calculated by two methods. The first combined all background counts into one large count and determined the average rate by dividing the total count by the duration. The error in the mean for this method is given by the square root of the count divided by the duration. The second method used each background count as an independent measurement and determined the mean and standard deviation of the collection of measurements. The standard error in the mean of this collection is given by the standard deviation divided by the square root of the number of samples. The first method provided a more accurate estimate of the mean since the duration of each sample is correctly accounted for. The second method provided additional insight into any non-Poisson variations in the background due to systematic changes during the measurement period. These systematic changes may have been due to diurnal cycles in the cosmic-ray rate, drift in the NaI(Tl) gain with temperature, or drift in the 511-keV energy window. However, no evidence for such effects was seen.

4.2 BACKGROUND DATA FOR A-OTSG MEASUREMENTS

Table 4.1 below lists the raw background measurements and the resulting estimates of the background rate for the first measurement set (A-OTSG). The background coincidence rate of 0.548 c/m for the A sensor pair and 0.545 c/m for the B sensor pair will be used for the A-OTSG measurements. As one can see, the two calculation methods used to determine the background estimate yielded results which agree within acceptable limits. The agreement in the standard error in the means indicates that the background was well behaved and Poisson during the measurement period.

TABLE 4.1. Background Rates for OTSG-A Measurements

DATE	TIME	DURATION (sec)	COUNTS-A (cts)	A-COUNT RATE (c/m)	COUNTS-B (cts)	B-COUNT RATE (c/m)	Comment
9-14-8B	0940	3,000	22	0.440	25	0.500	7 coupons
	1030	27,600	203	0.441	257	0.552	7 coupons
	2040	3,000	22	0.440	25	0.500	Empty cave
	2130	30,000	291	0.582	264	0.528	Empty cave
9-15-88	0907	3,000	32	0.640	28	0.560	Empty cave
	1001	3,000	35	0.700	29	0.580	Empty cave
9-16-88	0640	7,600	72	0.568	75	0.592	Empty cave
	0841	5,400	52	0.578	60	0.666	Empty cave
	1049	4,200	40	0.571	39	0.557	Empty cave
9-17-88	0800	16,000	154	0.578	169	0.634	Empty cave
	1230	15,100	135	0.536	155	0.616	Empty cave
	1655	12,100	93	0.461	103	0.511	Empty cave
	2025	14,000	138	0.591	129	0.553	Empty cave
9-18-88	0021	20,500	235	0.688	202	0.591	Empty cave
	0620	19,500	161	0.495	184	0.566	7 coupons
	1145	16,600	142	0.513	129	0.466	7 coupons
	1630	18,300	154	0.505	160	0.525	7 coupons
	2138	32,600	309	0.569	268	0.493	7 coupons
9-19-88	1045	3,000	28	0.560	28	0.560	Empty cave
	2240	31,800	310	0.585	293	0.553	Empty cave
9-20-88	1017	2,200	15	0.409	22	0.600	Empty cave
	2305	33,900	318	0.563	278	0.492	Empty cave
9-21-88	1030	9,600	90	0.563	91	0.569	Empty cave
	1315	15,000	146	0.584	136	0.544	Empty cave
	1730	16,600	139	0.502	164	0.593	Empty cave
	2210	33,300	292	0.526	291	0.524	Empty cave
totals		396,900	3628	14.188	3604	14.425	n=26
average			0.548 c/m	0.546	0.545 c/m	0.555	
standard error				0.072		0.047	
standard error in mean			0.009 c/m	0.014	0.010 c/m	0.009	

4.3 BACKGROUND DATA FOR B-OTSG MEASUREMENTS

Table 4.2 below lists the raw background measurements and the resulting estimate of the background rate for the second measurement set (B-OTSG). The background coincidence rate of 0.594 c/m for the A sensor pair and 0.535 c/m for the B sensor pair will be used for the B-OTSG measurements.

TABLE 4.2. Background Rates for OTSG-B Measurements

DATE	TIME	DURATION (sec)	COUNTS-A (cts)	A-COUNT RATE (c/m)	COUNTS-B (cts)	B-COUNT RATE (c/m)	Comment
9-21-88	1030	9,600	90	0.563	91	0.560	Empty cave
	1315	15,000	146	0.584	136	0.544	Empty cave
	1730	16,600	139	0.502	164	0.593	Empty cave
	2210	33,300	292	0.526	291	0.524	Empty cave
9-22-88	0924	10,800	105	0.583	89	0.494	Empty cave
	1230	17,700	180	0.610	157	0.532	Empty cave
	1730	50,000	480	0.576	463	0.556	Empty cave
9-23-88	1244	10,800	112	0.622	118	0.656	Empty cave
9-24-88	0920	10,080	101	0.601	78	0.464	Empty cave
	1210	18,600	179	0.577	151	0.487	Empty cave
	1725	52,200	522	0.600	472	0.543	Empty cave
9-25-88	0800	21,120	240	0.682	167	0.474	Empty cave
	1400	60,000	638	0.638	547	0.547	Empty cave
9-26-88	0930	3,600	46	0.767	21	0.350	Empty cave
	1036	3,900	34	0.523	29	0.446	Empty cave
	1140	3,600	34	0.567	34	0.567	Empty cave
	1245	3,600	29	0.483	31	0.517	Empty cave
	1350	4,300	44	0.614	34	0.474	Empty cave
totals		344,800	3411	10.618	3073	9.328	
average			.594 c/m	0.590	.535 c/m	0.518	n=18
standard error				0.066		0.066	
standard error in mean			.010 c/m	0.016	.010 c/m	0.016	

5.0 COPPER ACTIVATION MEASUREMENTS

5.1 INTRODUCTION

Two coincidence counting systems were used at GPU/TMI-2 to count ^{64}Cu activity following exposure of copper coupons in the OTSGs. This chapter contains a tabulation of the coincidence measurements.

The copper coupons were 1/4-inch diameter rods, 4 inches long with the ends machined to a convex surface to allow the string to bend slightly. Each coupon weighed 28.60 grams and was labeled with an alphabetic character identifying the string followed by a sequence number (1 to 18). Eighteen PNL supplied copper coupons were placed in a 1/2-inch diameter polypropylene tube for emplacement in the bottom of the OTSG by insertion from the manway at the top of the OTSG through a steam tube. The coupons were loaded sequentially in the polypropylene tube with coupon #1 at the bullet end (front) of the string and coupon #18 at the rear of the string. The 18 copper coupons were preceded and followed in the string by small GM counters to measure the local gamma-ray dose as the string was inserted. Additional copper rods were used as ballast behind the rear GM counter to insure that the string would not float up from the bottom surface of the OTSG bowl or J-leg.

The coincidence measurements are labeled by a three character-identifier. The first character is the character used to in labeling the string (A to K), the second character identifies the sensor (A or B) used for that measurement, and the third character is the sequence number of the measurement. Both A and B sensor systems were used for each measurement. For example, measurements JA1 and JB1 would be simultaneous and of the same duration.

5.2 GENERAL TABLE EXPLANATION

The coincidence count data is presented in a single table for each string. This section explains the meanings of the table entries.

5.2.1 Column Headings

The first column headed "LABEL" contains the measurement label (string, sensor, and measurement sequence number). The second column identifies the coupons used to make that measurement (string and coupon number).

The column headed "BKG" contains the expected background count for that measurement. This value is the average background rate times the duration of the count. The column headed "CNT" contains the actual total number of coincidence counts for that measurement. These two columns contain the basic observations (duration of count and actual count). The expected background count is listed rather than the duration to allow easy visual recognition that a count was or wasn't above the expected background and by how much.

The column headed "N-FLUX" contains the estimated neutron flux in the region of the coupons while they were in the OTSG. The estimated flux would produce the necessary ^{64}Cu activity at the time of the measurement to yield the actual count for that measurement. The column headed "NF-ERR" contains the standard error in the estimated neutron flux (N-FLUX). The column headed "%-ERR" contains the N-FLUX standard error estimate expressed as a percentage. These columns contain the basic results of the measurements.

The column headed "FAP" contains the statistical significance of the measurement. The column headed "MDL-FLX" contains the minimum detectable flux corresponding to satisfying the FAP=0.001 criteria with a 50% detection probability. To convert the MDL-FLUX into a less-than-value (LTV), which is also referred to as a lower limit of detection (LLD) multiply by 4.737/3.092 or 1.532. To convert a significant measurement (N-FLUX > MDL-FLX) into a less-than-value (LTV), add 1.645 times the NF-ERR value to the N-FLUX value. These LTVs have a 95% probability of being greater than the actual mean value of the neutron flux. The column headed "ZF-ERR" contains the standard error estimate in the N-FLUX if only background counts occurred. The ZF-ERR is used to find the MDL. These columns contain statistically useful information.

5.2.2 Table Organization

The counts of the same coupons are grouped together and offset by a blank line. These counts of the same coupons are combined by the various averaging schemes and the results listed below the independent counts. At the end of each table is the average of all the measurements on the string coupons.

The individual measurements which where significant at FAP=0.001 and DP=0.5 have been highlighted by bold type in these tables.

The "Data Set Title" identifies the location of the string during the measurement using the standard TMI labels. The "File" identifies the computer data file containing the data.

5.2.3 Combined Results

The individual measurements are combined primarily by the weighted averaging scheme. The weighted average is the averaging scheme commonly used to combine data of unequal precision. However, other schemes are also listed in these tables to show that the results of the weighted averaging scheme are reasonable. Since it is generally easy to become confused by statistical techniques and then to have no confidence in the results, every effort has been made to show that the results of combining the many independent measurements are reasonable.

Since each coupon sees a neutron flux produced in a very limited region surrounding it, this combined average can be viewed as a spatial averaging of the flux in the J-leg or bowl. In the conversion to a fuel estimate the average flux will be multiplied by the debris area, which is exactly equivalent to determining a flux and then a fuel estimate for each coupon area and summing up the fuel estimates. The difference is that the minimum detection level for the total string is far less than that for each individual coupon.

The entries on the "Weighted Average" line are 1) N-FLUX = the weighted average of the individual neutron flux estimates in the group, 2) NF-ERR = the error estimate associated with the weighted average flux estimate, 3) %-ERR = error estimate in percentage, 4) FAP = the false alarm probability calculated from a normal distribution N(0,1) using the mean [N-FLUX] divided by the error estimate [NF-ERR] as the deviation from zero, and 5) MDL-FLUX = the minimum detectable flux which is 3.092 times the error estimate [NF-ERR]. The second line of weighted average information titled "using Wtd ZF-ERR" contains the FAP and MDL values obtained using the ZF-ERR value as the standard deviation rather than the NF-ERR value. The ZF-ERR value is more correct since it is based on the null hypothesis of no activity.

The "Normal Average" line is included to double check that the weighted average line is reasonable. The entries are 1) N-FLUX = mean of the independent N-FLUX values and 2) NF-ERR = the standard error of that mean calculated from the standard deviation of the set of independent flux values. This standard error of the mean can be smaller than the standard error in the weighted average if the measurements are closely grouped.

The "Long Count" line combines the independent counts into one long count. The entries included 1) BKG = the expected background count and 2) CNT = the count for the long combined count. It is not possible to calculate a flux estimate from the long count to compare to the correctly calculated weighted mean estimate due to the ^{64}Cu decay during the measurement period. However, it is possible to calculate a percent error and FAP from the long count, which serve to check the values found with the weighted average scheme. The excellent agreement of the "Long Count" and "Weighted Average" %-ERR values inspires confidence that the weighted average estimates are very reasonable combinations of the individual measurements.

The "Combined FAP" is the probability of obtaining another set of independent measurements with the same-or-lower FAP values from coupons with the same ^{64}Cu activity. The combined FAP limits the significance of the set and serves as a lower limit for the weighted average FAP. A value for the combined FAP greater than 0.001 indicates that the measurement set can not satisfy the significance criteria and no statistical scheme could produce a significant non-zero estimate of the neutron flux from that data.

5.3 DATA

This section contains the experimental data (counts) and the results of the data reduction (neutron flux).

The bullet end of the J-string (coupons J01-J06) definitely saw a statistically significant neutron flux. One of the individual measurements was statistically significant. This region corresponded to the highest gamma-ray dose reading on the small GM sensors. The weighted mean neutron flux seen by the forward third of the string was 0.038(9) n/(sec*cm²). Note the error bars for the two individual measurements overlap the error bars for the weighted average showing statistical agreement. The LTV for the weighted average is 0.053 n/(sec*cm²).

The JB4 measurement at 0.062(16) is higher than the LTV since there is a 5% chance that the mean of the neutron flux distribution would exceed the LTV and a higher probability that a single measurement would exceed that value. One can not neglect the lower count rate during the longer JB8 measurement and claim that the JB4 measurement corresponds to the correct mean. Although the JB4 measurement is more significant in that it is less likely to be due to a fluctuation within the background distribution, it is less precise in that it has a greater error bar.

Late in the measurement cycle, an attempt was made to localize the ^{64}Cu activity in less than the 6-coupon group. It appears that the neutron flux in the region of coupons J01-J03 was greater than in the region of J04-J06. Since the ^{64}Cu had decayed significantly when these measurements were made and the ^{64}Cu activity in the 3-coupon group would be approximately half that in a 6-coupon group, it is reasonable that a significant individual count was not obtained.

The remaining two-thirds of the string saw a neutron flux of less than a minimum detectable level, based upon the results of the 6-coupon groups. The neutron flux corresponding to J07-J12 was less than LLD=0.023 n/(sec*cm²). The neutron flux corresponding to J13-J18 was less than LLD=0.020 n/(sec*cm²). The GM dose rate over this back two-thirds of the string was about 1/5th of that in the first third. If the neutron flux follows the gamma-ray dose, one would have expected a neutron flux on the order of 0.007 n/(sec*cm²). This would be below the MDL and thus no detectable neutron flux could be expected in the rear two-thirds.

TABLE 5.1. J-String Measurements in the J-leg, A-OTSG/RCP-2A

Data Set Title: A-OTSG/RCP-2A File: A:J.DAT

LABEL	COUPONS	BKG	CNT	N-FLUX n/s/cm²	NF-ERR n/s/cm²	%-ERR	FAP	MDL-FLX n/s/cm²	ZF-ERR n/s/cm²
JB4	J01-J06	27.25	55	0.0621	0.0166	27%	0.000001951	0.0420	0.0117
JB8	J01-J06	81.75	106	0.0262	0.0112	43%	0.005694522	0.0327	0.0099
Weighted Average				0.0374	0.0093	25%	0.000027723	0.0287	0.0070
using Wtd ZF-ERR							0.000000039	0.0215	
Normal Average				0.0442	0.0180	41%	0.006954405	0.0555	
Long Count		109.00	161			25%	0.000001916		
Combined FAP							0.000000022		
JB2	J07-J12	27.25	37	0.0197	0.0124	63%	0.043250150	0.0379	0.0106
JB3	J07-J12	27.25	28	0.0016	0.0113	709%	0.468184725	0.0398	0.0111
JA8	J07-J12	82.20	87	0.0052	0.0104	199%	0.312604445	0.0334	0.0101
JA9	J07-J12	155.27	159	0.0026	0.0093	354%	0.392837406	0.0286	0.0092
Weighted Average				0.0062	0.0053	86%	0.121583731	0.0165	0.0050
using Wtd ZF-ERR							0.104809479	0.0153	
Normal Average				0.0073	0.0042	58%	0.042012741	0.0130	
Long Count		291.97	311			86%	0.139421659		
Combined FAP							0.012316013		
JA3	J13-J18	27.40	25	-0.0051	0.0108	210%	0.702519377	0.0396	0.0112
JA4	J13-J18	27.40	34	0.0148	0.0132	89%	0.123728036	0.0417	0.0118
JB6	J13-J18	27.25	27	-0.0006	0.0130	2088%	0.544636620	0.0468	0.0131
JB7	J13-J18	90.83	99	0.0067	0.0083	124%	0.208752689	0.0266	0.0080
JB9	J13-J18	154.42	158	0.0025	0.0090	360%	0.397167599	0.0285	0.0089
Weighted Average				0.0035	0.0046	131%	0.222441331	0.0142	0.0043
using Wtd ZF-ERR							0.207309538	0.0133	
Normal Average				0.0037	0.0034	93%	0.140008650	0.0105	
Long Count		327.30	343			131%	0.199630258		
Combined FAP							0.050397173		
JA6	J19-J25	27.40	29	0.0032	0.0107	339%	0.404962722	0.0368	0.0104
JA7	J19-J25	91.33	99	0.0050	0.0067	133%	0.224333819	0.0207	0.0064
Weighted Average				0.0045	0.0057	126%	0.214407899	0.0176	0.0051
using Wtd ZF-ERR							0.191253397	0.0159	
Normal Average				0.0041	0.0009	22%	0.000002615	0.0028	
Long Count		118.73	128			126%	0.208863895		
Combined FAP							0.131368011		
JA1	J02-J08	16.44	27	0.0270	0.0134	50%	0.010315355	0.0372	0.0104
JB1	J11-J17	16.35	22	0.0162	0.0134	83%	0.104957788	0.0419	0.0116
JA2	J13-J15	27.40	31	0.0135	0.0210	156%	0.269957887	0.0695	0.0197
JA5	J01-J03	27.40	36	0.0374	0.0264	70%	0.065544216	0.0810	0.0230
JB5	J04-J06	27.25	29	0.0076	0.0235	309%	0.393780648	0.0815	0.0228
Wtd Ave for string				0.0092	0.0027	29%	0.000283112	0.0082	0.0024
using Wtd ZF-ERR							0.000056000	0.0073	
Norm Ave for string				0.0136	0.0039	28%	0.000209788	0.0120	

An extra 7-coupon group was counted for this J-leg (J19-J25). This group was farther back from the bullet end than the other 3 groups and behind the rear GM counter. These coupons saw a neutron flux less than LLD=0.024 n/(sec*cm^2).

Although the weighted mean flux estimates for the three rear groups were all below the MDL flux for the groups, the values were remarkably similar and within the error estimates for the weighted means.

When the entire set of measurements is combined by a weighted average to estimate the average flux in the 2A/J-leg, the estimate is 0.009(3) n/(sec*cm^2). This value is larger than the corresponding MDL value of 0.007 n/(sec*cm^2). The LTV corresponding to this weighted average of the J-string is 0.014 n/(sec*cm^2). Combining the data from all the coupon measurements is reasonable since the various coupon locations result is a spatial average of the flux in the J-leg. The normal average of the all the measurements is 0.014(4), which is not much higher and is in statistical agreement [overlapping error bars] with the weighted average. This lends credence to the weighted average value. The other viable alternative to determine a more conservative LTV for overall average flux in the J-leg is to average the LTV for the four groups to obtain 0.030 n/(sec*cm^2). However, this alternative scheme does not take into account the added precision available to the weighted average scheme and statistical practice justifies using the lower weighted average value.

TABLE 5.2. E-String Measurements in the J-leg, A-OTSG/RCP-1A

Data Set Title: A-OTSG/RCP-1A File: A:E.DAT

LABEL	COUPONS	BKG	CNT	N-FLUX n/s/cm²	NF-ERR n/s/cm²	%-ERR	FAP	MDL-FLX n/s/cm²	ZF-ERR n/s/cm²
EB3	E01-E06	27.25	41	0.0259	0.0121	47%	0.008299532	0.0354	0.0099
EA4	E01-E06	27.40	36	0.0171	0.0120	70%	0.065544216	0.0371	0.0105
EA5	E01-E06	76.72	101	0.0189	0.0080	42%	0.004548799	0.0228	0.0070
EB7	E01-E06	73.58	89	0.0160	0.0099	62%	0.044143880	0.0295	0.0090
Weighted Average				0.0190	0.0050	26%	0.000075370	0.0155	0.0043
using Wtd ZF-ERR							0.000003908	0.0132	
Normal Average				0.0195	0.0022	11%	0.000000000	0.0069	
Long Count		204.95	267			26%	0.000019071		
Combined FAP							0.000000738		
EA1	E07-E12	27.40	45	0.0301	0.0115	39%	0.001252918	0.0318	0.0090
EB4	E07-E12	27.25	34	0.0134	0.0117	87%	0.117746772	0.0373	0.0104
EB6	**E07-E12**	**68.67**	**100**	**0.0308**	**0.0099**	**33%**	**0.000230148**	**0.0278**	**0.0082**
EA7	E07-E12	73.98	71	-0.0031	0.0090	290%	0.651090608	0.0301	0.0091
Weighted Average				0.0161	0.0052	32%	0.000937115	0.0160	0.0045
using Wtd ZF-ERR							0.000155544	0.0138	
Normal Average				0.0178	0.0080	45%	0.013454107	0.0249	
Long Count		197.30	250			32%	0.000172063		
Combined FAP							0.000000085		
EA2	E13-E18	27.40	39	0.0209	0.0113	54%	0.021315538	0.0335	0.0095
EA3	E13-E18	27.40	31	0.0068	0.0106	156%	0.269957887	0.0351	0.0100
EB5	E13-E18	76.30	93	0.0130	0.0076	59%	0.034941311	0.0231	0.0069
EA6	E13-E18	69.05	82	0.0128	0.0091	71%	0.069959795	0.0275	0.0084
Weighted Average				0.0131	0.0047	36%	0.002463836	0.0144	0.0039
using Wtd ZF-ERR							0.000393806	0.0121	
Normal Average				0.0134	0.0029	22%	0.000001869	0.0089	
Long Count		200.15	245			36%	0.001182897		
Combined FAP							0.000086024		
EB2	E01-E03	27.25	29	0.0058	0.0179	309%	0.393780648	0.0621	0.0174
EB1	E04-E06	27.25	31	0.0118	0.0176	149%	0.260361097	0.0590	0.0165
Wtd Ave for string				0.0156	0.0028	18%	0.000000011	0.0086	0.0017
using Wtd ZF-ERR							0.000000000	0.0052	
Norm Ave for string				0.0157	0.0025	16%	0.000000000	0.0078	

The weighted average neutron flux in the forward third of string E (E01-E06) was 0.019(5) n/(sec*cm²) and is statistically significant. Although none of the four independent counts of the forward third was individually significant (FAP=0.001), the combined set of four measurements was statistically significant no matter how the significance is calculated. The normal average produced a lower error estimate and FAP than the weighted average since the individual flux measures closely agree. The LTV for the weighted average is 0.027 n/(sec*cm²). Since a higher flux level was expected in the 1A/J-leg than in the 2A/J-leg, an initial effort was made to use 3-coupon groups. The

3-coupon groups did not produce individually significant counts, but gave some indication that coupons E04-E06 had more activity than E01-E03. This observation was in agreement with the in-situ GM measurements.

There was one individually significant measurement in the central portion of the E-string (E07-E12) and one marginally significant measurement. The weighted average neutron flux was 0.016(5) n/(sec*cm²). The weighted average flux was lower than the forward third since one of the counts was lower than background. Statistically there are no grounds for discarding that one count since it is within reasonable limits of the weighted mean. This region did not correspond to the highest gamma-ray dose reading on the small GM sensors. In fact the actual section corresponded to the lowest gamma-ray dose. The LTV for the weighted average is 0.025 n/(sec*cm²).

The neutron flux was lowest in the rear third of the E-string (E13-E18). The weighted average flux was 0.013(5) n/(sec*cm²). Although the corresponding weighted average FAP=0.0024 calculated with the NF-ERR value was not quite 0.001 significant, the FAP=0.0004 is significant when calculated with the ZF-ERR value under the null hypothesis. The LTV for the weighted average is 0.021 n/(sec*cm²) which is not much different than the 0.022 n/(sec*cm²) LLD based on the NF-ERR. One should note that the combined FAP was significant. For agreement with the GM measurements, the rear third should have had more ^{64}Cu activity than the central third.

Since the weighted average flux estimates for each region are relatively close in value, one can easily feel comfortable using a spatial average for the entire J-leg. The weighted average for the set of measurements in the 1A/J-leg is 0.016(3) n/(sec*cm²), which is in agreement with the weighted mean values for each of the three regions. The weighted average is statistically significant and can be accepted. The LTV for the weighted average is 0.020 n/(sec*cm²).

The weighted average for the 1A/J-leg (0.016) was higher than the weighted average for the 2A/J-leg (0.009). This is consistent with expectation and the greater significance of measurements in the 1A/J-leg.

TABLE 5.3. H-String Measurements in the Bowl of A-OTSG

Data Set Title: A-OTSG/BOWL ZW QUADRANT File: A:H.DAT

LABEL	COUPONS	BKG	CNT	N-FLUX n/s/cm²	NF-ERR n/s/cm²	%-ERR	FAP	MDL-FLX n/s/cm²	ZF-ERR n/s/cm²
HA2	H01-H06	27.40	22	-0.0100	0.0088	88%	0.872529102	0.0343	0.0097
HA3	H01-H06	27.40	26	-0.0027	0.0099	368%	0.631160238	0.0359	0.0102
HA4	H01-H06	127.87	124	-0.0018	0.0055	300%	0.645632085	0.0175	0.0055
HB6	H01-H06	168.95	161	-0.0046	0.0076	164%	0.739787703	0.0250	0.0078
Weighted Average				-0.0040	0.0037	92%	0.862420802	0.0114	0.0035
using Wtd ZF-ERR							0.876572425	0.0107	
Normal Average				-0.0048	0.0018	38%	0.995333097	0.0057	
Long Count		351.62	333			92%	0.846167206		
Combined FAP							0.501645982		
HB5	H07-H12	136.25	149	0.0070	0.0069	98%	0.147230907	0.0214	0.0066
HA6	H07-H12	169.88	176	0.0036	0.0081	228%	0.329400775	0.0251	0.0080
Weighted Average				0.0056	0.0053	94%	0.144462486	0.0162	0.0048
using Wtd ZF-ERR							0.122928218	0.0148	
Normal Average				0.0053	0.0017	32%	0.000911572	0.0053	
Long Count		306.13	325			94%	0.147063823		
Combined FAP							0.075319014		
HB2	H13-H18	27.25	30	0.0051	0.0101	200%	0.323866473	0.0345	0.0096
HB3	H13-H18	27.25	32	0.0091	0.0109	120%	0.204537823	0.0361	0.0101
HB4	H13-H18	127.17	146	0.0088	0.0058	66%	0.054431751	0.0173	0.0054
HA5	H13-H18	137.00	133	-0.0022	0.0067	301%	0.645151767	0.0215	0.0067
Weighted Average				0.0048	0.0038	78%	0.100287544	0.0117	0.0033
using Wtd ZF-ERR							0.073532753	0.0103	
Normal Average				0.0052	0.0026	51%	0.023967966	0.0081	
Long Count		318.67	341			78%	0.111509948		
Combined FAP							0.013784481		
HA1	H04-H09	27.40	23	-0.0077	0.0085	110%	0.824657604	0.0325	0.0092
HB1	H10-H15	27.25	24	-0.0057	0.0086	152%	0.758970818	0.0327	0.0091
Wtd Ave for string				0.0003	0.0022	739%	0.446189262	0.0068	0.0013
using Wtd ZF-ERR							0.409191569	0.0040	
Norm Ave for string				-0.0001	0.0019	2073%	0.519241621	0.0059	

TABLE 5.4. G-String Measurements in the Bowl of A-OTSG

Data Set Title: A-OTSG/BOWL-ZY QUADRANT File: A:G.DAT

LABEL	COUPONS	BKG	CNT	N-FLUX n/s/cm²	NF-ERR n/s/cm²	%-ERR	FAP	MDL-FLX n/s/cm²	ZF-ERR n/s/cm²
GB2	G01-G07	72.67	70	-0.0021	0.0065	318%	0.638516915	0.0218	0.0066
GA3	G01-G07	71.24	71	-0.0002	0.0069	3592%	0.527111989	0.0230	0.0069
GB4	G01-G06	81.75	92	0.0103	0.0098	95%	0.140957988	0.0304	0.0092
Weighted Average				0.0010	0.0043	440%	0.410104709	0.0132	0.0038
using Wtd ZF-ERR							0.400391588	0.0119	
Normal Average				0.0027	0.0039	145%	0.244598835	0.0119	
Long Count		225.66	233			440%	0.321285949		
Combined FAP							0.131899372		
GA1	G10-G16	65.76	60	-0.0035	0.0048	138%	0.777501604	0.0166	0.0051
GB1	G03-G09	65.40	76	0.0073	0.0060	83%	0.107706428	0.0189	0.0056
GA4	G07-G12	82.20	88	0.0058	0.0097	166%	0.275363471	0.0310	0.0094
Weighted Average				0.0014	0.0035	254%	0.347024924	0.0108	0.0033
using Wtd ZF-ERR							0.337998815	0.0102	
Normal Average				0.0032	0.0034	106%	0.171732056	0.0104	
Long Count		213.36	224			254%	0.241923066		
Combined FAP							0.088047102		
GA2	G12-G18	73.07	78	0.0034	0.0062	183%	0.297063405	0.0199	0.0060
GB3	G12-G18	70.85	75	0.0037	0.0078	211%	0.326480113	0.0252	0.0076
Weighted Average				0.0035	0.0049	138%	0.234392435	0.0150	0.0046
using Wtd ZF-ERR							0.220103967	0.0141	
Normal Average				0.0036	0.0002	4%	0.000000000	0.0005	
Long Count		143.92	153			138%	0.235137304		
Combined FAP							0.105723932		
Wtd Ave for string				0.0018	0.0024	134%	0.228409186	0.0073	0.0011
using Wtd ZF-ERR							0.057390238	0.0034	
Norm Ave for string				0.0031	0.0017	55%	0.033326561	0.0052	

There was no indication of ^{64}Cu activity in any of the A/BOWL coupons for either string (H or G). None of the combined FAP values for the various coupon groups are significant at even the 0.01 level, which implies that no statistical combinations could provide a significant flux estimate other than zero. The weighted averages for both complete strings [H at 0.000(2) n/(sec*cm²) and G at 0.002(2) n/(sec*cm²)] are consistent with zero and less than the corresponding MDL values [0.007 n/(sec*cm²) using NF-ERR or 0.004 using ZF-ERR]. The average neutron flux in the bowl is less than the LLD=0.011 n/s/cm² using NF-ERR or 0.006 n/(sec*cm²) using ZF-ERR.

None of the individual measurements was significant at even a marginal FAP level. Note, however, that out of the 20 individual A/BOWL measurements, one was significant at the 1/20 level which shows 1) the FAPs are accurate and 2) there was really nothing to see.

TABLE 5.5. F-String Measurements in the J-leg, B-OTSG/RCP-2B

Data Set Title: B-OTSG/RCP-2B File: A:F.DAT

LABEL	COUPONS	BKG	CNT	N-FLUX n/s/cm²	NF-ERR n/s/cm²	%-ERR	FAP	MDL-FLX n/s/cm²	ZF-ERR n/s/cm²
FA2	F01-F06	35.64	40	0.0087	0.0128	147%	0.253691571	0.0407	0.0121
FB4	F01-F06	64.20	83	0.0217	0.0108	50%	0.013673132	0.0309	0.0095
FA5	F01-F06	71.87	91	0.0246	0.0126	51%	0.016584667	0.0362	0.0112
Weighted Average				0.0188	0.0069	37%	0.003253501	0.0213	0.0060
using Wtd ZF-ERR							0.000908183	0.0186	
Normal Average				0.0183	0.0049	27%	0.000088441	0.0151	
Long Count		171.71	214			37%	0.001022451		
Combined FAP							0.000194157		
FB3	F07-F12	32.10	38	0.0125	0.0132	106%	0.169325266	0.0421	0.0122
FA4	F07-F12	71.28	84	0.0147	0.0108	74%	0.076648295	0.0332	0.0100
FB6	F07-F12	64.20	94	0.0434	0.0144	34%	0.000290178	0.0390	0.0120
FA9	F07-F12	213.84	256	0.0283	0.0115	41%	0.002766621	0.0316	0.0105
Weighted Average				0.0233	0.0061	26%	0.000072069	0.0189	0.0054
using Wtd ZF-ERR							0.000009244	0.0168	
Normal Average				0.0247	0.0071	29%	0.000266504	0.0221	
Long Count		381.42	472			26%	0.000004196		
Combined FAP							0.000000061		
FB2	F13-F18	32.10	48	0.0317	0.0140	44%	0.005190545	0.0397	0.0115
FA3	F13-F18	35.64	54	0.0390	0.0157	41%	0.002484868	0.0432	0.0128
FB5	F13-F18	64.74	80	0.0196	0.0117	60%	0.036624051	0.0350	0.0106
FA6	F13-F18	71.28	100	0.0419	0.0148	36%	0.000760619	0.0419	0.0126
FB9	F13-F18	192.60	242	0.0331	0.0111	34%	0.000337090	0.0304	0.0101
Weighted Average				0.0317	0.0059	18%	0.000000032	0.0181	0.0049
using Wtd ZF-ERR							0.000000000	0.0151	
Normal Average				0.0331	0.0039	12%	0.000000000	0.0119	
Long Count		396.36	524			18%	0.000000001		
Combined FAP							0.000000000		
FA7	F13-F15	29.70	33	0.0231	0.0407	176%	0.295896016	0.1353	0.0386
FB8	F13-F15	26.75	31	0.0313	0.0414	132%	0.229448183	0.1343	0.0385
Weighted Average				0.0271	0.0290	107%	0.174955814	0.0897	0.0269
using Wtd ZF-ERR							0.156324935	0.0831	
Normal Average				0.0272	0.0041	15%	0.000000000	0.0127	
Long Count		56.45	64			107%	0.173214626		
Combined FAP							0.083139144		
FB7	F16-F18	26.75	20	-0.0472	0.0318	67%	0.924987590	0.1277	0.0366
FA8	F16-F18	29.70	29	-0.0052	0.0402	778%	0.575651419	0.1424	0.0406
Weighted Average				-0.0310	0.0249	80%	0.893313527	0.0771	0.0268
using Wtd ZF-ERR							0.876931703	0.0827	
Normal Average				-0.0262	0.0210	80%	0.893914614	0.0649	
Long Count		56.45	49			80%	0.855824170		
Combined FAP							0.733566284		

TABLE 5.5 con't. F-String Measurements in the J-leg, B-OTSG/RCP-2B

Data Set Title: B-OTSG/RCP-2B File: A:F.DAT

LABEL	COUPONS	BKG	CNT	N-FLUX n/s/cm²	NF-ERR n/s/cm²	%-ERR	FAP	MDL-FLX n/s/cm²	ZF-ERR n/s/cm²
FA1	F03-F09	29.70	38	0.0149	0.0111	75%	0.080148336	0.0346	0.0099
FB1	**F10-F16**	**26.75**	**47**	**0.0407**	**0.0139**	**34%**	**0.000248867**	**0.0367**	**0.0105**
FA6x	**F13-F18**	**40.59**	**69**	**0.0711**	**0.0213**	**30%**	**0.000030612**	**0.0561**	**0.0162**
FB6x	**F07-F12**	**36.56**	**63**	**0.0660**	**0.0203**	**31%**	**0.000044786**	**0.0535**	**0.0153**
Wtd Ave for string				0.0242	0.0033	14%	0.000000000	0.0101	0.0010
using Wtd ZF-ERR							0.000000000	0.0032	
Norm Ave for string				0.0209	0.0050	24%	0.000015559	0.0155	

We were certainly able to detect a measurable neutron flux in the 2B/J-leg. Four of the individual measurements meet the FAP=0.001 significance criteria.

The flux measurements in the front third of the string [F01-F06] is significant for three of the four measures of significance listed in the table when three successive over background measurements are combined. The weighted average flux estimate is 0.019(7) n/(sec*cm²) and the corresponding LTV is 0.030 n/(sec*cm²). The NF-ERR based MDL-FLX could also be used to determine a LLD of 0.033 n/(sec*cm²) if the significance based on the ZF-ERR is not acceptable.

The middle third of the string [F07-F12] does have a measurable neutron flux. A weighted average neutron flux was 0.023(6) n/s/cm² with a corresponding LTV of 0.033 n/(sec*cm²). The FB6 measurement is statistically significant by itself. The FB6x measurement, listed at the end of the table, corresponds to the count halfway through the 2-hour FB6 measurement. Therefore, these two measurements are not statistically independent. The FB6x measurement is the most statistically significant measurement of the string. The "x" measurements were not included in the weighted average of the set.

The rear third of the string [F13-F18] also has a measurable neutron flux of 0.032(6) n/s/cm². The LTV for the weighted average is 0.041 n/(sec*cm²). The FA6x measurement also corresponds to the count half way through the 2-hour FA6 measurement. The rear third was slightly more active than the middle third when looking at the measurements as a group. Note that counts FA7 and FB8 seem to indicate that most of the ^{64}Cu activity was in coupons F13-F15 rather than in F16-F18, since coupons F16-F18 produced lower than background counts in FB7 and FB8. Although not statistically significant, the flux estimates for coupons F16-F18 agreed reasonably well with the activity estimate in the rear third.

The count FB1 [F10-F16] was also individually significant and supports the significant activity in the rear two-thirds of the string.

Taken as a whole the weighted average neutron flux in the 2B/J-leg was 0.024(3) n/s/cm^2. This is well above the corresponding minimum detectable flux level and is statistically very significant. The LTV for the weighted average is 0.030 n/(sec*cm^2). Again the measurements in all three regions are relatively close in value and support using an average over the entire J-leg.

TABLE 5.6. I-String Measurements in the J-leg, B-OTSG/RCP-1B

Data Set Title: B-OTSG/RCP-1B File: A:I.DAT

LABEL	COUPONS	BKG	CNT	N-FLUX n/s/cm^2	NF-ERR n/s/cm^2	%-ERR	FAP	MDL-FLX n/s/cm^2	ZF-ERR n/s/cm^2
IA2	I01-I06	29.70	37	0.0178	0.0149	84%	0.108639193	0.0469	0.0134
IB3	I01-I06	64.20	67	0.0031	0.0093	300%	0.379772780	0.0295	0.0091
IA5	I01-I06	89.10	101	0.0140	0.0122	87%	0.114959276	0.0376	0.0115
IA6	I01-I06	99.00	99	0.0000	0.0126	--%	0.513365802	0.0405	0.0126
Weighted Average				0.0072	0.0059	81%	0.109002269	0.0181	0.0055
using Wtd ZF-ERR							0.093164823	0.0169	
Normal Average				0.0087	0.0043	49%	0.020314560	0.0132	
Long Count		282.00	304			81%	0.101271420		
Combined FAP							0.013212949		
IA3	I07-I12	71.28	73	0.0019	0.0097	509%	0.434940150	0.0317	0.0096
IB5	I07-I12	80.25	81	0.0009	0.0109	1242%	0.481450097	0.0349	0.0109
IB6	I07-I12	89.17	82	-0.0088	0.0116	132%	0.789889822	0.0390	0.0120
Weighted Average				-0.0014	0.0061	432%	0.591443631	0.0190	0.0058
using Wtd ZF-ERR							0.596089316	0.0181	
Normal Average				-0.0020	0.0034	171%	0.721104781	0.0106	
Long Count		240.70	236			432%	0.627636729		
Combined FAP							0.323978692		
IB2	I13-I18	26.75	23	-0.0091	0.0118	130%	0.791531733	0.0443	0.0127
IA4	I13-I18	95.04	92	-0.0029	0.0094	327%	0.636148581	0.0312	0.0095
Weighted Average				-0.0053	0.0074	139%	0.764795435	0.0227	0.0072
using Wtd ZF-ERR							0.769464012	0.0223	
Normal Average				-0.0060	0.0031	52%	0.973534577	0.0096	
Long Count		121.79	115			139%	0.742819270		
Combined FAP							0.602378607		
IA1	I07-I09	29.70	39	0.0396	0.0269	68%	0.057880482	0.0821	0.0234
IB1	I10-I12	26.75	22	-0.0202	0.0202	100%	0.845604572	0.0775	0.0222
IB4	I04-I09	85.60	96	0.0098	0.0096	98%	0.142749165	0.0296	0.0091
Wtd Ave for string				0.0021	0.0034	160%	0.266375271	0.0104	0.0010
using Wtd ZF-ERR							0.016667969	0.0030	
Norm Ave for string				0.0038	0.0044	115%	0.192926360	0.0137	

There appears to be only a minimal neutron flux present in the 1B/J-leg. None of the individual measurements was significantly different from background in a statistical sense. The collection of measurements taken as a group can not be made statistically significant. The weighted average flux in the J-leg is 0.002(3) which is consistent with zero and is not a statistically significant increase from zero. It is also less than the corresponding MDL values [0.010 n/(sec*cm^2) using NF-ERR or 0.003 using ZF-ERR]. Therefore, the average neutron flux in this J-leg is less than the LLD=0.016 n/s/cm^2 using NF-ERR or 0.005 n/(sec*cm^2) using ZF-ERR. Based on the I01-I06 combined FAP, there appears to be a slight ^{64}Cu activity in the forward third of the string, which makes the LLD calculated with NF-ERR higher than that calculated with ZF-ERR.

The lack of neutron flux in this J-leg is a somewhat unexpected result, since flux in the 2B/J-leg was considerably larger.

TABLE 5.7. C-String Measurements in Bowl of B-OTSG

Data Set Title: B-OTSG/BOWL ZW QUADRANT File: A:C.DAT

LABEL	COUPONS	BKG	CNT	N-FLUX n/s/cm^2	NF-ERR n/s/cm^2	%-ERR	FAP	MDL-FLX n/s/cm^2	ZF-ERR n/s/cm^2
CB5	C01-C06	65.81	78	0.0120	0.0089	74%	0.077531147	0.0268	0.0082
CA7	C01-C06	60.39	54	-0.0097	0.0115	118%	0.811221791	0.0406	0.0121
CA8	C01-C06	181.17	190	0.0054	0.0089	166%	0.265488032	0.0268	0.0087
Weighted Average				0.0045	0.0055	124%	0.209602034	0.0171	0.0051
using Wtd ZF-ERR							0.191724301	0.0158	
Normal Average				0.0026	0.0064	250%	0.344710846	0.0199	
Long Count		307.37	322			124%	0.209161168		
Combined FAP							0.069630146		
CA6	C07-C12	81.18	86	0.0044	0.0086	198%	0.310769795	0.0269	0.0084
CB7	C07-C12	54.39	57	0.D040	0.0118	296%	0.379590191	0.0390	0.0115
CB8	C07-C12	163.18	146	-0.0105	0.0080	76%	0.918724702	0.0255	0.0083
Weighted Average				-0.0021	0.0052	251%	0.654656667	0.0162	0.0050
using Wtd ZF-ERR							0.660932809	0.0156	
Normal Average				-0.0007	0.0049	700%	0.556782879	0.0152	
Long Count		298.75	289			251%	0.721317095		
Combined FAP							0.279757857		
CA5	C13-C18	73.06	76	0.0029	0.0088	304%	0.380913304	0.0286	0.0087
CB6	C13-C18	73.12	67	-0.0055	0.0076	139%	0.778193534	0.0260	0.0080
Weighted Average				-0.0019	0.0058	301%	0.630169820	0.0178	0.0057
using Wtd ZF-ERR							0.632274617	0.0175	
Normal Average				-0.0013	0.0042	323%	0.621538369	0.0130	
Long Count		146.18	143			301%	0.61478271D		
Combined FAP							0.447753608		

TABLE 5.7 con't. C-String Measurements in Bowl of B-OTSG

Data Set Title: B-OTSG/BOWL ZW QUADRANT File: A:C.DAT

LABEL COUPONS		BKG	CNT	N-FLUX n/s/cm²	NF-ERR n/s/cm²	%-ERR	FAP	MDL-FLX n/s/cm²	ZF-ERR n/s/cm²
CA3	C01-C07	29.70	32	0.0036	0.0089	248%	0.360385437	0.0302	0.0086
CB4	C01-C07	67.77	67	-0.0006	0.0064	1100%	0.553301808	0.0213	0.0064
Weighted Average				0.0008	0.0052	625%	0.436424871	0.0161	0.0048
using Wtd ZF-ERR							0.431229784	0.0148	
Normal Average				0.0015	0.0021	140%	0.237525184	0.0065	
Long Count		97.47	99			625%	0.451838643		
Combined FAP							0.268926173		
CA1	C03-C09	19.80	16	-0.0081	0.0087	106%	0.832897145	0.0347	0.0096
CA2	C03-C09	29.70	31	0.0019	0.0084	433%	0.429868992	0.0287	0.0082
Weighted Average				-0.0029	0.0060	207%	0.685796280	0.0187	0.0060
using Wtd ZF-ERR							0.687623565	0.0185	
Normal Average				-0.0031	0.0050	161%	0.732371153	0.0155	
Long Count		49.50	47			207%	0.657931770		
Combined FAP							0.531285942		
CB1	C10-C16	17.83	15	-0.0068	0.0094	138%	0.780807052	0.0364	0.0102
CB2	C10-C16	26.75	19	-0.0129	0.0074	57%	0.951089945	0.0304	0.0087
Weighted Average				-0.0106	0.0058	55%	0.965406895	0.0180	0.0062
using Wtd ZF-ERR							0.954619063	0.0193	
Normal Average				-0.0099	0.0031	31%	0.999379920	0.0094	
Long Count		44.58	34			55%	0.956392610		
Combined FAP							0.875575781		
CB3	C12-C18	26.75	30	0.0057	0.0097	170%	0.289520755	0.0320	0.0092
CA4	C12-C18	75.24	78	0.0019	0.0061	328%	0.390350283	0.0194	0.0060
Weighted Average				0.0030	0.0052	173%	0.282140005	0.0160	0.0050
using Wtd ZF-ERR							0.275487489	0.0154	
Normal Average				0.0038	0.0019	50%	0.022750035	0.0059	
Long Count		101.99	108			173%	0.288705981		
Combined FAP							0.142206743		
Wtd Ave for string				-0.0010	0.0021	202%	0.689427284	0.0064	0.0009
using Wtd ZF-ERR							0.877619069	0.0027	
Norm Ave for string				-0.0008	0.0018	234%	0.665766874	0.0056	

There appears to be only a minimal neutron flux present in the bowl of the B-OTSG. None of the individual measurements was significantly different than zero. The collection taken as a whole is not statistically significant. The weighted average flux in the bowl is -0.001(2), which is consistent with zero and not significant. It is also less than the corresponding MDL values [0.006 n/(sec*cm²) using NF-ERR or 0.003 using ZF-ERR]. The average neutron flux in the bowl is less than the LLD=0.010 n/s/cm² using NF-ERR or 0.004 n/(sec*cm²) using ZF-ERR.

5.4 SUMMARY

A summary of the neutron flux measurements in the steam generators appears in Table 5.8. These values are less than the preliminary neutron flux estimates, which used a lower sensor efficiency value and were not based on the weighted means.

The weighted average values for each area (J-leg or bowl) should be used since these contain the most experimental information. Additionally the counting errors have been properly propagated for these estimates. The weighted values of all the independent measurements in each string are highlighted in bold print. The flux estimates for subregions in these areas are less precise but are included where significant to provide insight as to relative magnitudes of the flux. The higher flux estimates in these subregions should not be used to increase the amount of neutron flux in the weighted average values.

In Table 5.8, the column labeled "LTV" is a less-than-value where the mean of the neutron flux has a 95% chance of being below that value and only a 5% chance of being above it. The column labeled "FAP" contains the probability that no neutron flux was observed and any net count can be explained by statistical variations in background only.

The number of measurements made for each estimate is included in the table. Some of the measurements were for longer duration than others in an attempt to obtain better counting statistics. Fewer measurements were made on the G-string, but all were for longer duration since the activity was expected to be low.

Note that the LTV approaches the 0.007 n/(sec*cm^2) background neutron flux over land value. However, one must remember that the flux measured was the thermal capture component of the total flux. The detection system was not able to statistically distinguish counts using rods with ^{64}Cu activity induced by the cosmic background neutron flux from counts with no rods in the detector system. The thermal component of the background neutron flux is less than 1/4 the total background neutron flux, so the experimentally observed MDL was not limited by exposure of the coupons to background neutron flux after removal from the OTSGs. Also the calculated MDL value for two simultaneous 12 hour counts of 6 coupons approached this 0.007 n/(sec*cm^2) value. Therefore, these limits are reasonable.

TABLE 5.8. Summary for OTSG Measurements

LOCATION	COUPONS	NEUTRON FLUX n/(aec*cm²)	LTV n/(sec*cm²)	FAP zf-err	Number of Measurements
1A/J-leg	E01-E18 Wtd Ave	0.016(3)	0.020	0.0000	14
	E01-E06	0.019(5)	0.027	0.0000	4
	E07-E12	0.016(5)	0.025	0.0002	4
	E13-E18	0.013(5)	0.021	0.0004	4
2A/J-leg	J01-J25 Wtd Ave	0.009(3)	0.014	0.0000	18
	J01-J06	0.038(9)	0.053	0.0000	2
	J07-J12	--	0.023	0.10	4
	J13-J18	--	0.020	0.21	5
	J19-J25	--	0.024	0.19	2
A/BOWL ZW	H01-H18 Wtd Ave	--	0.006	0.41	12
A/BOWL ZY	G01-G18 Wtd Ave	--	0.006	0.057	8
1B/J-leg	I01-I18 Wtd Ave	--	0.005	0.017	12
2B/J-leg	F01-F25 Wtd Ave	0.024(3)	0.030	0.0000	18
	F01-F06	0.019(7)	0.030	0.0009	3
	F07-F12	0.023(6)	0.033	0.0000	4
	F13-F18	0.032(6)	0.041	0.0000	5
B/BOWL ZW	C01-C18 Wtd Ave	--	0.004	0.88	16

In the bowls and the 1B/J-leg where a significant non-zero estimate of the neutron flux was not obtained, no additional measurements following our last measurements would have enabled us to make a significant estimate, since the combined FAP values were high and the ^{64}Cu activity was decaying away. Likewise, no different arrangement of the measurements during the time we counted coupons would have enabled us to make a significant estimate. The high FAP associated with the H and C strings indicates that a neutron flux measuring system would have to be at least a factor of 20 more sensitive than the one used to make a statistically significant measurement.

6.0 RESIDUAL FUEL ESTIMATES

6.1 INTRODUCTION

This chapter outlines several calculation models that facilitate estimating the quantity of residual fuel in the OTSG sections. The estimated fuel weight is based on the neutron flux, Φ, measured by copper coupon activation measurements. There are several important parameters for obtaining an accurate estimate of the quantity of fuel in the debris.

More than one model will be presented to show the sensitivity of fuel estimates to either the parameter values or the calculation model used. The goal is to find a calculation scheme that is relatively independent of the unknown parameters. The several possible models can be useful in setting upper and lower limits on the amount of fuel present. Some relatively simple models are examined to provide insight into the problem. Often a simple calculation can provide a good deal of reasonably accurate information.

Two generic models exist 1) neutron production models and 2) neutron capture models.

A neutron production model examines the expected neutron flux from a diffuse volume source when assumptions are made about the distribution of the source. The source parameters needed for this model include 1) density of the debris, 2) depth of the debris, 3) area covered by debris, 4) fraction of fuel in the debris, and 5) total amount of debris. These parameters are not well known, but an estimate of the values can be constructed from the video examination accompanying each string emplacement.

A neutron capture model ignores the details of the source distribution but estimates the neutron source strength based on knowing where the neutrons are captured or leave the system. The parameters needed for this model are the attenuation lengths of fission neutrons in both the borated water and the steel walls. In most cases one would start with the neutron production model, but in this case, most of the neutrons will be captured in known materials distributed in a known manner. Therefore neutron capture models will be addressed first.

A third modeling scheme would use complex computer codes for neutron transport to provide a an accurate flux/fuel conversion. The drawbacks of a transport code are that one needs to input specific geometry and can not easily see the affects of approximations and changes in various parameter values. To obtain an accurate result with a Monte Carlo transport code, a very large number of neutrons must be tracked to produce a statistically significant number of captures in the relatively small copper coupon.

6.2 GENERAL INFORMATION

This section will provide reference data required by any physical model of the debris in the OTSG.

6.2.1 Geometry

The J-leg sections containing debris are nominally 6-foot long, 28-inch diameter pipes with a 2-inch thick steel wall. A 6-foot (72 inch = 182.88 cm) length is selected as the length seen by the eighteen 4-inch long copper coupons. The inner diameter of each J-leg is 28.791 inches (73.129 cm) and the outer diameter is 33.5 inches (85.09 cm). The wall thickness is 2.625 inches (6.67 cm) with the inner 0.375 inches (0.95 cm) a 304 stainless steel cladding and the outer 2.25 inches (5.72 cm) carbon steel. The internal volume of the J-leg is filled with water with a boron concentration of 5720 ppm by weight.

The internal volume of a 73.129-cm diameter, 182.88-cm long cylinder is $V = \pi * r^2 * L = 7.681E5\ cm^3$. The internal volume of a 85.09-cm diameter, 182.88-cm long cylinder is $1.040E6\ cm^3$. The volume of the 6-foot section of pipe wall is $2.718E5\ cm^3$. The inner surface area of the pipe is $A = 2*\pi*r*L = 4.202E4\ cm^2$. We will assume that debris is located only on the bottom quarter of the pipe which means that the debris is distributed across $1.1E4\ cm^2$. If a quantitative evaluation of the video records in the J-legs supports a different debris area, all the estimates will scale linearly to the new area.

The OTSG bowl sections containing debris are nominally 10-foot diameter hemispheres, with a 6-inch thick steel wall. The hemisphere inner radius is 59.34 inches (150.7 cm) and the outer radius is 66.03 inches (167.7 cm) and the wall thickness is 6.69 inches (16.99 cm). As in the J-legs, there is 0.375 inches (0.95 cm) of 304 stainless steel cladding on 6.31 inches (16.03 cm) of carbon steel.

The surface area of a hemisphere of radius 150.7 cm is $A = 2*\pi*r^2 = 1.427E5\ cm^2$. If the debris is limited to a portion sampled by the 6-foot long string, the half-angle of the spherical section is 0.6 radians = 34.4 degrees. The surface area within the cone subtended by the half-angle θ is $A = 2*\pi*r^2*[1-\cos(\theta)] = 2.492E4\ cm^2$.

The video scans perhaps indicate that the area covered by debris is less than the above areas. However, without the quantitative photo interpertation, a smaller area estimate is not reasonably available. All the fuel estimates in this section scale linearly with the debris area and should be adjusted to more realistic area estimates should they become available.

6.2.2 Source Strength

The source strength of the TMI-2 fuel is reported by B. R. Brosey[a] to be 190 neutrons/second per kilogram of uranium dioxide. We will use this as the neutron source strength.

6.2.3 Number Densities and Material Compositions

Nearly all models will require the number density of the various materials found in the OTSGs. The number density values are listed in Table 6.1 below. To avoid later confusion, "N_g" is the weight based number density in atoms/gram, "N_c" is the volume based number density in atoms/cm^3, and "N" is the total number of atoms of a given material in the problem. The weight based atomic number density, N_g, of a element equals Avogadro's number, 6.022045E23 number/mole (#/mole) divided by the gram atomic weight (g/mole). For mixtures of elements in a material (alloys or compounds) the atomic number density of the element can be multiplied by the percent by weight of that element in the mixture. To obtain the volume based number density, N_c (#/cm^3), multiply N_g (#/g) by the specific gravity (g/cm^3).

The water in the OTSG contains 5720 ppm boron. In Table 6.1, the number of boron atoms in 5.72 mg of boron has been added to the number of hydrogen and oxygen atoms in a gram of water (the added weight of the boric acid is neglected). The isotopic abundance of ^{63}Cu atoms is 69.2%. The compositions of carbon steel and 304 stainless are selected as the averages of the ranges given for each element.

[a] B. R. Brosey. January 1988. GPU Nuclear Planning Study, Reactor Vessel Post Defueling Special Nuclear Materials Survey. TPO/TMI 189, Table 1 page 21.

TABLE 6.1. Number Density of Various Materials in OTSG

Material	MolecularWt or AtomicWt	N_g element or molecule #/g	N_g in mix (incl %wt) atoms/g	Specific gravity g/cm^3	N_c atoms/cm^3
Boron	10.81	5.5708E22		2.34	1.3036E23
Water H_2O	18.01528	3.3427E22		1.000	
11.19% H	1.00794	5.9746E23	6.6855E22		6.6855E22
88.81% O	15.9994	3.7639E22	3.3427E22		3.3427E22
H_2O +5 ppt B	# of B	in 5.00 mg =	2.7854E20		2.7854E20
H_2O +5.72 ppt B	# of B	in 5.72 mg =	3.1865E20		3.1865E20
Copper	63.546	9.4767E21	9.4767E21	8.96	8.4911E22
69.2% ^{63}Cu			6.5579E21		5.8758E22
30.8% ^{65}Cu			2.9188E21		2.6153E22
Fe	55.847	1.0783E22	1.0783E22	7.874	8.49E22
Carbon Steel				7.75	
99.1% Fe	55.847	1.0783E22	1.07E22		8.28E22
1.0% Mn	54.938	1.0962E22	1.10E20		8.50E20
0.9% C	12.011	5.0138E22	4.51E20		3.50E21
304 Stainless				8.02	
69% Fe	55.847	1.0783E22	7.44E21		5.97E22
19% Cr	51.996	1.1582E22	2.20E21		1.76E22
9% Ni	58.69	1.0261E22	9.23E20		7.41E21
2% Mn	54.938	1.0962E22	2.19E20		1.76E21
1% Si	28.086	2.1441E22	2.14E20		1.72E21
0.08% C	12.011	5.0138E22	4.01E19		3.22E20
0.04% P	30.974	1.9442E22	7.78E18		6.24E19
0.03% S	32.06	1.8784E22	5.64E18		4.52E19
Polypropylene $(CH_2)_x$				0.90	
85.63% C	12.011	5.0138E22	4.293E22		3.86E22
14.37% H	1.00794	5.9746E23	8.586E22		7.73E22
U	238.0289	2.5300E21	2.5300E21	19.05	4.82E22
UO_2	270.03	2.2301E21		10.96	
U 1	238.0289	2.5300E21	2.230E21		2.44E22
O 2	15.9994	3.7639E22	4.460E21		4.89E22

6.2.4 Neutron Cross Sections and Mean Free Paths

In addition to number density values, cross section and mean free path data is required by the models. Table 6.2 follows and lists useful cross section and mean free path data for the materials found in the OTSG. The table lists the cross sections in barns (1 barn = 1E-24 cm²). The mean free path

(MFP) is the average distance a neutron travels between collisions of a given type. The MFP is given by

$$MFP\ (cm) = 1\ /\ [\ \sigma(cm^2)\ *\ N_c(\#/cm^3)\ ]$$

where "σ" is the cross section in cm^2 and "N_c" is the volume based atomic number density in cm^{-3}. The cross section data in the table are of three types 1) thermal neutron capture cross section, 2) thermal neutron scattering cross section, and 3) total cross section at the 2 MeV peak of the fission spectrum. The $\sigma * N_c$ products within a material add, so the MFP characteristic of the mixed material is given by

$$1/MFP = \sum [1/MFP_i]$$

Values for mixed materials are also found in the Table 6.2.

The total neutron cross section at 2 MeV is primarily a scattering cross section. A 2-MeV neutron in the peak of the fission spectra will travel about 5 cm in the water before colliding with a hydrogen atom. This collision will cause the 2-MeV neutron to lose half of its energy on the average. The neutron will continue to collide with other hydrogen atoms until it has lost most of its energy (i.e., it becomes a thermal neutron). The MFP will be shorter after each collision as the neutron loses energy. After several (20-25) collisions the neutron will have approximately thermal energy (1/40 eV). Since the MFP (total) for the boron in the water is much larger than for hydrogen, the added boron will have very little affect on the moderation process.

Once a neutron has been thermalized, the thermal neutron scattering and capture cross sections apply. The thermalized neutron will not lose energy (on the average) during subsequent collisions since the hydrogen atoms also have thermal energy in the material. For thermal neutrons, without boron added to the water, the MFP to capture in hydrogen is 61.5 times larger than the MFP to the next hydrogen scatter. Thus a thermalized neutron will scatter many times before being captured without the added boron.

TABLE 6.2. Neutron Cross Section and Mean Free Path Data

Material	Number Density #/cc	Thermal Capture σ(c) barns	Thermal Capture MFP(c) cm	Thermal Scatter σ(s) barns	Thermal Scatter MFP(s) cm	2 MeV Total σ(t) barns	2 MeV Total MFP(t) cm
Borated Water H_2O							
H	6.69E22	0.3326(7)	44.9	20.491(14)	0.73	2.9	5.2
O	3.34E22	0.00019(2)	1.6E5	3.761(6)	7.96	1.5	20.
B 5.00 ppt	2.79E20	767.(8)	4.67	4.27(7)	839.	1.8	2000
B 5.72 ppt	3.19E20	767.(8)	4.09	4.27(7)	734	1.8	1700
5 ppt mix	1.01E23	2.34	4.23	14.82	0.67	2.4	4.1
5.72pptmix	1.01E23	2.64	3.75	14.82	0.67	2.4	4.1
Copper	8.49E22	3.78(2)	3.11	7.78(3)	1.51	3.0	3.9
69.2% ^{63}Cu	5.88E22	4.50(2)	3.78	5.1(2)	3.33		
30.8% ^{65}Cu	2.62E22	2.17(3)	17.6	14.1(5)	2.71		
Fe	8.49E22	2.56(3)	4.6	11.35(3)	1.04	3.0	3.9
Carbon Steel wall 17 cm thick							
99.1% Fe	8.28E22	2.56(3)	4.7	11.35(3)	1.06	3.0	4.0
1.0% Mn	8.50E20	13.3(2)	88.5	2.2(2)	530	3.5	340
0.9% C	3.50E21	0.00350(7)	8.2E4	4.740(5)	60.3	1.7	170
mixture	8.72E22	2.55	4.5	11.03	1.04	2.9	3.9
304 Stainless cladding 0.95 cm thick							
69% Fe	5.97E22	2.56(3)	6.54	11.35(3)	1.48	3.0	5.6
19% Cr	1.76E22	3.07(8)	18.5	3.38(1)	16.8	3.0	19.
9% Ni	7.41E21	4.49(16)	30.1	17.8(4)	7.58	3.0	45.
2% Mn	1.76E21	13.3(2)	42.7	2.2(2)	260	3.5	160
1% Si	1.72E21	0.171(3)	3.40E3	2.0437(17)	284	2.5	230
0.08% C	3.22E20	0.00350(7)	8.87E5	4.740(5)	655	1.7	1.8E3
0.04% P	6.24E19	0.172(6)	9.32E4	3.134(10)	5.11E3	3.0	5.3E3
0.03% S	4.52E19	0.52(1)	4.3E4	0.98(5)	2.3E4	3.0	3.4E3
mixture	8.86E22	2.98	3.79	9.89	1.14	3.0	3.8
Polypropylene $(CH_2)_x$							
85.63% C	3.86E22	0.00350(7)	7.4E3	4.740(5)	5.47	1.7	15.
14.37% H	7.73E22	0.3326(7)	38.9	20.491(14)	0.63	2.9	4.5
mixture	1.16E23	0.2228	38.7	15.26	0.56	2.5	3.5
U	4.82E22	11.8	1.76			7.3	2.8
UO_2							
U 1	2.44E22	7.57+4.2f	3.5			7.3	5.6
O 2	4.89E22	0.00019(2)	1.6E5	3.761(6)	7.96	1.5	20.

When 5000 ppm boron is added to the water, most of the neutrons will be captured in the boron rather than hydrogen since the MFP to boron capture is much less than the MFP to hydrogen capture for this boron concentration. Note that the MFP to thermal capture in the boron is 5.6 [4.09/0.73] times longer than the hydrogen thermal scattering MFP. This means that non-thermal capture of neutrons into boron is not significant. Therefore, 5000 ppm boron loading does not significantly interfere with the moderation process. Since moderation is not disturbed, a relatively uniform thermal neutron flux distribution is produced near the fuel by the hydrogen scattering/moderation process.

The thermal neutron capture cross section is the cross section per atom for neutron capture at thermal energies. The energy dependence of the capture cross section is basically $1/\sqrt{E}$ for these materials. Although the energy distribution of fuel produced neutrons is a fission spectrum (which peaks at 2 MeV), the ratio of neutron captures in the OTSG materials follows the product of the thermal neutron capture cross section and the number density of the materials. Since the copper thermal capture MFP is the shortest of the materials in the OTSG, the copper will compete favorably with the boron and iron for thermal neutron capture.

The measurements of the neutron activation of ^{64}Cu in copper coupons (0.25-inch diameter, 4-inch long copper rods) have been converted to a neutron flux estimate. A summary of the neutron flux estimates in the steam generators appears in Table 6.3. The table contains weighted average values in the column headed "Wtd Ave FLUX" for each area (J-leg or bowl) of the OTSG where non-zero flux estimates were indicated. In some areas a significant non-zero flux estimate was not possible since the flux was below the limit of detection. In the column labeled "LTV" is a "less-than value" or upper limit where the mean of the neutron flux has a 95% chance of being below that value and only a 5% chance of being above it. The "LTV" is 1.645-sigma above either the mean flux or the minimum detectable flux.

6.3 FUEL ESTIMATE BASED ON THE DEBRIS VOLUME

A model of the debris volume, based on the video made during string emplacement, can be used to obtain a starting point estimate of the fuel weight in a J-leg of between 0.8 kg and 4.6 kg. In a bowl, the starting point estimate is 1.8 kg. The justification for these estimates is detailed below.

The debris in the OTSG J-legs appeared in the video to be relatively shallow, on the order of 1-3 centimeters deep. It also appeared to settle slowly when stirred up by the TV camera suggesting a density between 1-2 g/cm^3. Additional evidence by R. Lancaster and P. Babel[a] indicates that approximately 7% of the pressurizer debris is fuel. Using this information, the fuel weight estimate is

$$\text{Fuel} = \text{Depth} * \text{Area} * \text{Density} * \text{Fraction Fuel}$$

[a] R. Lancaster and P. Babel. April 8, 1988. TMI-2 Engineering Calculation 4550-3233-3223-88-011.

Using this scheme limits on the amount of fuel in a J-leg will he set.

Using 1.1E4 cm^2 as the area covered with debris in a J-leg, a lower limit is

$$\text{FUEL} = [1\ cm]*[1.1E4\ cm^2]*[1\ g/cm^3]*[0.001\ kg/g]*[0.07]$$

$$= 0.77\ kg$$

The upper limit for fuel in the J-leg is

$$\text{FUEL} = [3\ cm]*[1.1E4\ cm^2]*[2\ g/cm^3]*[0.001\ kg/g]*[0.07]$$

$$= 4.6\ kg$$

The depth of debris in the bowl was less than observed in the J-legs. The average debris depth appear to be less than 1 cm. The corresponding upper and lower limits for the OTSG bowls with an area of 2.5E4 cm^2 would be 1.75 kg and 3.5 kg, assuming 1 g/cm^3 and 2 g/cm^3 densities for the debris, respectively.

Note the debris volume estimate did not use the measured neutron flux but is included in this section to show that fuel weights based on the neutron flux measurements are reasonable.

Also this model uses the same parameters for both the A and B OTSGs, so the fuel estimates from this model listed in Table 6.3 are the same for both systems. It is not the purpose of this report to provide detailed analysis of the video records but to use the general impressions from the video to insure reasonable fuel estimates based on the neutron flux measurements.

6.4 SIMPLE MODEL

The simplest method to obtain an estimate of the amount of fuel in the OTSG is to merely multiply 1) the neutron flux, Φ, measured by the ^{64}Cu activation, 2) the area, A, of the debris, and 3) the neutron production rate in the fuel. This simple model converts the neutron flux to fuel by

$$\text{Fuel} = [\Phi\ n/(s*cm^2)] * [A\ cm^2] / [190\ n/(s*kg)]$$

The corresponding fuel estimates are listed below in Table 6.3 based on the measured flux estimates, which are also listed in the table.

TABLE 6.3. Summary of OTSG Neutron Flux Measurements with Fuel Estimates Using Both the Simplest Flux Based Model and the Debris Volume Estimates

LOCATION	Wtd Ave FLUX n/sec/cm²	FLUX LTV n/sec/cm²	DEBRIS AREA cm²	Simple Model FUEL EST kg	Simple Model FUEL LTV kg	Debris Volume FUEL EST kg	Debris Volume FUEL LTV kg
1A/J-leg	0.016(3)	0.020	1.1E4	0.93	1.16	0.77	4.6
2A/J-leg	0.009(3)	0.014	1.1E4	0.52	0.81	0.77	4.6
A/BOWL	----	0.006	2.5E4	----	0.79	1.75	3.5
A sum				1.45	2.87	3.29	12.7
1B/J-leg	----	0.005	1.1E4	----	0.29	0.77	4.6
2B/J-leg	0.024(3)	0.030	1.1E4	1.39	1.73	0.77	4.6
B/BOWL	----	0.004	2.5E4	----	0.53	1.75	3.5
B sum				1.39	2.55	3.29	12.7

This simple model is more than just dimensionally correct. Without the water to moderate the fission spectrum neutrons, the fission neutron flux would have to be reduced to an effective flux corresponding to only the lower-energy component where thermal neutron capture dominates. However, with water filling the OTSG the fission spectrum neutrons produced by the fuel are moderated and generally are captured within a mean free path (corresponding to the neutron's original energy) of the source point. During the neutron moderation process, neutrons collide about 25 times and travel on a random path through the region surrounding the source point. Since neutrons produced in the vicinity of a coupon will be moderated to thermal energy in that vicinity, it is not necessary to reduce the effective neutron flux to only the low-energy, thermal component.

The model assumes that neutrons can escape the fuel debris without significant absorption in the fuel debris. Assuming as much as 10 kg of uranium in a J-leg, one only has 0.91 g/cm² of uranium in a debris layer. At standard uranium density (19.05 g/cm³) this would be 0.047 cm thick. The MFP for a 2-MeV neutron though standard uranium is 2.8 cm which is about 60 times greater than the thickness of uranium in the debris. Thus, assuming neutrons can escape the fuel debris is justified for the high-energy portion of the fission spectra.

The model does not take into account neutrons which escape directly out through the steel wall. Initially half of the neutrons produced in the fuel are headed out through the steel wall. However, the wall thickness (17 cm) is large compared to the MFP for collision with an iron nucleus. Neutrons colliding with the much heavier iron nuclei are more likely to be back scattered without much energy loss than when colliding with the much lighter hydrogen or oxygen atoms in water. Thus one can expect that a significant fraction of neutrons initially headed out of the OTSG through the wall will return to the region of the coupons.

There will be some tendency for the thermal neutron flux to be higher a short distance above the source plane since the mean free path of the 2-MeV neutrons is about 5 cm in water and neutrons will have to wander back to the wall, with which the copper coupon is in contact, with shorter MFP values after each collision. However since the source plane is large, and most neutrons escape in a direction other than normal to the plane, this effect should not be large.

Without the boron loading of the water, neutrons would scatter many times [MFP(H-c)/MFP(H-s) = 44.9/0.73 = 61.5] before eventually being captured in hydrogen. Since this would allow neutrons several passes at the copper rod, one would have an effective increase in the thermal neutron flux relative to that expected from the source strength. However, with the boron loading the number of thermalized neutron scatters [MFP(B-c)/MFP(H-s) = 4.01/0.73 = 5.5] is much less.

With these competing effects, one can expect the prediction of this simple model to be reasonably correct.

6.5 NEUTRON CAPTURE MODELS

The neutron capture model converts the measured neutron flux into estimates of the total fuel remaining in each OTSG. The total fuel in the A-OTSG is about equal to that in the B-OTSG and is less than 5 or 10 kg depending on the parameter values used in the capture model. The capture model is discussed in detail below.

The neutron capture model considered assumes 1) that the neutron flux can be treated as relatively uniform throughout a relatively small volume element near the water/fuel/steel interface at the bottom of the bowl and J-legs and 2) that the neutron production rate in the volume element equals the neutron capture rate in the volume element. When this occurs, neutrons will be captured in the various materials found in the volume element in the ratio of the σ*N products for each material.

The key to applying this model is finding a reasonable volume element. One must first realize that the neutrons will not travel across the 28-inches of water in the J-leg, so the entire J-leg volume would not be a useful basis for the model.

The problem can be reduced to two infinite half planes (borated water in one and steel in the other) in the region of a single copper coupon. When the fuel is considered a planar neutron source at the water/steel interface, the number of thermal neutrons can be expected to fall off exponentially into either the water or iron half planes. Most of the neutrons will not be able to cross 28-inches of borated water to interact in the far wall of the J-leg. Also it will make no difference to the model if a few neutrons penetrate the J-leg wall and escape since the result is the same if the model considers them captured in non-existent material or they leave the outer wall. Also, the wall curvature can be neglected compared to the other problem dimensions.

The number of neutrons captured within an infinitely thick volume from a planar source is calculated as an integral into the volume with an exponential weighting factor, exp(-x/a), where "a" is the attenuation length. This volume integral is equivalent to a uniform weighting up to the attenuation length and to zero weighting beyond that distance.

$$\int_0^{\infty} e^{-(x/a)} * dx = -a * e^{-(x/a)} \Big]_0^{\infty} = -a * \left[e^{-\infty} - e^{0} \right] = a$$

$$\int_0^{a} 1 * dx = a$$

The uniform weighting or uniform neutron flux over a region is assumed by the simple capture model. An appropriate value of the attenuation length, "a", is required.

One reasonable choice for the attenuation length is the MFP associated with the total cross section at 2 MeV. The 2-MeV MFP is the distance the neutron travels from the source point before interacting. The general rule of thumb is that neutrons are captured in the region of first interaction due to the random walk path of the neutron during the moderation process. The MFP value for the borated water is 4.1 cm and the value for the steel wall is 3.9 cm. The slightly lower value for the cladding, 3.8, will not be used since most 2-MeV neutrons pass through the clad without interacting. One can argue that these distances should be increased to allow for a region for the neutron to moderate in following the first interaction. Conversely, one can argue that these distances are too large to apply to the planar geometry since only a very few neutrons are emitted from the fuel normal to the plane.

Another reasonable choice for the attenuation length, from an engineering point of view, is the effective removal cross section. It has been demonstrated that the attenuation of fission neutrons through most shields can be expressed by a simple exponential function using an effective removal cross section. The removal cross section data are obtained from shielding measurements and corresponds to removal of the fission spectra neutron flux by a given thickness of material. This approximation assumes water following the shielding material. The following table lists these cross sections and associated mean free paths.

TABLE 6.4. Fission Spectra Removal Cross Section Data

Material	Fission spectra removal cross section (/cm)	Mean Free Path MFP (cm)
Water	0.103	9.71
B	0.180	5.56
Fe	0.168	5.95
Cu	0.173	5.76

The attenuation length in water, a_w, and in iron, a_i, will be used to determine the dimensions of a rectangular volume element surrounding the copper coupon. This volume element will then be used to convert the measured neutron flux into a neutron source strength and subsequently to a fuel weight estimate. Figure 6.1 provides the geometry for our model where the dimensions of a rectangular box surrounding the copper coupon are expressed in terms of the attenuation lengths. The copper coupon is shown as the "O" in the center of the box. The rectangle of water above the coupon extends one attenuation length, "a_w", into the water. The rectangle of iron below the coupon also extends one attenuation length, "a_i", into the iron. The width, "W", of both boxes is the sum of these attenuation lengths. The desired conversion factor will not depend strongly on the value used for the width since both the source strength and the number of neutrons captured in the box increase linearly with "W". The dimension of the box into the page we will take as the 10-cm length of the coupon. In fact since the 18-coupon string used for the measurement is long compared to the box dimensions, any value consistently used is exact. The neutron source plane is at the iron/water interface.

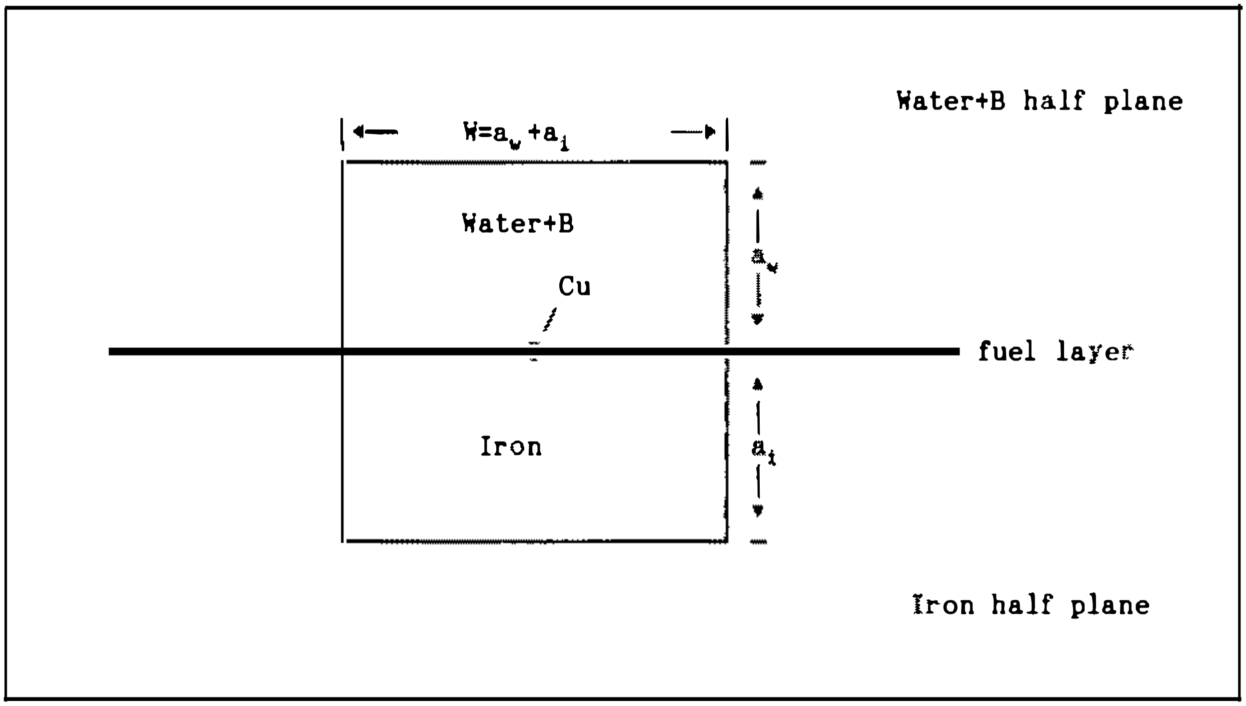

FIGURE 6.1. Geometry for Capture Model

The model assumes that all the neutrons produced in the box are captured in the box, since any neutrons escaping the box will be replaced by an equal number from outside the box by symmetry. The copper coupon breaks the symmetry, but since the width of the box is sufficiently large so that the copper coupon will not see a significant number of neutrons produced outside the box, it does not need to use the symmetric escape/replacement argument for neutrons it affects.

The neutron capture rate in the copper rods is

$$CR_{Cu}(n/s) = \sigma_{Cu} * \Phi * N_{Cu} = 1.025 * \Phi(n/s/cm^2)$$

where σ_{Cu}=3.78E-24 cm^2 is the thermal neutron capture cross section in copper (natural mix of both ^{63}Cu and ^{65}Cu), Φ is the measured neutron flux in $n/(s*cm^2)$, and N_{Cu}=2.7103E23 is the number of copper atoms in one 28.60-gram coupon.

Since the neutrons will be captured in the ratio of the $\sigma*N$ products, the neutron capture rate in the borated water portion of the box is

$$CR_{Bwater}(n/s) = \frac{\sigma_{Bwater} * N_{Bwater}}{\sigma_{Cu} * N_{Cu}} * CR_{Cu}(n/s)$$

$$= \sigma_{Bwater} * N_{Bwater} * \Phi$$

where σ_{Bwater}=2.64E-24 cm² is the thermal neutron capture cross section in the mixture of water with 5720 ppm B added, and N_{Bwater} is the number of atoms in the water volume. N_{Bwater} is the product of the volume based number density of the mixture which is 1.01E23 atoms/cm³ and the water volume which is V_{Bwater}= 10 cm * (a_w+a_i) * a_w in terms of the box dimensions. Therefore, the neutron capture rate in the water is

$$CR_{Bwater}(n/s) = [2.64E-24\ cm^2]*[1.01E23\ \#/cm^3]*[10\ cm]$$

$$*[a_w+a_i]*[a_w]*\Phi(n/s/cm^2)$$

$$CR_{Bwater}(n/s) = 2.67*[a_w+a_i]*[a_w]*\Phi(n/s/cm^2)$$

Likewise, the number of neutrons captured in the iron portion of the box is

$$CR_{Fe}(n/s) = \sigma_{Fe} * N_{Fe} * \Phi$$

where σ_{Fe}=2.56E-24 cm² is the thermal neutron capture cross section in iron and N_{Fe} is the number of atoms in the iron volume. The number density is 8.49E22 atoms/cm³ and the iron volume is given by V_{Fe}= 10 cm * (a_w+a_i) * a_i. Therefore, the capture rate in the water is

$$CR_{Fe}(n/s) = [2.56E-24\ cm^2]*[8.49E22\ \#/cm^3]*[10\ cm]$$

$$*[a_w+a_i]*[a_i]*\Phi(n/s/cm^2)$$

$$CR_{Fe}(n/s) = 2.17*[a_w+a_i]*[a_i]*\Phi(n/s/cm^2)$$

Now the total capture rate is

$$CR(n/s) = CR_{Cu}(n/s) + CR_{Bwater}(n/s) + CR_{Fe}(n/s)$$

$$CR(n/s) = 1.025*\Phi + 2.67*[a_w+a_i]*[a_w]*\Phi + 2.17*[a_w+a_i]*[a_i]*\Phi$$

If SS is a source strength per unit area on the source plane, the neutron production rate inside the box is given by

$$PR(n/s) = SS(n/s/cm^2) * [10\ cm] * [a_w+a_i]$$

where a_w and a_i are in centimeters. But the model assumes that the production rate in the box equals the capture rate in the box, therefore CR = PR, which solving for SS yields

$$SS(n/s/cm^2) = [1.025/(a_w+a_i) + 2.67*a_w + 2.17*a_i] * \Phi / 10$$

where a_w and a_i are in centimeters and Φ is in $n/s/cm^2$. The length of the coupon exactly divides out of the expression, making the result completely insensitive to the length of the coupon. Also, the width of the box divides out of the major terms in the sum making the result relatively insensitive to the box width.

The amount of fuel in the region is related to the source strength per unit area by

$$SS(n/s/cm^2) = [190\ n/s/kg]*[Fuel(kg)]/[Debris\ area(cm^2)]$$

so the amount of fuel in the region is given by

$$Fuel(kg) = \frac{Area(cm^2)*[1.025/(a_w+a_i)+2.67*a_w+2.17*a_i]*\Phi(n/s/cm^2)}{10 * [190\ n/s/kg]}$$

where a_w and a_i are in centimeters.

Consider two cases with the box dimensions determined by 1) the 2-MeV MFPs and 2) the effective removal MFPs. In the first case, using the 2-MeV MFPs, we have a_w=4.1 cm and a_i=3.9 cm so the fuel estimate becomes

$$[Fuel(kg)] = [Debris\ area(cm^2)] * 0.0103 * \Phi(n/s/cm^2)$$

This is the formula used in Table 6.5 for the first estimates. In the second case, using removal cross sections, a_w=9.7 cm and a_i=6.0 cm, so the fuel estimate becomes

$$[\text{Fuel(kg)}] = [\text{Debris area}(\text{cm}^2)] * 0.0205 * \Phi(\text{n/s/cm}^2)$$

The results for these two cases are shown in the following table.

TABLE 6.5. Summary of OTSG Neutron Flux Measurements with Fuel Estimates Using the Neutron Capture Model with Two Parameter Selections

LOCATION	Wtd Ave FLUX n/sec/cm²	FLUX LTV n/sec/cm²	DEBRIS AREA cm²	2 MeV σ total FUEL EST kg	2 MeV σ total FUEL LTV kg	Removal σ FUEL EST kg	Removal σ FUEL LTV kg
1A/J-leg	0.016(3)	0.020	1.1E4	1.81	2.26	3.61	4.51
2A/J-leg	0.009(3)	0.014	1.1E4	1.02	1.58	2.03	3.16
A/BOWL	----	0.006	2.5E4	----	1.54	----	3.08
A sum				2.83	5.38	5.64	10.75
1B/J-leg	----	0.005	1.1E4	----	0.56	----	1.13
2B/J-leg	0.024(3)	0.030	1.1E4	2.71	3.39	5.42	6.77
B/BOWL	----	0.004	2.5E4	----	1.03	----	2.05
B sum				2.71	4.98	5.42	9.95

Next, the possible errors that this model might include are addressed.

Throughout this derivation of the amount of fuel, the measured neutron flux was only multiplied by the thermal neutron cross section. In the conversion of the measured count rates to the neutron flux, the flux was an effective thermal flux since the product of the thermal cross section and the measured flux was used rather than a more complex energy convolution. The same has been done here, so the fuel estimate has not been compromised by the simple effective thermal flux approach.

The model also assumes a uniform neutron flux, Φ, within the box. However there will be an asymmetry in the flux at the interface due to the albedo of the interface. As mentioned before, the flux on the iron side is likely to be lower than on the water side due to the greater tendency of neutrons to backscatter off the heavier iron nuclei. The actual flux measurement was made on the water side of the interface so the model would overestimate the number of neutrons captured on the iron side (less flux there). If one assumed a 20%

backscatter off the iron, the flux on the iron side would be 67% (80/120) of the water side flux. As a result, the fuel estimate in the table would be about 15% high as a result. Note that the lower removal MFP for iron compared to water is likely due to the greater backscatter off the iron.

The copper captured less than 1% of the neutrons in the box so any adjustment of the box width, which impacted only the neutrons captured in the copper, would have only a very small impact on the fuel estimate.

The amount of fuel in the box also does not interact with a very large number of neutrons. First from Table 6-2, note that the MFP for a 2-MeV neutron is 2.8 cm in uranium, which is greater than the thickness of uranium in the debris. Assuming as much as 10 kg of uranium evenly dispersed in a J-leg, one only has a 0.91 g/cm^2 layer of uranium in the debris. That would correspond to a solid uranium layer only 0.048 cm thick given the 19.05 g/cm^3 density of uranium. Once the high-energy neutrons escape the debris they have a chance of again entering the debris as thermal neutrons and being captured there. With a 11.77 barn [7.57 capture +4.2 fission] cross section for natural uranium to interact with thermal neutrons, the interaction rate in the uranium is

$$IR_U(n/s) = [11.77E\text{-}24cm^2] * [2.5300E21\ \#U/g] * [0.91\ g/cm^2] * [10\ cm] * [a_w + a_i] * \Phi$$

$$IR_U(n/s) = 0.271 * [a_w + a_i] * \Phi$$

which can be compared to the capture rate in water

$$CR_{Bwater}(n/s) = 2.67 * [a_w + a_i] * [a_w] * \Phi$$

Since CR_{Bwater} is 9.85*a_w times larger than IR_U, the 10 kg of uranium would interact with less than 2.5% of the neutrons captured in the boron loaded water if a_w=4.1 cm, or less than 1.0% of the neutrons if a_w=9.7 cm. Therefore the fuel distribution parameters are not a major source of error for this model. Although the fuel has more than the natural abundance of ^{235}U (capture σ=98 barns and fission σ=580 barns), the ^{235}U enrichment of the fuel should not reduce the fuel estimate significantly.

This fuel calculation considered the major neutron poison, boron [σ_{scat} = 4.27(7) barns, σ_{capt} = 767(8) barns, and resonance integral I_a = 344(1) barns] at 5.72 ppt. If large amounts of other neutron capturing materials like cadmium [σ_{scat} = 5.6(6) barns, σ_{capt} = 2520(50) barns, and resonance integral I_Y = 70(10) barns] or silver [σ_{scat} = 5.08(3) barns, σ_{capt} = 63.3(4) barns, and

I_γ = 756(20) barns] were mixed in with the debris, the amount of fuel could be greater than estimated with this model. However, without information on amounts of other neutron poisons present, any attempt to adjust the fuel estimate would be speculation. Since most of the fuel produced neutrons spend far more time in the water volume than the solid debris, the relative affect of neutron poisons on the fuel estimate should scale as the ratio of concentration in water times capture cross section. Silver and cadmium are much less water soluble than boron, therefore the boron poison should dominate. If the neutron poisons were mixed in with the fuel debris, the danger of criticality is greatly decreased. In fact, the neutron flux measured is probably the best estimator for criticality danger from the unknown mixture.

The major uncertainty in the neutron capture model involves the values used for a_w and a_i. The fuel estimate will vary linearly with changes in these parameters. Since the model is most sensitive to these parameters, the formula for the fuel estimate left these explicitly in the equation.

Some estimation of the proper value of a_w is available from calibration experiments performed at PNL. These experiments were performed in borated water using a ^{252}Cf point source and a 5-inch long, 0.25-inch diameter ^{3}He sensor. The ^{252}Cf source strength was 6.3E6 n/s. A series of measurements were made with varying distances between source and sensor. The problem of determining the appropriate value of a_w for the capture model is difficult since the measurements were made with a point source and an extended cylindrical sensor. The raw data appear in the following table.

TABLE 6.6. ^{3}He Sensor to Source Data

Source-sensor distance (cm)	Sensor Count	a_w est cm
1.3	20,000	0.23
3.2	18,000	0.67
5.7	11,000	1.2
8.3	8,000	1.8
10.8	3,500	2.2
13.3	1,600	2.5
15.9	980	2.8
18.4	610	3.2
21.0	290	3.3
23.5	85?	3.2
26.0	68	3.5

The a_w estimates shown in the table are the values required at each distance to equate the measured count rate with the value calculated for that distance assuming 100% detection efficiency for thermal neutrons in a ^{3}He sensor. The $\exp(-r/a_w)/r^2$ model of distance dependence was used. The extended sensor was numerically integrated over it length. As one can see the model does not exactly apply since the counts at short distances were lower than would be predicted with a constant a_w value. At short distances from the source there will be a significant high-energy neutron component to the flux that the ^{3}He will not efficiently detect. At larger distances an attenuation constant of about 3 cm appears consistent with the data.

When plotting the raw data on log/log paper there is a knee (or inflection point) at 7.6 cm with a relatively linear log/log relationship beyond 7.6 cm. This would correspond to the length of the sensor becoming less important. Beyond this point neutron scattering may obscure the difference between a point and extended source. One also would expect a largely thermalized neutron field past this point. Beyond about 8-cm separation, the data fits the function

$$Cnt = 29,700*exp[-x(cm)/7.25]$$

reasonably well. This would point to an a_w value of 7.25 cm. The other view would be that since the function starts to drop rapidly beyond 7.6 cm, an a_w value of 7.6 cm would be supported.

Simply integrating (numerically) the limited raw data over the separation yields a value equal to the product of 20,000*6.3 cm. This is an indication that a_w is on the order of 6.3 cm.

The experimental data can not be made to fit the crude model more accurately, since the model is only an approximation. It is somewhat frustrating that the point source data can not be readily transformed into planar source information. However, one must recognize that the neutron scattering/moderation process obscures information about the source geometry. The experimental data is consistent with an a_w value less than the removal MFP of 9.7 cm used in case II above. Thus the LTV for case II (10 kg fuel per OTSG) appears to be a very reasonable upper limit for the fuel present.

6.6 EMPIRICAL NEUTRON PRODUCTION MODEL

This section will examine the calibration measurements made at PNL. These measurements used a ^{252}Cf neutron source behind various metal plates under boron-loaded water and over a thick steel plate as a mockup for the measurements in the steam generator. These measurements were made using a ^{3}He proportional counter in a water tight polypropylene tube as the neutron sensor. The experiments measured the relative contribution to the neutron flux for a point source displaced from the sensor location. The experimental results allow calculation of the activity produced by selected distributions of fuel.

Since these mockup experiments were done at PNL before the measurements at TMI, only a few experimental cases match the OTSG situations. One of the most direct calibrations involved placing the 6.5E6 n/s ^{252}Cf source in a tank over a 4-inch thick steel plate. The 0.5-inch diameter source was placed in a slot milled in a half-inch thick aluminum plate. The source was covered over with an additional 2-inch thick aluminum plate to simulate attenuation in some fuel debris. Then a string of eight copper coupons (in the same plastic jacket used at TMI) was placed on top of the plate for a 2-hour activation by the neutron source. The tank above the aluminum plate was filled with 5000 ppm borated water. The coupons were counted on a NaI(Tl) coincidence counter at PNL (in a manner similar to the way the TMI coupons were counted). This counter is referred to as the Packard-5. Measurements were made with the 0.25-inch diameter, 5-inch long ^{3}He sensors alongside the copper coupons for cross calibration between the copper coupon measurements and the ^{3}He sensors. The ^{64}Cu activation data from Packard-5 was reduced to a neutron flux estimate (N-FLUX) in the same manner as the coupons from the OTSG measurements. These flux estimates are listed in Table 6.7.

TABLE 6.7. Results of PNL Copper Coupon Activation with 6.5E6 n/s Source

Data Set Title: K-COUPONS PNL ACTIVATION File: A:KALE.DAT

COUPON LABEL	BKG	CNT	N-FLUX n/(s*cm²)	NF-ERR n/(s*cm²)	%-ERR	FAP	MDL-FLUX n/(s*cm²)
K1	1.23	2244	964.8710	20.3796	2%	0.000000000	2.4827
K1-2	2.46	2775	966.7588	18.3685	2%	0.000000000	2.6298
K2	1.23	3998	1643.0067	25.9927	2%	0.000000000	2.3723
K3	1.23	2649	1149.5175	22.3448	2%	0.000000000	2.5054
K3-2	2.46	3281	1171.6233	20.4698	2%	0.000000000	2.6951
K4	2.46	1732	392.1895	9.4372	2%	0.000000000	1.7102
K5	2.46	523	143.1458	6.2891	4%	0.000000000	2.0739
K6	4.92	359	51.8844	2.7769	5%	0.000000000	1.3310
K7	7.37	240	24.2833	1.6183	7%	0.000000000	1.1092
K8	7.37	91	9.3204	1.0651	11%	0.000000000	1.1842
K8-2	103.00	969	10.7009	0.3973	4%	0.000000000	0.4201

The coupon K2 was directly above the source. Note that coupons K1 and K3 were each centered 4 inches away but the flux seen by K1 was 16% lower than K3 due to K1 being closer to the edge of the tank where neutrons could escape the tank. Counts labeled "Kn-2" were recounts of the same coupon at a later time. The recounts agree statistically with the initial counts.

The next step is to take these point source measurements and attempt to estimate the amount of planar distributed neutron source required to produce the ^{64}Cu activity corresponding to the measured flux values. One approach is to assume a uniform planar source producing 1 n/s/cm². Then to divide up the source plane into concentric rings 4-inches wide. Since 4-inches corresponds to the length of the copper coupon, finer spatial resolution of the source plane would not be distinguishable in either the calibration data or the TMI measurements. Since the measured neutron flux does not fall off rapidly with displacement from the point source and the moderation process obscures the details of the source geometry, the value of each point source measurement can be reasonably used as representative of any point source within a 2-inch radius. Although it is not possible to match the experimental data to an attenuated point source model $\exp(-r/a)/r^2$, it is possible to use linear superposition of point sources to model a planar source.

A point source could be placed anywhere in the ring corresponding to a given displacement and the copper coupon in the center of the concentric ring model would see a neutron flux consistent with our flux measurement for that source/sensor displacement. Since a planar source strength of 1 n/s/cm^2 has been assumed, the contribution from each ring is our measured flux times the ring area divided by the source strength of our point source. This is like placing a 1 n/s source on every square centimeter of the ring. Linear superposition of these small sources implies that the flux from the planar source equals the sum of these small point sources.

All the mathematically complex neutron scattering applies identically to both our large point source and the several smaller ones. Any necessary spatial averaging over the point sources has been done by the spatial extent of the copper coupon. The contributions from each concentric ring to the estimated neutron flux seen by the coupon from our planar 1 n/s/cm^2 source are listed in Table 6.8 below. In the table, the inner (R1) and outer (R2) radii of the concentric rings are listed. The values under "MeasFLUX" are the values of the flux required to produce the ^{64}Cu activity measured in the copper coupons. The values under "EstFLUX" equal MeasFLUX*AREA/6.5E6 and are the estimated flux that a planar neutron source of 1.0 n/s/cm^2 would produce based on our measurements. Also in the table are the count rates on the ^{3}He sensor at the positions of the copper coupons. The last column is the ratio between the ^{3}He count and the "MeasFLUX" value. The ^{3}He sensor projected area is 8.06 cm^2, so the average efficiency for measuring the flux responsible for ^{64}Cu activation was 51%, which seems reasonable.

TABLE 6.8. Flux Conversion of PNL Copper Coupon Data

REGION (Coupon)	R1 cm	R2 cm	AREA cm^2	MeasFLUX $n/s/cm^2$	EstFLUX $n/s/cm^2$	^3He Count	Ratio
K2	0	5.1	81.0	1640	0.0204	7391	4.51
K3	5.08	15.2	648.6	1150	0.1148	4028	3.50
K4	15.2	25.4	1297.2	392	0.7823	1253	3.20
K5	25.4	35.6	1945.8	143	0.0428	818	5.72
K6	35.6	45.7	2594.3	52	0.0208	321	6.20
K7	45.7	55.9	3242.9	24	0.0120	135	5.62
K8	55.9	66.0	3884.5	10	0.0060		
			sum = 13694.3		sum = 0.9991		ave = 4.80 se ave = 0.72

The systematic errors in this experiment are such that the values in the "MeasFLUX" column are smaller than they should be. This means that the planar source strength required to match a measured flux value will be a lower limit. The limited extent of the tank and limited depth of borated water in the tank allowed neutrons to escape the system which in the larger OTSG would continue to scatter and increase the measured flux value. The magnitude of this underestimate is indicated by the measured flux in K1 being 16% lower than in K3. The K1 coupon was closer to a wall than any of the other coupons so the underestimation for the coupons used was probably less than 10%. The aluminum plate between the source and the coupons is thicker than necessary to match the attenuation due to the amount of fuel debris seen by video. The ^3He count directly over the source with only the slotted aluminum plate was 2.8 times that with the extra 2-inch thick plate. At an 8-inch offset it was 1.5 times larger and at 20-inch offset it was about the same. The error due to the thicker plate will be addressed later. Likewise, any contribution to the flux when the source is at greater distances than the dimensions of the tanks have been ignored. Since the contribution of the larger rings is dropping rapidly this should contribute no more than a 5% error.

To estimate the amount of fuel in the region of a copper coupon one can scale from this calibration data by using the ratio

$$\frac{[\text{EstFlux } n/s/cm^2]}{[\text{SourceStrength } n/s/cm^2]} = \frac{[\Phi\ n/(s*cm^2)]}{[\text{Fuel(kg)}]*[190\ n/(s*kg)]/[A\ cm^2]}$$

where "Φ" is the neutron flux measured at TMI by the copper coupon activation, and "A" is the fuel debris area. The assumed source strength of the planar source was 1 $n/s/cm^2$. From Table 6.8, the sum of the estimated flux contributions from the rings is 1.0 $n/s/cm^2$. Thus the scaling formula becomes

$$\text{Fuel} = [\Phi \ n/(s*cm^2)] * [A \ cm^2] / [190 \ n/(s*kg)]$$

for this data. This is identical to the formula for the simplest model discussed previously and values obtained with that formula were listed in Table 6.3. However, now there is some experimental evidence to indicate that these values are a reasonable lower limit to the amount of fuel. These values are also listed in Table 6.10 below.

Since the fuel debris was relatively thin, the PNL ^{252}Cf measurements with slotted plates of three different materials with zero vertical separation between source and sensor (no plates covering the source) under the borated water cover are probably more applicable than the previously discussed measurement with 2-inch vertical separation between source and sensor using a 2-inch thick aluminum covering plate. These measurements were made only with the ^{3}He sensor. The ^{3}He count rates will be converted to estimated fluxes from the 1 n/s/cm² planar source by multiplying the count rate by the area, dividing by the source strength and dividing by the average value of the count/flux ratio, 4.8, from Table 6.8. These measurements are listed in the following table.

TABLE 6.9. Flux Conversion of PNL ^{3}He Sensor Data

Offset inch	R2 cm	AREA cm²	Al ^{3}HeCnt c/s	Al EstFLUX n/s/cm²	Fe ^{3}HeCnt c/s	Fe EstFLUX n/s/cm²	Cu ^{3}HeCnt c/s	Cu EstFLUX n/s/cm²
0	2.54	20	20,546	0.0132	22,891	0.0147	23,419	0.0150
2	7.62	162	15,314	0.0795	15,492	0.0804	18,349	0.0953
4	12.7	324	8,695	0.0903	7,547	0.0784	10,052	0.1044
6	17.8	486	4,465	0.0696	2,874	0.0448	3,870	0.0603
8	22.9	649	1,930	0.0401	1,465	0.0305	1,893	0.0394
10	27.9	811	1,295	0.0337	793	0.0206	908	0.0236
12	33.0	973	695	0.0217	429	0.0134	505	0.0157
14	38.1	1135	417	0.0152	227	0.0083	274	0.0100
16	43.2	1297	246	0.0102	137	0.0057	159	0.0066
18	48.3	1459	121	0.0057	105	0.0049	136	0.0064
20	53.3	1621	138	0.0072	88	0.0046	97	0.0050
			sum =	0.3864	sum =	0.3063	sum =	0.3817

Using an average value of 0.36 n/s/cm² as the estimated flux the scaling formula becomes

$$\text{Fuel} = 2.8 * [\Phi\ n/(s*cm^2)] * [A\ cm^2] / [190\ n/(s*kg)]$$

Thus the total fuel is less than 8 kg in the A-OTSG and less than 7.1 kg in the B-OTSG.

The error estimates on this model are 1) 15% random measurement error associated with converting the ^{3}He count to flux value, 2) possible 10% underestimation of the neutron flux due to neutrons escaping the tank, and 3) possible 5% contribution to the flux from rings beyond our measurements. An estimate of the upper limit for the fuel from the PNL calibration measurements can be obtained by increasing the scaling factor by to 3.7 [3.7 = 2.8*1.15*1.1*1.05]. This gives a more conservative scaling formula of

$$\text{Fuel} = 3.7 * [\Phi\ n/(s*cm^2)] * [A\ cm^2] / [190\ n/(s*kg)]$$

Thus the total fuel is less than 10.6 kg in the A-OTSG and less than 9.4 kg in the B-OTSG. This is still less than the 12.7 kg upper limit estimated with the debris volume model. The values for the fuel estimates with this error correction formula are listed in Table 6.10 below. The values in the table are based experimental PNL data using 1) the conversion factor for the activation of copper coupons at PNL (no corrections for possible systematic error or change in fuel attenuation) and 2) the best estimates using ^{3}He sensor data (increased to cover systematic error estimates).

TABLE 6.10. Summary of OTSG Neutron Flux Measurements with Fuel Estimates from the Mockup Experimental Data

LOCATION	Wtd Ave FLUX n/sec/cm²	FLUX LTV n/sec/cm²	DEBRIS AREA cm²	copper direct FUEL EST kg	copper direct FUEL LTV kg	^{3}He corrected FUEL EST kg	^{3}He corrected FUEL LTV kg
1A/J-leg	0.016(3)	0.020	1.1E4	0.93	1.16	3.43	4.3
2A/J-leg	0.009(3)	0.014	1.1E4	0.52	0.81	1.93	3.0
A/BOWL	----	0.006	2.5E4	----	0.79	----	2.9
A-OTSG				1.45	2.87	5.36	10.2
1B/J-leg	----	0.005	1.1E4	----	0.29	----	1.1
2B/J-leg	0.024(3)	0.030	1.1E4	1.39	1.73	5.14	6.4
B/BOWL	----	0.004	2.5E4	----	0.53	----	1.9
B-OTSG				1.39	2.55	5.14	9.4

6.7 CONCLUSIONS

These residual fuel estimates agree with estimates based on debris volume (video evidence) and the gamma-ray measurements. In spite of modeling uncertainties, these estimates could not underestimate reality by more than the factor of two originally agreed to. In fact, The LTVs in the table may be considered reasonable upper limits without an additional multiplicative factor.

The neutron flux measurements indicate that the amount of residual fuel in the OTSGs is less than 10 kg each. This estimate should be scaled down to the best available debris area estimate.

Appendix A

FLUX.BAS LISTING

```
1 CLS
2 PRINT "BASIC PROGRAM TO CALCULATE THE FLUX SEEN BY A COUPON(S)"

10 INPUT "NAME OF DATA DISK [B]: ", DISK$
11 INPUT "NAME OF STRING [J]: ", ROPE$
12 FILENAM$ = DISK$ + ":" + ROPE$

14 DFILE$ = FILENAM$ + ".DAT"
15 PRINT "NAME OF INPUT DAT FILE [B:J.DAT]: ", DFILE$
16 OPEN DFILE$ FOR INPUT AS #1

17 PFILE$ = FILENAM$ + ".PRN"
18 PRINT "NAME OF OUTPUT PRN FILE [B:J.PRN]: ", PFILE$
19 OPEN PFILE$ FOR OUTPUT AS #2

25 SFILE$ = FILENAM$ + ".SUM"
26 PRINT "NAME OF OUTPUT SUM FILE [B:J.SUM]: ", SFILE$
27 OPEN SFILE$ FOR OUTPUT AS #3


30 INPUT #1, TITLE$
31 PRINT #2, "Data Set Title:  "; TITLE$; TAB(50); "File:  "; DFILE$
32 PRINT #2,
33 PRINT #3, "Data Set Title:  "; TITLE$; TAB(50); "File:  "; DFILE$

40 PRINT #3, CHR$(174); "RM100"; CHR$(175)
41 PRINT #3, CHR$(174); "TS6,15,22,27,38,48,56,68,78"; CHR$(175)
42 PRINT #3,
"________________________________________________________________________
_"
45 PRINT #3, "LABEL COUPONS BKG  CNT   N-FLUX NF-ERR  %-ERR FAP MDL-FLUX ZF-
ERR"
46 PRINT #3, "         n/(s*cm²) n/(s*cm²)   n/(s*cm²) n/(s*cm²)"
47 PRINT #3,
"________________________________________________________________________
_"

50 DIM BKGM(2), BKGSEM(2), BKGSD(2), EFF(2)
51 INPUT "A or B OSTG, Packard [A,B,P] "; A$
52 IF A$ = "A" OR A$ = "a" THEN 60
53 IF A$ = "B" OR A$ = "b" THEN 70
54 IF A$ = "P" OR A$ = "p" THEN 80
58 GOTO 51
```

```
60 ' Background data for A-OTSG measurements
61 BKGM(1) = .548     'Mean background rate--sensor #1 during A-OSTG
62 BKGM(2) = .545     'Mean background rate--sensor #2 during A-OSTG
63 BKGSEM(1) = .014   'StdErr in Mean background rate--sensor #1
64 BKGSEM(2) = .01    'StdErr in Mean background rate--sensor #2
65 BKGSD(1) = .072    'StdDev in background distribution--sensor #1
66 BKGSD(2) = .047    'StdDev in background distribution--sensor #2
67 EFF(1) = .048      '19.3% of Cu-64 positron decay
68 EFF(2) = .048      '
69 GOTO 100

70 ' Background data for B-OTSG measurements
71 BKGM(1) = .594     'Mean background rate--sensor #1 during B-OSTG
72 BKGM(2) = .535     'Mean background rate--sensor #2 during B-OSTG
73 BKGSEM(1) = .016   'StdErr in Mean background rate--sensor #1
74 BKGSEM(2) = .016   'StdErr in Mean background rate--sensor #2
75 BKGSD(1) = .066    'StdDev in background distribution--sensor #1
76 BKGSD(2) = .066    'StdDev in background distribution--sensor #2
77 EFF(1) = .048      '19.3% of Cu-64 positron decay
78 EFF(2) = .048      '
79 GOTO 100

80   ' Background data for PACKARD-5
81 BKGM(1) = .12291     'Background rate sensor #1
82 BKGM(2) = 0!         'Background rate sensor #2 --ZERO==> NO 2nd sensor
83 BKGSEM(1) = .0096    'StdErr in Mean background rate--sensor #1
84 BKGSD(1) = .0096     'StdDev in background distribution--sensor #1
85 EFF(1) = .05252      '19.3% of Cu-64 positron decay
89 GOTO 100


100 DIM EFIX(2, 7) 'average relative efficiency for multi rod counts
101 EFIX(1, 1) = 1!: EFIX(2, 1) = 1!
102 EFIX(1, 2) = .974: EFIX(2, 2) = .989
103 EFIX(1, 3) = .981: EFIX(2, 3) = .983
104 EFIX(1, 4) = .965: EFIX(2, 4) = .967
105 EFIX(1, 5) = .943: EFIX(2, 5) = .946
106 EFIX(1, 6) = .904: EFIX(2, 6) = .906
107 EFIX(1, 7) = .981: EFIX(2, 7) = .876

150 PRINT #2, TAB(32); "SYSTEM #A"; TAB(48); "SYSTEM #B"
151 PRINT #2, "Background Rate"; TAB(32); BKGM(1); TAB(48);
152 PRINT #2, BKGM(2); TAB(64); "c/m"
153 PRINT #2, "Std Err in Bkg estimate"; TAB(32); BKGSEM(1); TAB(48);
154 PRINT #2, BKGSEM(2); TAB(64); "c/m"
155 PRINT #2, "Std Dev in Bkg distribution"; TAB(32); BKGSD(1); TAB(48);
156 PRINT #2, BKGSD(2); TAB(64); "c/m"
```

```
157 PRINT #2, "Sensor Efficiency for Cu-64"; TAB(32); EFF(1); TAB(48);
158 PRINT #2, EFF(2); TAB(64); "ct/decay"
159 PRINT #2,

170 LAMDA = .054583   'decay constant of Cu-64 in decays/hour
171 PRINT #2, "Cu-64 Decay constant                =";  LAMDA; " decays/hour"
180 CROSS = 4.4E-24   'cross section for Cu-63 in sq cm
181 PRINT #2, "Cu-63 Thermal Neutron Cross section ="; CROSS; " cm²"
185 NATOM = 1.875E+23 'number of atoms in a standard coupon
186 PRINT #2, "Atoms per standard Copper coupon    ="; NATOM; "Atoms"
190 FAPMDL# = .001 'FAP level for MDL
191 PRINT #2, "FAP for minimum detectable level    = ";
192 PRINT #2, USING "#.########"; FAPMDL#
195 PRINT #2,

200 ' ***********************************************************
210 ' File input of total time exposed to neutron flux in hours
220 INPUT #1, Tact
230 ' ***********************************************************
240 PRINT "Total activation time ="; Tact; " Hours"
250 PRINT #2, "Activated for"; Tact; "hours";

300 FRACT = 1 - EXP(-LAMDA * Tact)  'Fraction of maximum activity made
310 PRINT #2, " producing"; FRACT * 100; "% of maximum activity"

500 ' ***********************************************************
510 ' File input of clock time [hours,minute] removed from neutron flux
520 INPUT #1, THR, TMIN
530 ' ***********************************************************
540 PRINT "Time activation ended: "; THR; ":"; TMIN
550 PRINT #2, "Activation ended at [hr:min] ";
551 PRINT #2, USING "##"; THR;
552 PRINT #2, ":";
553 PRINT #2, USING "##"; TMIN
560 TOUT = THR + TMIN / 60!  'Time in hours

600 'Loop back point
610 IF EOF(1) THEN 6000   'Quit if input file empty
650 PRINT #2,
660 PRINT #2,
"================================================================="
670 PRINT #2,

700 ' ***********************************************************
701 ' File input of clock time [hours,minute] at start of count
702 '       NOTE:  24 hours added for each day after end of activation
703 ' File input of count duration in seconds
710 INPUT #1, THR, TMIN, Tcnt
```

```
711 ' ***************************************************************
720 Tdecay = THR + TMIN / 60 - TOUT  'Time (hours) since removal from flux
730 PRINT "Counting started at:"; THR; ":"; TMIN; " for"; Tcnt; "sec"
750 PRINT #2, "Counting started at ";
751 PRINT #2, USING "##"; THR;
752 PRINT #2, ":";
753 PRINT #2, USING "##"; TMIN;
754 PRINT #2, " which was ";
755 PRINT #2, USING "###.##"; Tdecay;
756 PRINT #2, " hours after the end of activation"
770 TcntM = Tcnt / 60!   'Convert time in seconds to minutes
780 TcntH = Tcnt / 3600!   'Convert time in seconds to hours
790 PRINT #2, "Duration of count was"; Tcnt; "seconds or"; TcntM; "minutes"

810 CDFRAC = EXP(-LAMDA * TcntH)   'Time units are hours here
820 DDFRAC = EXP(-LAMDA * Tdecay)
830 PRINT #2, "Activity at start of count was ";
831 PRINT #2, USING "###.####"; DDFRAC * 100;
832 PRINT #2, "% of original activity."
840 PRINT #2, "Activity at  end  of count was ";
841 PRINT #2, USING "###.####"; CDFRAC * DDFRAC * 100;
842 PRINT #2, "% of original activity."
850 PRINT #2, "                              or   ";
851 PRINT #2, USING "###.####"; CDFRAC * 100;
852 PRINT #2, "% of activity at start of count."

1300 FOR SYS = 1 TO 2
1301 IF BKGM(SYS) = 0 THEN 4200
1305 PRINT #2, ""
1306 PRINT #2, "- - - - - - - - - - - - - - - - - - - - - - - - - - - - - - - - - -
- -"
1307 PRINT #2, ""
1320 PRINT "System #"; SYS;

1400 ' ***************************************************************
1401 ' File input of count title string in quotes "Name"
1402 ' File input of number of coupons counted
1403 ' File input of raw count
1410 INPUT #1, SAMP$, NCOUP, CNT
1420 ' ***************************************************************
1430 PRINT "Title: "; SAMP$; "   with"; NCOUP; "coupons  CNT="; CNT;
1450 PRINT #2, "System #"; CHR$(SYS + 64); " with"; NCOUP; "coupons";
1460 PRINT #2, TAB(30); SAMP$; TAB(60); TITLE$
1470 PRINT #2,
1480 PRINT #2, "Coincidence"; TAB(16); "Count"; TAB(32); "Background";
1481 PRINT #2, TAB(48); "Net Signal"

1500 BKG = BKGM(SYS) * TcntM      'mean background estimate for count
```

```
1510 SDBKG = BKGSEM(SYS) * TcntM  'standard error in mean background estimate
1520 NET = CNT - BKG              'Net Signal count
1530 PRINT #2, "Counts"; TAB(16); CNT; TAB(32); BKG; TAB(48); NET;
1531 PRINT #2, TAB(64); " counts"

1600 RCNT = CNT / TcntM           'Rates in cts/min
1610 RBKG = BKG / TcntM
1620 RNET = NET / TcntM
1630 PRINT #2, "Rates"; TAB(16); RCNT; TAB(32); RBKG; TAB(48); RNET;
1631 PRINT #2, TAB(64); " c/m"

1700 SQCNT = SQR(CNT)             'Error estimates
1701 SQBKG = SQR(BKG)
1702 SQNET = SQR(CNT + SDBKG * SDBKG)  'Includes small error in mean bkg est
1703 SQZER = SQR(BKG + SDBKG * SDBKG)  'Includes small error in mean bkg est
1710 ECNT = SQCNT / TcntM         'Rate errors
1720 EBKG = SDBKG / TcntM
1730 ENET = SQNET / TcntM
1740 PRINT #2, "Rate Error"; TAB(16); ECNT; TAB(32); EBKG; TAB(48);
1741 PRINT #2, ENET; TAB(64); " c/m"

1750 PCNT = 100! * ECNT / RCNT    'Conversion to percent error estimates
1760 PBKG = 100! * EBKG / RBKG
1770 PNET = 0!
1775 IF RNET <> 0 THEN PNET = 100! * ENET / ABS(RNET)
1780 PRINT #2, "% Err"; TAB(16); PCNT; "%"; TAB(32); PBKG; "%"; TAB(48);
1781 PRINT #2, PNET; "%"
1790 PRINT #2,

1900 MDTEST# = 1! - FAPMDL#' Require a FAP < 0.001 for MDL
1902 MDCNT = 0                    'Minimum Detection CNT
1910 X1 = 5 * SQBKG + BKG         'Find limit for the Poisson sum loop
1911 IF X1 < CNT THEN X1 = CNT
1912 IF X1 < 20 THEN X1 = 20
1920 PM# = BKG                    'Poisson mean
1921 P0# = EXP(-PM#)              '1st term in sum
1925 PSUM# = P0#                  'Poisson sum
1927 PFAP# = 0                    'False alarm probability
1930 FOR X = 1 TO X1              'LOOP START
1940 P0# = P0# * PM# / X
1945 ' LPRINT X, P0#, PSUM# + P0#, 1 - PSUM# '<<<<<<< Debug -- check P,C,D
1950 IF X = CNT THEN PFAP# = 1 - PSUM#
1960 IF PSUM# < MDTEST# THEN MDCNT = X
1965 PSUM# = PSUM# + P0#
1980 NEXT X                       'LOOP END
1982 MDCNT = MDCNT + 1            'Minimum Detection CNT
1985 ' RETURN                 '<<<<<< Debug return for FAP LOOP test at 8000
1990 PRINT #2, "Poisson FAP ="; PFAP#, "MDCNT="; MDCNT, "X1="; X1
```

```
1995 XFAP = PFAP#
1996 PRINT XFAP

2100 SIGNIF = NET / SQBKG
2110 PRINT #2, "Signal significant at";
2111 PRINT #2, USING "####.##"; SIGNIF;
2112 PRINT #2, "-sigma -- Poisson using sqr(bkg)";
2113 IF SIGNIF > 3 THEN PRINT #2, "   <<<<<";
2114 PRINT #2,

2210 SIGNIF = NET / (BKGSD(SYS) * TcntM)
2220 PRINT #2, "Signal significant at";
2221 PRINT #2, USING "####.##"; SIGNIF;
2222 PRINT #2, "-sigma -- Normal using SD of bkg";
2223 IF SIGNIF > 3 THEN PRINT #2, "   <<<<<";
2224 PRINT #2,
2225 PRINT #2,

2300 ' ********************************
2301 ' **   FLUX CALCULATION START   **
2302 ' ********************************
2305 EFFEC = EFF(SYS)
2310 IF NCOUP <= 7 THEN EFFEC = EFFEC * EFIX(SYS, NCOUP)
2320 PRINT #2, "Sensor efficiency with"; NCOUP; "coupons="; EFFEC * 100; "%"

3030 N64S1 = 1! / (EFFEC * (1! - CDFRAC))  'Atoms per net count
3040 N64S = N64S1 * NET                    'Atoms with this net count
3050 ACTX = LAMDA * N64S / 60!             'Lamda(d/hr)  ACTX(d/m)
3060 PRINT #2, "Cu-64 at start of count ="; N64S; "atoms";
3070 PRINT #2, TAB(55); ACTX; "d/min"

3100 N64A1 = N64S1 / DDFRAC              'Atoms per net count
3110 N64A = N64S / DDFRAC                'Atoms with this net count
3120 ACT = LAMDA * N64A / 60!            'Lamda(d/hr)  ACTX(d/m)
3130 PRINT #2, "Cu-64 at OTSG exit      ="; N64A; "atoms";
3140 PRINT #2, TAB(55); ACT; "d/min"

3200 N63 = NATOM * NCOUP
3210 LAMDAS = LAMDA / 3600!   'Lamdas(d/s)
3220 FLUXO = LAMDAS / (CROSS * N63 * FRACT)
3230 FLUX = FLUXO * N64A      'Flux to produce this net count
3240 FLUX1 = FLUXO * N64A1    'Flux to produce one net count
3250 PRINT #2, "Neutron flux seen       ="; FLUX; "neutrons/(second*cm²)"
3290 ' ********************************
3291 ' **   FLUX CALCULATION END     **
3292 ' ********************************

3300 PFLUX = PNET           '% err in flux is same as % err in net count
```

```
3310 PFLUXN = PFLUX        'Extra 5% error added for multiple coupon counting
3311 IF NCOUP > 1 THEN PFLUXN = SQR(PFLUXN * PFLUXN + 25)
3320 EFLUX = ABS(FLUX) * PFLUX / 100!
3330 EFLUXN = ABS(FLUX) * PFLUXN / 100!
3335 EFLX = EFLUXN
3336 PFLX = PFLUXN
3338 ZFLX = FLUX1 * SQZER    'Flux error if only background seen
3340 EFLUX1 = FLUX1 * SQNET
3341 IF EFLUX1 = EFLUX THEN 3350
3342 EFLX = EFLUX1
3345 PRINT #2, "Neutron flux error ALT  ="; EFLUX1; "n/(s*cm²)"

3350 PRINT #2, "Neutron flux error      ="; EFLUX; "n/(s*cm²)";
3351 PRINT #2, TAB(55); "Flux error="; PFLUX; "%"
3360 IF NCOUP = 1 THEN 3380
3370 PRINT #2, "plus 5% efficiency error="; EFLUXN; "n/(s*cm²)";
3371 PRINT #2, TAB(55); "Flux error="; PFLUXN; "%"
3380 ' Extra 5% error added in quadrature for multiple coupon counting"
3390 PRINT #2, "Zero neutron flux error ="; ZFLX; "n/(s*cm²)"

3400 MDNET = MDCNT - BKG           'Minimum detectable net count
3405 MDFLUX = MDNET * FLUX1        'Minimum detectable neutron flux
3410 PRINT #2, "Minimum Detectable Flux ="; MDFLUX; "n/(s*cm²)"
3420 PRINT #2, "Minimum detection count ="; MDCNT; "cts";
3430 PRINT #2, "    net count needed = "; MDNET; "cts"

4000 PRINT #3, SAMP$; CHR$(9);
4010 PRINT #3, USING "###.##"; BKG;
4011 PRINT #3, CHR$(9);
4020 PRINT #3, USING "####"; CNT;
4021 PRINT #3, CHR$(9);
4030 PRINT #3, USING "####.####"; FLUX;
4031 PRINT #3, CHR$(9);
4040 PRINT #3, USING "####.####"; EFLX;
4041 PRINT #3, CHR$(9);
4050 PRINT #3, USING "#####"; PFLX;
4051 PRINT #3, "%"; CHR$(9);
4060 PRINT #3, USING "#.#########"; PFAP#;
4061 PRINT #3, CHR$(9);
4070 PRINT #3, USING "##.####"; MDFLUX;
4080 PRINT #3, CHR$(9);
4081 PRINT #3, USING "####.####"; ZFLX
4200 NEXT SYS


5100 GOTO 600

6000 CLOSE #1  'End of program -- close up files used
```

```
6010 CLOSE #2
6020 CLOSE #3
6100 STOP


8000 WIDTH LPRINT 100
8005 LPRINT "Test of the Poisson FAP loop"
8010 FAPMDL# = .001 'FAP level for MDL
8020 LPRINT "FAP for minimum detectable level    ="; FAPMDL#
8030 BKG = 25
8040 SQBKG = SQR(BKG)
8050 CNT = 34
8080 GOSUB 1900
8100 LPRINT "        BKG ="; BKG, "  CNT="; CNT
8110 LPRINT "Poisson FAP ="; PFAP#, "MDCNT="; MDCNT, "X1="; X1
8120 STOP
```

Appendix B

COMB.BAS LISTING

```
10 CLS
15 PRINT "BASIC PROGRAM TO CALCULATE WEIGHTED MEAN AND COMBINED FAPS"
17 WIDTH LPRINT 96

20 INPUT "NAME OF DATA DISK [B]: ", DISK$
21 INPUT "NAME OF INPUT FILE [DATA]: ", INFIL$
25 FILENAM$ = DISK$ + ":" + INFIL$

30 DFILE$ = FILENAM$ + ".DAT"
31 PRINT "NAME OF INPUT DAT FILE [B:DATA.DAT]: ", DFILE$
32 OPEN DFILE$ FOR INPUT AS #1

35 PFILE$ = FILENAM$ + ".CMB"
36 PRINT "NAME OF OUTPUT PRN FILE [B:DATA.CMB]: ", PFILE$
37 OPEN PFILE$ FOR OUTPUT AS #2

40 DIM LA$(10)
41 DIM BKG(10), CNT(10)
42 DIM FLX(10), EFL(10), PFL(10)
43 DIM FAP(11), MDL(10), ZFE(10)
45 DIM FL$(10), VL(10)
46 DIM P(11)
47 NDF = 9'Number of data fields

50 T$ = " "                    'TAB character to separate fields
55 LBCNT = 0

60 FAPMDL# = .001              'FAP level for MDL
61 PRINT #2, "FAP for minimum detectable level    = ";
62 PRINT #2, USING "#.########"; FAPMDL#

70 PRINT #2, CHR$(174); "RM100"; CHR$(175);
71 PRINT #2, CHR$(174); "TS6,15,22,27,38,48,56,68,80"; CHR$(175)
72 PRINT #2,
"______________________________________________________________________________________
_"
75 PRINT #2, "LABEL COUPONS BKG  CNT   N-FLUX   N-ERR  %-ERR FAP   MDL-FLUX"
76 PRINT #2, "        n/(s*sqcm) n/(s*sqcm)   n/(s*sqcm)"
78 PRINT #2,
"______________________________________________________________________________________
_"

100 NM = 0                     'Number of measurements in set
```

```
110 IF LBCNT > 0 THEN 200
120 LBCNT = LBCNT + 1
140 ' LPRINT "LABEL COUPONS BKG  CNT   N-FLUX   N-ERR  %-ERR FAP   MDL-FLUX"
150 ' LPRINT "         n/(s*sqcm) n/(s*sqcm)   n/(s*sqcm)"

200 IF EOF(1) THEN 6000        'Quit if input file empty
210 ' ************************************************************
220 ' File input of total time exposed to neutron flux in hours
230 INPUT #1, IS$
240 ' ************************************************************

250 NL = LEN(IS$)              'Divide line into fields
260 IF NL < I THEN 1000        'Empty string (blank line) ends the set
280 IF NL < 15 THEN 200        'Not long enough for real data (tab stops)

310 NF = 0                     'Number of data fields in line
320 N1 = 1
330 WHILE N1 < NL
340 N2 = INSTR(N1, IS$, T$)
350 IF N2 = 0 THEN N2 = NL
360 NF = NF + 1
370 FL$(NF) = MID$(IS$, N1, N2 - N1)
380 N1 = N2 + 1
390 WEND

400 IF INSTR(IS$, "Title") = 0 THEN 450
405 GOSUB 8000
410 PRINT #2, CHR$(174); "BB"; CHR$(175); CHR$(174); "NB"; CHR$(175)
430 ' LPRINT IS$
440 LBCNT = 0
450 PRINT #2, IS$
455 IF FL$(1) = "LABEL" THEN 100
460 IF NF <> NDF THEN 100   'Wrong number of fields ends the set - NO PROCESS
470 ' LPRINT IS$
490 GOTO 700

500 FOR I = 1 TO NF            'Remove any leading or trailing spaces
510 V$ = FL$(I)                'if necessary for VAL function
520 WHILE LEFT$(V$, 1) = " "             'Remove any leading spaces
530 V$ = MID$(V$, 2)
540 WEND
550 WHILE RIGHT$(V$, LEN(V$)) = " "      'Remove any trailing spaces
560 V$ = LEFT$(V$, LEN(V$) - 1)
570 WEND
580 FL$(I) = V$
590 NEXT I

600 FOR I = 1 TO NF
```

```
610 PRINT I, "["; FL$(I); "]", VL(I)
620 NEXT I

700 FOR I = 1 TO NF            'Evaluate the fields
720 VL(I) = VAL(FL$(I))
750 NEXT I

800 NM = NM + 1                'Number of measurements in set
810 LA$(NM) = FL$(1)
820 BKG(NM) = VL(2)
830 CNT(NM) = VL(3)
840 FLX(NM) = VL(4)
850 EFL(NM) = VL(5)
860 PFL(NM) = VL(6)
873 FAP(NM) = VL(7)
880 MDL(NM) = VL(8)
890 ZFE(NM) = VL(9)

900 GOTO 200                   'Loop back for more input

1000 IF NM < 2 THEN 100        'Calculate combined values for the set
1010 SBKG = 0         'Sum of BKGs
1020 SCNT = 0         'Sum of CNTs
1030 SFLX = 0         'Weighted Sum of FLXs
1040 SWTS = 0         'Sum of WTs
1045 SZWTS = 0        'Sum of WTs for ZFEs
1050 SF1# = 0         'Sum of FLXs
1060 SF2# = 0         'Sum of (FLX*FLX)s
1090 ' LPRINT NM; " Measurements in this set"
1095 LBCNT = 0

1100 FOR I = 1 TO NM
1110 SBKG = SBKG + BKG(I)
1120 SCNT = SCNT + CNT(I)
1130 WT = EFL(I)
1131 IF WT = 0 THEN WT = 1E-10
1132 WT = 1! / (WT * WT)
1140 SFLX = SFLX + WT * FLX(1)
1150 SWTS = SWTS + WT
1151 ZWT = ZFE(I)
1152 IF ZWT = 0 THEN ZWT = 1E-10
1153 ZWT = 1! / (ZWT * ZWT)
1155 SZWTS = SZWTS + ZWT
1160 SF1# = SF1# + FLX(I)
1165 SF2# = SF2# + FLX(I) * FLX(I)
1170 NEXT I
1180 GNM = GNM + NM                'Save for weighted average of full set
1181 GSFLX = GSFLX + SFLX
```

```
1182 GSWTS = GSWTS + SWTS
1183 GSZWTS = GSZWTS + SZWTS
1185 GSF1# = GSF1# + SF1#
1186 GSF2# = GSF2# + SF2#
1195 IF SBKG <= 0 THEN SBKG = 1E-10
1198 SQBKG = SQR(SBKG)

1200 FLUX = SFLX / SWTS
1210 EFLX = 1! / SQR(SWTS)
1215 PFLX = ABS(100 * EFLX / FLUX)
1216 ZFLX = 1! / SQR(SZWTS)
1220 PRINT #2, "Weighted Average"; T$; T$;
1221 PRINT #2, USING "####.####"; FLUX;
1222 PRINT #2, T$;
1223 PRINT #2, USING "####.####"; EFLX;
1224 PRINT #2, T$;
1225 PRINT #2, USING "#####"; PFLX;
1226 PRINT #2, "%"; T$;
1230 X = FLUX / EFLX
1231 GOSUB 7000                'Calculate FAP based on N(0,1) with NF-ERR
1232 WFAP# = Q#
1235 WMDL = 3.092 * EFLX
1241 PRINT #2, USING "#.#########"; WFAP#;
1242 PRINT #2, T$;
1245 PRINT #2, USING "##.####"; WMDL;
1247 PRINT #2, T$;
1249 PRINT #2, USING "####.####"; ZFLX

1250 X = FLUX / ZFLX
1251 GOSUB 7000                'Calculate FAP based on N(0,1) with ZF-ERR
1252 WZFAP# = Q#
1255 WZMDL = 3.092 * ZFLX
1270 PRINT #2, "FAP using Wtd 0-Flux error "; T$; T$; T$;
1271 PRINT #2, USING "#.#########"; WZFAP#;
1272 PRINT #2, T$;
1275 PRINT #2, USING "##.####"; WZMDL

1290 ' LPRINT "Weighted Mean Flux ="; FLUX; TAB(40);
1291 ' LPRINT X; "sigma N(0,1) FAP ="; WFAP#
1292 ' LPRINT "Error in Mean Flux ="; EFLX; TAB(40); PFLX; "%"
1293 ' LPRINT "3.1-sigma MDL Flux ="; WMDL;
1294 ' LPRINT TAB(40); " 4.66-sigma MDL Flux ="; WMDL * 4.66 / 3.1
1299 ' LPRINT

1300 AVEFLX = SF1# / NM
1310 NMX = NM - 1
1311 IF NM < 2 THEN NMX = 1
1320 S# = (SF2# - SF1# * SF1# / NM) / NMX
```

```
1321 SEFLUX = S#
1325 IF SEFLUX > 0 THEN SEFLUX = SQR(SEFLUX)
1330 SEAVEF = SEFLUX / SQR(NM)
1340 PEAVEF = ABS(100 * SEAVEF / AVEFLX)
1350 PRINT #2, "Normal Average"; T$; T$; T$;
1351 PRINT #2, USING "####.####"; AVEFLX;
1352 PRINT #2, T$;
1353 PRINT #2, USING "####.####"; SEAVEF;
1354 PRINT #2, T$;
1355 PRINT #2, USING "#####"; PEAVEF;
1356 PRINT #2, "%"; T$;
1360 X = AVEFLX / SEAVEF
1361 GOSUB 7000              'Calculate FAP based on N(0,1)
1362 SAFAP# = Q#
1365 SAMDL = 3.092 * SEAVEF
1370 PRINT #2, USING "#.#########"; SAFAP#;
1371 PRINT #2, T$;
1375 PRINT #2, USING "##.####"; SAMDL
1380 ' LPRINT "Mean Flux          ="; AVEFLX; TAB(40);
1381 ' LPRINT X; "sigma N(0,1) FAP ="; SAFAP#
1385 ' LPRINT "Std Dev in Flux    ="; SEFLUX
1386 ' LPRINT "Std Error in mean  ="; SEAVEF; TAB(40); PEAVEF; "%"
1388 ' LPRINT "3.1-sigma MDL Flux ="; SAMDL;
1389 ' LPRINT TAB(40); " 4.66-sigma MDL Flux ="; SAMDL * 4.66 / 3.1
1390 ' LPRINT

1400 MDTEST# = 1! - FAPMDL#        'Require a FAP < 0.001 for MDL
1402 MDCNT = 0                     'Minimum Detection CNT
1410 X1 = 5 * SQBKG + SBKG         'Find limit for the Poisson sum loop
1411 IF X1 < SCNT THEN X1 = SCNT
1412 IF X1 < 20 THEN X1 = 20
1420 PM# = SBKG                    'Poisson mean
1421 PO# = EXP(-PM#)               '1st term in sum
1425 PSUM# = PO#                   'Poisson sum
1427 PFAP# = 0                     'False alarm probability
1430 FOR X = 1 TO X1               'LOOP START
1440 PO# = PO# * PM# / X
1450 IF X = SCNT THEN PFAP# = 1 - PSUM#
1460 IF PSUM# < MDTEST# THEN MDCNT = X
1465 PSUM# = PSUM# + PO#
1480 NEXT X                        'LOOP END
1482 MDCNT = MDCNT + 1             'Minimum Detection CNT

1500 ' LPRINT "SBKG="; SBKG; "   SCNT="; SCNT; "   MDCNT="; MDCNT
1510 ' LPRINT "All one count Poisson FAP ="; PFAP#

1550 PRINT #2, "Combined Count"; T$;
1560 PRINT #2, USING "###.##"; SBKG;
```

```
1561 PRINT #2, T$;
1562 PRINT #2, USING "####"; SCNT;
1563 PRINT #2, T$; T$; T$;
1570 PCNT = 0
1571 X = ABS(SCNT - SBKG)
1572 IF X <> 0 THEN PCNT = SQR(SCNT) / X
1575 PRINT #2, USING "#####"; PFLX;
1576 PRINT #2, "%"; T$;
1580 PRINT #2, USING "#.#########"; PFAP#


1700 IF NM < 2 THEN 1790           'Order the FAPs
1710 FOR I = 1 TO NM - 1
1720 FOR J = I + 1 TO NM
1730 IF FAP(I) >= FAP(J) THEN 1770
1740 X = FAP(I)
1750 FAP(I) = FAP(J)
1760 FAP(J) = X
1770 NEXT J
1780 NEXT I
1790 'FAPs no in order largest to smallest

1800 FAP(NM + 1) = 0               'Convert FAPs to Ps
1810 FAP(0) = 1
1820 PRODFAP = 1
1830 FOR I = I TO NM
1840 P(I) = FAP(I) - FAP(I + 1)
1850 PRODFAP = PRODFAP * FAP(I)
1860 NEXT I

1910 P1 = P(1)
1920 P2 = P(2)
1930 P3 = P(3)
1940 P4 = P(4)
1950 P5 = P(5)
1960 P6 = P(6)
1970 P7 = P(7)
1980 P8 = P(8)
1990 P9 = P(9)

2000 ON NM GOTO 2100, 2200, 2300, 2400, 2500, 2600, 2700, 2800, 2900
2010 ' LPRINT "NEED TO PROGRAM FOR NM="; NM
2020 CFAP = 1
2030 GOTO 3000

2100   ' 1 measurement in the set
2110 CFAP = FAP(1)
2190 GOTO 3000
```

```
2200   ' 2 measurements in the set
2210 CFAP = P2 * P2 + 2 * P1 * P2
2290 GOTO 3000

2300   ' 3 measurements in the set
2310 C# = P3 * P3
2320 C# = C# + 3 * (P1 * P3 + P2 * P3 + P2 * P2)
2330 C# = C# + 6 * P1 * P2
2380 CFAP = C# * P3
2390 GOTO 3000

2400   ' 4 measurements in the set

2410 C# = P4 ^ 3
2420 C# = C# + 4 * (P1 * P4 ^ 2 + P2 * P4 ^ 2 + P3 * P4 ^ 2 + P3 ^ 3)
2430 C# = C# + 6 * (P2 ^ 2 * P4 + P3 ^ 2 * P4)
2440 C# = C# + 12 * (P1 * P2 * P4 + P1 * P3 * P4 + P1 * P3 ^ 2)
2450 C# = C# + 12 * (P2 * P3 * P4 + P2 * P3 ^ 2 + P2 ^ 2 * P3)
2460 C# = C# + 24 * P1 * P2 * P3 * P4
2480 CFAP = C# * P4
2490 GOTO 3000

2500   ' 5 measurements in the set
2510 C# = P5 ^ 5
2520 C# = C# + 5 * P1 * P5 ^ 4 + 5 * P2 * P5 ^ 4 + 5 * P3 * P5 ^ 4
2521 C# = C# + 5 * P4 * P5 ^ 4 + 5 * P4 ^ 4 * P5
2530 C# = C# + 10 * P2 ^ 2 * P5 ^ 3 + 10 * P3 ^ 2 * P5 ^ 3
2531 C# = C# + 10 * P4 ^ 2 * P5 ^ 3
2532 C# = C# + 10 * P3 ^ 3 * P5 ^ 2 + 10 * P4 ^ 3 * P5 ^ 2
2540 C# = C# + 20 * P1 * P2 * P5 ^ 3 + 20 * P1 * P3 * P5 ^ 3
2541 C# = C# + 20 * P1 * P4 * P5 ^ 3 + 20 * P1 * P4 ^ 3 * P5
2542 C# = C# + 20 * P2 * P3 * P5 ^ 3 + 20 * P2 * P4 * P5 ^ 3
2543 C# = C# + 20 * P2 * P4 ^ 3 * P5 + 20 * P3 * P4 * P5 ^ 3
2544 C# = C# + 20 * P3 * P4 ^ 3 * P5
2550 C# = C# + 30 * P1 * P3 ^ 2 * P5 ^ 2 + 30 * P1 * P4 ^ 2 * P5 ^ 2
2551 C# = C# + 30 * P2 * P3 ^ 2 * P5 ^ 2 + 30 * P2 * P4 ^ 2 * P5 ^ 2
2552 C# = C# + 30 * P2 ^ 2 * P3 * P5 ^ 2 + 30 * P2 ^ 2 * P4 * P5 ^ 2
2553 C# = C# + 30 * P2 ^ 2 * P4 ^ 2 * P5 + 30 * P3 * P4 ^ 2 * P5 ^ 2
2554 C# = C# + 30 * P3 ^ 2 * P4 * P5 ^ 2 + 30 * P3 ^ 2 * P4 ^ 2 * P5
2560 C# = C# + 60 * P1 * P2 * P3 * P5 ^ 2 + 60 * P1 * P2 * P4 * P5 ^ 2
2561 C# = C# + 60 * P1 * P3 * P4 * P5 ^ 2 + 60 * P1 * P2 * P4 ^ 2 * P5
2562 C# = C# + 60 * P1 * P3 * P4 ^ 2 * P5 + 60 * P1 * P3 ^ 2 * P4 * P5
2563 C# = C# + 60 * P2 * P3 * P4 * P5 ^ 2 + 60 * P2 * P3 * P4 ^ 2 * P5
2564 C# = C# + 60 * P2 * P3 ^ 2 * P4 * P5 + 60 * P2 ^ 2 * P3 * P4 * P5
2570 C# = C# + 120 * P1 * P2 * P3 * P4 * P5
2580 CFAP = C#
2590 GOTO 3000
```

```
2600   ' 6 measurements in the set

2700   ' 7 measurements in the set

2800   ' 8 measurements in the set

2900   ' 9 measurements in the set
2910 ' LPRINT "NEED TO PROGRAM FOR NM="; NM
2920 CFAP = 1
2990 GOTO 3000

3000 PRINT #2, "Combined FAP"; T$; T$; T$; T$; T$; T$;
3050 PRINT #2, USING "#.#########"; CFAP
3052 PRINT #2,

3100 ' LPRINT "Correctly Combined FAP    ="; CFAP
3110 ' LPRINT "Product of the FAPs       ="; PRODFAP
3170 ' LPRINT
3180 ' LPRINT "-------------------------------------"
3190 ' LPRINT

4000 GOTO 100

5000 STOP

6000 CLOSE #1  'End of program -- close up files used
6010 CLOSE #2
6020 PRINT "END OF FILE STOP"
6100 STOP

7000 'Subroutine to find Normal N(0,1) FAP based on A&S 26.2.17
7010 'Call with X = (X-MEAN)/SIGMA
7020 'Error < 7.5E-8 for 0 <= X < infinity
7030 XX = ABS(X)
7100 SQ2PI = 2.5066283#'sqr(2*PI)
7110 Z = EXP(-XX * XX / 2) / SQ2PI
7120 T# = 1! / (1! + .2316419# * XX)
7130 T2# = T# * T#
7140 T4# = T2# * T2#
7150 Q# = .31938153# * T# - .356563782# * T2# + 1.781477937# * T# * T2#
7160 Q# = Q# - 1.821255978# * T4# + 1.330274429# * T# * T4#
7170 Q# = Z * Q#
7180 IF X > 0 THEN 7190
7181 Q# = 1 - Q#
7190 RETURN

7200 'Subroutine to find X given a FAP=Q(X) based on A&S 26.2.23
```

```
7210 'Call with Q=FAP
7220 'Error < 4.5E-4 for 0<FAP<=.5
7230 X = 0
7240 IF Q > .5 THEN 7390
7250 IF Q <= 0 THEN Q = 1E-09
7300 QQ# = Q
7303 QL# = LOG(QQ#)
7305 T2# = -2! * QL#
7310 T# = SQR(T2#)
7320 XD# = 1! + 1.432788 * T# + .189269 * T2# + .001308 * T# * T2#
7330 XN# = 2.515517 + .802853 * T# + .010328 * T2#
7340 X = T# - XN# / XD#
7355 PRINT "QQ#="; QQ#; "  QL#="; QL#; "  T#="; T#; "  T2#="; T2#; "  X="; X
7390 RETURN

8000 'GRAND WEIGHTED AVERAGE FOR TITLED SET
8100 IF GNM < 2 THEN 9400     'Calculate combined values for the set
8200 FLUX = GSFLX / GSWTS
8210 EFLX = 1! / SQR(GSWTS)
8215 PFLX = ABS(100 * EFLX / FLUX)
8218 GZFLX = 1! / SQR(GSZWTS)
8220 PRINT #2, "Wtd Ave for set "; T$; T$;
8221 PRINT #2, USING "####.####"; FLUX;
8222 PRINT #2, T$;
8223 PRINT #2, USING "####.####"; EFLX;
8224 PRINT #2, T$;
8225 PRINT #2, USING "#####"; PFLX;
8226 PRINT #2, "%"; T$;
8230 X = FLUX / EFLX
8231 GOSUB 7000               'Calculate FAP based on N(0,1)
8232 WFAP# = Q#
8235 WMDL = 3.092 * EFLX
8260 PRINT #2, USING "#.#########"; WFAP#;
8261 PRINT #2, T$;
8270 PRINT #2, USING "##.####"; WMDL;
8285 PRINT #2, T$;
8287 PRINT #2, USING "####.####"; GZFLX

8290 ' LPRINT "Set Wtd Ave   Flux ="; FLUX; "    ";
8291 ' LPRINT X; "sigma N(0,1) FAP ="; WFAP#
8292 ' LPRINT "Error in Mean Flux ="; EFLX; "    "; PFLX; "%"
8293 ' LPRINT "3.1-sigma MDL Flux ="; WMDL;
8294 ' LPRINT TAB(40); " 4.66-sigma MDL Flux ="; WMDL * 4.66 / 3.1
8295 ' LPRINT

8340 X = FLUX / GZFLX
8341 GOSUB 7000               'Calculate FAP based on N(0,1) with ZF-ERR
8342 GWZFAP# = Q#
```

```
8345 GWZMDL = 3.092 * GZFLX
8350 PRINT #2, "FAP using Wtd 0-Flux error "; T$; T$; T$;
8371 PRINT #2, USING "#.#########"; GWZFAP#;
8372 PRINT #2, T$;
8375 PRINT #2, USING "##.####"; GWZMDL

9300 AVEFLX = GSF1# / GNM
9310 GNMX = GNM - 1
9320 S# = (GSF2# - GSF1# * GSF1# / GNM) / GNMX
9321 SEFLUX = S#
9325 IF SEFLUX > 0 THEN SEFLUX = SQR(SEFLUX)
9330 SEAVEF = SEFLUX / SQR(GNM)
9340 PEAVEF = ABS(100 * SEAVEF / AVEFLX)
9350 PRINT #2, "Normal Average"; T$; T$; T$;
9351 PRINT #2, USING "####.####"; AVEFLX;
9352 PRINT #2, T$;
9353 PRINT #2, USING "####.####"; SEAVEF;
9354 PRINT #2, T$;
9355 PRINT #2, USING "#####"; PEAVEF;
9356 PRINT #2, "%"; T$;
9360 X = AVEFLX / SEAVEF
9361 GOSUB 7000              'Calculate FAP based on N(0,1)
9362 SAFAP# = Q#
9365 SAMDL = 3.092 * SEAVEF
9370 PRINT #2, USING "#.#########"; SAFAP#;
9371 PRINT #2, T$;
9375 PRINT #2, USING "##.####"; SAMDL
9380 ' LPRINT "Mean Flux          ="; AVEFLX; TAB(40);
9381 ' LPRINT X; "sigma N(0,1) FAP ="; SAFAP#
9385 ' LPRINT "Std Dev in Flux    ="; SEFLUX
9386 ' LPRINT "Std Error in mean  ="; SEAVEF; TAB(40); PEAVEF; "%"
9388 ' LPRINT "3.1-sigma MDL Flux ="; SAMDL;
9389 ' LPRINT TAB(40); " 4.66-sigma MDL Flux ="; SAMDL * 4.66 / 3.1
9390 ' LPRINT
9396 ' LPRINT "**************************************"
9399 ' LPRINT

9400 GNM = 0          'Setup for next time through
9410 GSFLX = 0        'Weighted Sum of FLXs
9420 GSWTS = 0        'Sum of WTs
9450 GSF1# = 0        'Sum of FLXs
9460 GSF2# = 0        'Sum of (FLX*FLX)s
9580 PRINT #2,
"________________________________________________________________________________
_"
9490 RETURN
```

DISTRIBUTION

No. of
Copies

OFFSITE

10 DOE/Office of Scientific and
Technical Information

10 John Schork
GPU Nuclear Corp.
P.O. Box 480, Rt. 441 S.
Middletown, PA 17057-0191

Michelle Davis
EG&G
P.O. Box 1625
Idaho Falls, ID 83401

Steve Metzger
EG&G TMI Technical Integration
P.O. Box 88
Middletown, PA 17057

No. of
Copies

ONSITE

DOE Richland Operations Office

E. C. Norman

17 Pacific Northwest Laboratory

K. H. Abel (5)
B. D. Geelhood (5)
R. L. Brodzinski
Publishing Coordination
Technical Report Files (5)